Improving Efficiencies in Water-Based Separators Using Mathematical Analysis Tools

by

Jaisen N. Kohmuench

Dissertation submitted to the Faculty of the
Virginia Polytechnic Institute and State University in partial
fulfillment of the requirements for the degree

of

DOCTOR OF PHILOSOPHY

in

Mining and Minerals Engineering

Approved
by:

G.H. Luttrell, Chairman
R.H. Yoon
G.T. Adel
E.C. Westman
M.J. Mankosa

December, 2000
Blacksburg, Virginia

Keywords: Coal Spirals, Circuit Analysis, CrossFlow Separator, HydroFloat Separator, Classification, Density Separation.

Improving Efficiencies in Water-Based Separators Using Mathematical Analysis Tools

by

Jaisen N. Kohmuench

Committee Chairman: Gerald H. Luttrell
Department of Mining and Minerals Engineering

(ABSTRACT)

A better understanding of several mineral processing devices and applications was gained through studies conducted with mathematical analysis tools. Linear circuit analysis and population balance modeling were utilized to remedy inefficiencies found in a number of popular mineral processing water-based unit operations. Improvements were made in areas, including unit capacity and separation efficiency.

One process-engineering tool, known as linear circuit analysis, identified an alternative coal spiral circuit configuration that offered improved performance while maintaining a reasonable circulating load. In light of this finding, a full-scale test circuit was installed and evaluated at an existing coal preparation facility. Data obtained from the plant tests indicate that the new spiral circuit can simultaneously reduce cut-point and improve separation efficiency.

A mathematical population balance model has also been developed which accurately simulates a novel hindered-bed separator. This device utilizes a tangential feed presentation system to improve the performance of conventional teeter-bed separators. Investigations utilizing the mathematical model were carried out and have predicted solid feed rates of up to 71 tph/m^2 (6 tph/ft^2) can be achieved at acceptable efficiencies. The model also predicts that the

unfavorable impact of operating at low feed percent solids is severely reduced by the innovative feed presentation design. Tracer studies have verified that this system allows excess feed water to cross over the top of the separator without entering the separation chamber, thereby reducing turbulence.

A hindered-bed separator population balance model was also developed whose results were utilized to improve the efficiencies encountered when using a teeter-bed separator as a mineral concentrator. It was found that by altering the apparent density of one of the feed components, the efficiency of the gravity separation could be greatly improved. These results led to the development of a new separator which segregates particles based on differences in mass after the selective attachment of air bubbles to the hydrophobic component of the feed stream. Proof-of-concept and in-plant testing indicate that significant improvements in separation efficiency can be achieved using this air-assisted teeter-bed system. The in-plant test data suggest that in some cases, recoveries of the plus 35 mesh plant feed material can be increased by more than 40% through the application of this new technology.

ACKNOWLEDGEMENTS

The author wishes to express his deepest thanks and gratitude to Dr. Gerald H. Luttrell for his guidance and advice during this investigation. The opportunity to work on a project of such breadth was greatly appreciated as was the freedom allowed the author in completing this research. The author also wishes to thank the rest of the Luttrell Clan, Kay, Sarah, and Greg, for their fellowship and friendship.

The author is also grateful to Dr. Greg Adel for his friendship and advice, especially his counsel in the area of population balance modeling. Thank you also is expressed to Dr. Roe-Hoan Yoon for his helpful suggestions and recommendations.

A sincere thank you is also expressed to Dr. Mike Mankosa for his friendship and guidance. His in-field instruction and insight were invaluable. Thanks also to Cathy Mankosa, his wife, for her continued support and encouragement.

Thanks are also expressed to several companies whose support, both monetary and otherwise, made this work possible. This gratitude is expressed to Eriez Magnetics, PCS Phosphate, and the Pittston Coal Management Company. Individual thanks must also be expressed to Mr. Joe Shoniker, Mr. Fred Stanley and particularly, Mr. Richard Merwin.

The author wishes to acknowledge Wayne and Billy Slusser for their technical advice, assistance, and instruction. Their effort and ability are greatly appreciated.

The author would like to thank his parents, William and Carolyn Kohmuench, for their continued support and encouragement. And finally, the author expresses his deepest appreciation to his wife, and most loyal fan, Kathryn, for her support, encouragement and love.

TABLE OF CONTENTS

LIST OF FIGURES

Chapter 1: Improving Spiral Performance Using Circuit Analysis

Chapter 2: Improving Performance of Hindered-Bed Separators

Chapter 3: Improving Coarse Particle Recovery in Hindered-Bed Separators

LIST OF TABLES

Chapter 1: Improving Spiral Performance Using Circuit Analysis

Chapter 2: Improving Performance of Hindered-Bed Separators

Chapter 3: Improving Coarse Particle Recovery in Hindered-Bed Separators

ORGANIZATION

This dissertation is separated into three major chapters, each addressing a different aspect of improving efficiency in water-based separations. Chapter 1 discusses alternative circuitry which can improve overall spiral performance in coal preparation plants. Chapter 2 addresses the development of an efficient novel hindered-bed classifier. In Chapter 3, the improvements gained by the addition of air to hindered-bed density separators are discussed.

A great majority of each chapter has been constructed from articles that the author has published in several journals and proceedings. As a result, there is a literature review and a reference section for each of the three major chapters in this dissertation. Listed below are the reference data for the works from which these chapters were constructed.

Chapter 1: Improving Spiral Performance Using Circuit Analysis.

1) Luttrell, G.H., Kohmuench, J.N., Stanley, F.L. and Trump, G.D., 1998. "Improving Spiral Performance Using Circuit Analysis," SME Annual Meeting and Exhibit, Orlando, Florida, March 9-11, 1998, *Preprint No. 98-161*, 8 pp, (accepted on basis of abstract).
2) Luttrell, G.H., Kohmuench, J.N., Stanley, F.L. and Trump, G.D., 1998. "Improving Spiral Performance Using Circuit Analysis," *Minerals and Metallurgical Processing*, November 1998, Vol. 15, No. 4, pp. 16-21, (full peer review).
3) Luttrell, G.H., Kohmuench, J.N., Stanley, F.L. and Trump, G.D., 1999. "An Evaluation of Multi-Stage Spiral Circuits," *Proceedings*, 16th International Coal Preparation Conference and Exhibit, Lexington, Kentucky, April 27-29, 1999, pp.79-88, (accepted on basis of abstract).

Chapter 2: Improving Performance of Hindered-Bed Classifiers

1) Dunn, P.L., Stewart, S.O., Kohmuench, J.N. and Cadena, C.A., 2000. "A Hydraulic Classifier Evaluation: Upgrading Heavy Mineral Concentrates," *Preprint No. 00-155*, SME Annual Meeting, February 28 - March 1, 2000, Salt Lake City, Utah, (accepted on basis of abstract).

2) Kohmuench, J.N., Mankosa, M.J., Luttrell, G.H. and Adel, G.T., 2001. "A Process Engineering Evaluation of the CrossFlow Separator," SME Annual Meeting, February 26-28, 2001, Denver, Colorado, (accepted on basis of abstract-in preparation).

Chapter 3: Improving Coarse Particle Recovery in Hindered-Bed Separators

1) Kohmuench, J.N., Luttrell, G.H. and Mankosa, M.J., 1998. "Testing of the HydroFloat Cell for Recovery of Coarse Phosphate," *Proceedings*, Engineering Foundation Conference on Beneficiation of Phosphate, Palm Coast, Florida, December 6-11, 1998, pp. 1-6, (accepted on basis of abstract).

2) Kohmuench, J.N., Luttrell, G.H. and Mankosa, M.J., 2000. "Coarse Particle Concentration Using the HydroFloat Separator," *Preprint No.* 00-100, SME Annual Meeting, February 28 - March 1, 2000, Salt Lake City, Utah, (accepted on basis of abstract).

3) Mankosa, M.J., Kohmuench, J.N. and Luttrell, G.H., 2000. "Evaluation of the HydroFloat Separator for Coarse Coal Recovery," Proceedings, 17th International Coal Preparation Conference and Exhibit, May 2-4, 2000, Lexington, Kentucky, (accepted on basis of abstract).

4) Mankosa, M.J., Merwin, R.A., Kohmuench, J.N. and Luttrell, G.H., 2000. "In-Plant Testing of the HydroFloat Separator," 21st International Mineral Processing Congress, Rome, Italy, July 23-28, 2000, 9 pp., (full peer review).

CHAPTER 1

Improving Spiral Performance Using Circuit Analysis

1.1 Introduction

Spirals have become one of the most effective and low-cost methods for cleaning 1 mm x 100 mesh coals. Unfortunately, the specific gravity cut-points obtained using spirals are typically much higher than those employed by the coarse coal dense medium circuits. This imbalance creates either a loss of clean coal or a decrease in product quality. Also, water-based separators such as spirals tend to be much less efficient than dense medium devices due to misplaced coal and refuse. As a result, spirals are often used in multi-stage circuits in which the clean coal and/or middling streams from primary spirals are rewashed using secondary spirals. Plant operators are then faced with the decision to either (i) discard the secondary middlings and sacrifice yield or (ii) retain the middlings and accept a lower coal quality.

Studies carried out at Virginia Tech indicate that a third alternative exists for handling the middlings problem. This option involves the use of a rougher-cleaner configuration in which the middlings from the cleaner spirals are recycled back to the feed of the rougher spirals. Preliminary analyses indicate that this approach can improve separation efficiency (i.e., lower *Ep*) while simultaneously reducing cut-point.

1.2 Literature Review

Since its introduction by Humphreys in the 1940's (Thompson *et al*., 1990), spirals have proved to be a cost effective and efficient means of concentrating a variety of ores. Their success can be attributed to the fact that they are perceived as environmentally friendly, rugged, compact, and cost effective (Kapur *et al*., 1998). During the 1980's, there had been an increased interest in recovering coal fines. Since then, spirals have become a common method for the concentration of 0.1 mm – 3 mm coal. Spirals are able to maintain high combustible recoveries while treating material too coarse for flotation and too fine for dense media separation. Nonetheless, coal spiral efficiencies have not been able to match the separation results generally found in metalliferous concentration processes (Holland-Batt, 1995).

A spiral is comprised of helical conduit of semicircular cross-sections (Wills, 1992). Feed is introduced at the top of the spiral between 15-45% solids and is allowed to flow downward. Complex mechanisms, including the combined effects of centrifugal force, differential particle settling rates, interstitial trickling, and possibly hindered-settling (Mills, 1978), effect the stratification of particles. Generally, high density material reports to the inner edge of the spiral, while lower density material reports to the highwall of the spiral. Classification can also occur, predominantly misplacing the coarse, high density particles to the outer edge of the spiral. The center of the spiral trough contains any middling material present in the feed. The schematic cross-section seen in Figure 1.1 illustrates this separation. The band of high density material that forms near the inner edge can be removed through the use of adjustable splitters. *Ep* (Ecart Probable) values generally range between 0.10 and 0.15, with cut-points ranging between 1.70 and 2.00 SG.

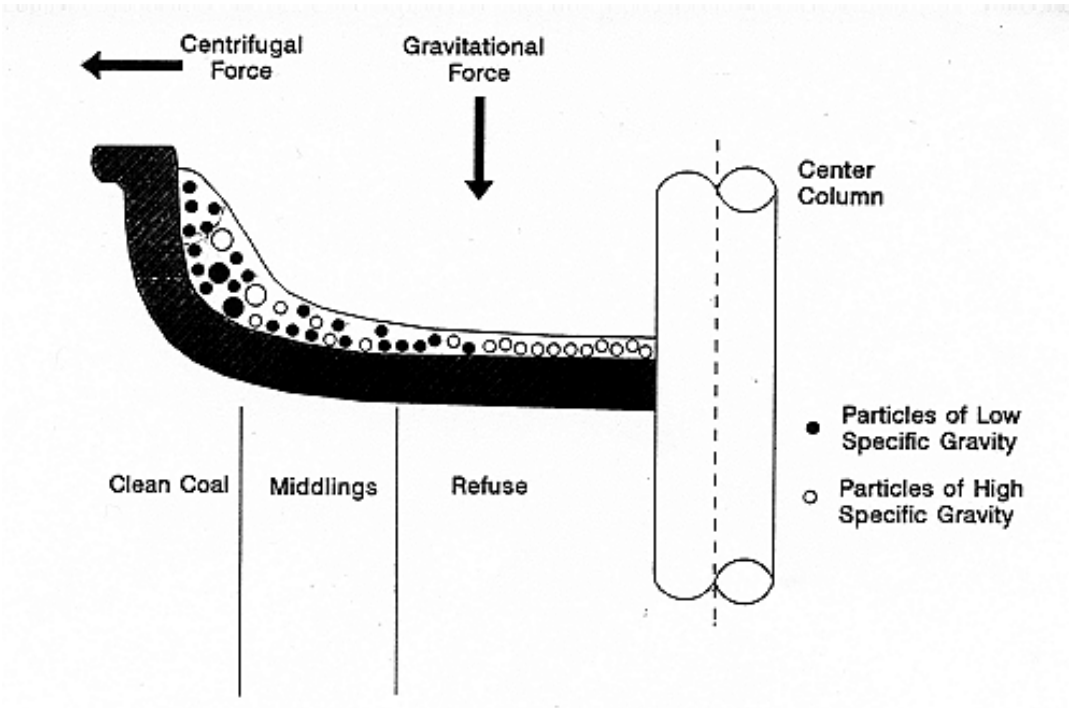

Figure 1.1 – Cross-section of a spiral trough flow (Chedgy *et al*., 1990).

Several improvements in coal spiral performance have been seen over the years. Recent studies have concentrated on optimizing the number of turns required on a spiral. This effort is an attempt to standardize the required number of turns needed on a spiral for different ores. As recent as the 1960's, Australian coal spirals had as few as 2 full turns, while modern spirals can employ as many as 7 turns to achieve the required separation (Holland-Batt, 1995).

Improvements in mineral spiral efficiencies have also been noted by Edward, *et al.* (1993) after the removal of products and subsequent repulping of the remaining flow after approximately four spiral turns. Generally, without repulping, the spiral flow can reach steady-state after only two turns. However, the recovery of the mineral can continue slowly for up to four or more turns. Repulping the spiral flow after only a few turns can restore the initial high

rate of recovery (Holland-Batt, 1995). Several spiral manufacturers have introduced designs that have successfully incorporated repulping.

Repulping in coal applications is less effective. When treating coal, the number of necessary turns increases due to the relatively low specific gravity of the pulp. For instance, if a mineral spiral, treating 4.0 SG material, requires 2 to 3 turns in order to effectively make a separation, it can be expected that a coal spiral will need 5 to 6 turns. Repulping after only 3 turns can destroy a partial separation occurring in the finer material which would normally require 6 turns to complete. In addition, repulpers in mineral spirals add solids and water to the concentrate zone, while repulpers in coal spiral applications add slurry to the reject zone thereby decreasing combustible recovery. Holland-Batt (1995) confirmed this in his work, which showed repulpers do not improve efficiency in coal spiral separations, and can actually decrease efficiency.

Studies have also shown that the feed rate, especially the total volumetric flow, introduced onto a spiral can greatly affect the performance of a spiral. Walsh and Kelly (1992) have stated in their work that the total mass feed rate is among one of the most important factors for determining coal spiral capacity. Their work goes on to show that for any feed pulp density, there is an associated optimum feed rate. Further studies by Holland-Batt (1990) show that there is indeed a performance envelope that is greatly affected by slurry density, and further indicates that a more dominant control of spiral performance is seen when combining slurry density with the solids flow rate (i.e., volumetric feed rate). As volumetric feed rate is increased, an increasing amount of entrained material will report to the outer wall and effectively reduce efficiency. These misplaced particles find it hard to escape the high velocity flow regimes and ultimately report to the clean coal product.

Mikhail, *et al*. (1988) also studied the performance of spirals with relation to feed rate and feed solids. This work found that feed rate may actually have a greater effect on separation cut-point than even splitter position. If solids are held constant as feed rate increases, the volumetric velocity of slurry down the spiral also increases. Consequently, the effect of the centrifugal force exerted on the slurry particles is greater, forcing more material to report to the clean coal launder. This higher recovery reflects a higher cut-point. Figure 1.2 illustrates this point.

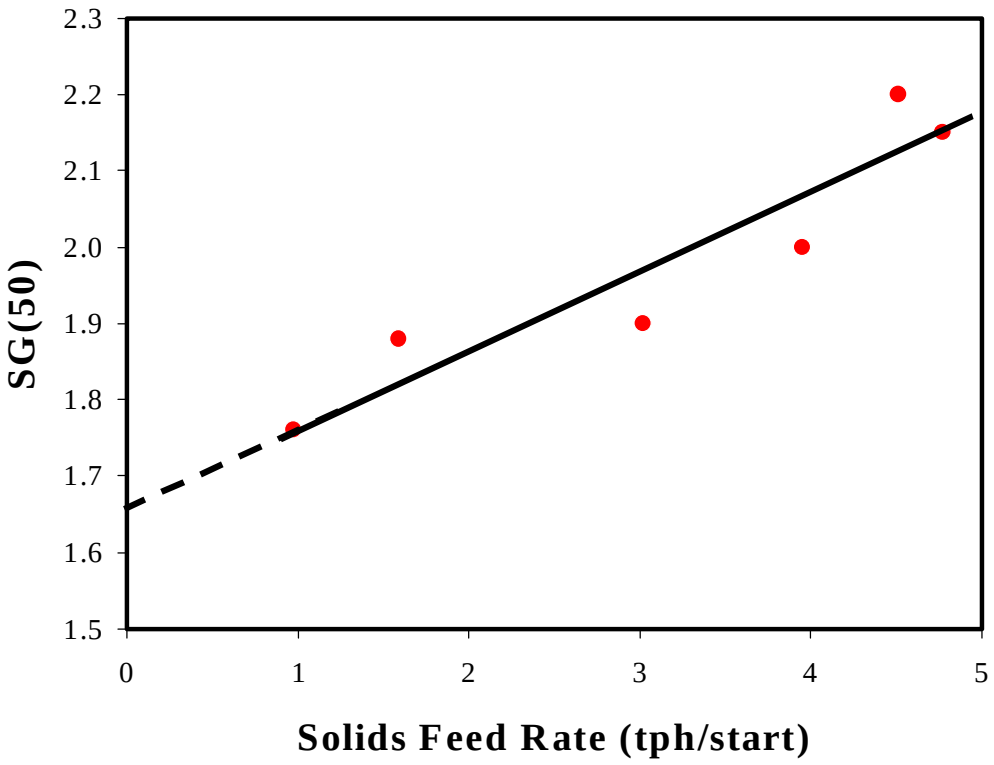

Figure 1.2 – Feed rate versus cut-point of a spiral separation (Mikhail *et al*., 1988)

Unexpectedly, little or no literature was found in the area of advanced coal spiral circuitry for the reason of improving separation efficiency. However, there were a few exceptions. A new process, utilizing rotating spirals, was studied by Holland-Batt (1992). His studies suggest that by rotating the downward volumetric flow (the spiral flow turns over itself during its descent), rotating spirals can improve the separation potentials by applying one or more additional force to the flowing film of particles. These studies were an extension of work completed in the early 1980's. Ultimately, it was found that the finer feed particles benefited from a flow that rotated over itself. Unfortunately, little or no improvement was found for the coarser feed particles.

Another advance in spiral circuitry was the advent of the compound spiral. The compound spiral is essentially a two-stage, middlings reclean circuit arranged on one column (MacNamara *et al*., 1995, 1996). A short primary and short secondary spiral are positioned on the same center tube, where a first stage clean and reject product can be removed, after which, the first stage middlings are repulped and retreated on the secondary spiral. Advantages of this design include lower cut-points, reduced floor space, elimination of interstage pumping, and improved recovery (Weldon *et al*., 1997).

1.3 Theoretical Framework

1.3.1 Circuit Analysis

Circuit analysis can be used to evaluate the overall effectiveness of various configurations of unit operations in mineral and coal processing circuits. This powerful tool, which was first developed and advocated by Meloy (1983), has regretfully seen only limited application in the analysis of coal processing circuits. Strictly speaking, this method can only be applied if particle-particle interactions do not influence the probability that a particle will report to a particular stream. In other words, the partition (or Tromp) curve should remain unchanged during variations in the characteristics of the feed stream. This assumption is generally valid for dense medium separations. This may also be a reasonable assumption for water-based processes such as spirals provided that the changes in feed characteristics are not too large. In fact, circuit analysis will always provide useful insight into how unit operations should be configured in a multi-stage circuit, even if the exact numerical predictions are not completely accurate.

Consider the one-stage unit operation shown below. The concentrate-to-feed ratio is given by:

$$C/F = P \qquad [1.1]$$

As a result, the mass of particles of a given property reporting to either the concentrate (C) or refuse (R) streams can be calculated as seen in Figure 1.3:

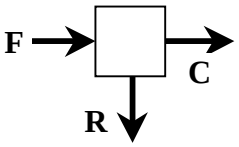

C = (P) F
R = (1-P) F

Figure 1.3 - Analysis of a single-stage separator.

where *P* is a dimensionless probability function that selects particles to report to a given stream based on their physical properties. For density-based separations, the probability function can often be estimated from an S-shaped transition function commonly referred to as the Lynch-Rao equation (1975), i.e.:

$$P = (e^{\alpha}-1)/(e^{\alpha X}+e^{\alpha}-2) \qquad [1.2]$$

in which *X* is the SG/SG_{50} ratio and α is a sharpness index. Note that the specific gravity cut-point (SG_{50}) is represented by a value of X=1 at which P=0.5.

The slope of the probability function evaluated at X=1 can be used to represent the separation efficiency of the process. The slope is obtained by taking the derivative of the concentrate-to-feed ratio at X=1. For the Lynch-Rao (1975) equation, this gives:

$$\partial(C/F)/\partial X = \partial P/\partial X = \alpha e^{\alpha} / (4-4e^{\alpha})) \qquad [1.3]$$

However, efficiencies of dense medium separators are more commonly reported in terms of an Ecart probable error (*Ep*). *Ep* values may be calculated directly from the probability function using the expression:

$$Ep = SG_{50} (X_{25}-X_{75}) / 2 \qquad [1.4]$$

where X_{25} and X_{75} are defined at P=0.25 and P=0.75, respectively. Therefore, the following approximation may be used in this case:

$$\partial(C/F)/\partial X = \partial P/\partial X \approx \Delta P/\Delta X = -0.25\ SG_{50}/Ep \qquad [1.5]$$

Now consider a similar analysis of the rougher-cleaner circuit shown in Figure 1.4.

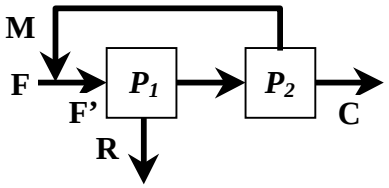

$F' = F + M$
$C = (P_2)(P_1)F'$
$R = (1-P_1)F'$
$M = (1-P_2)(P_1)F'$

Figure 1.4 - Analysis of a rougher-cleaner circuit.

By simple algebraic substitution, the concentrate-to-feed ratio (C/F) for this circuit can be calculated as:

$$C/F = P_2P_1 / (1-P_1+ P_1P_2) \qquad [1.6]$$

If the probability function (P) is assumed to be the same for both separators, then the separation efficiency for the rougher-cleaner circuit is:

$$\partial(C/F)/\partial X = (2P-P^2) / (P^2-P+1)^2 \, \partial P/\partial X \qquad [1.7]$$

Using the Lynch-Rao (1975) equation and noting that P=0.5 at X=1, the following relationship may be obtained:

$$\partial(C/F)/\partial X = 1.33 \, \partial P/\partial X = 1.33 \, \alpha e^{\alpha} / (4-4e^{\alpha}) \qquad [1.8]$$

Likewise, for the case involving *Ep* values, the following approximation will also hold:

$$\partial(C/F)/\partial X = 1.33 \, \partial P/\partial X \approx 1.33 \, (-0.25 \, SG_{50}/Ep) \qquad [1.9]$$

According to this analysis, the separation efficiency (defined by the slope of the circuit partition curve) of a rougher-cleaner circuit should be 1.33 times that of the single-stage circuit.

The relative efficiencies of other circuit configurations can be evaluated by circuit analysis using the same approach. Several of these are summarized in Table 1.1. As shown, the standard rougher-cleaner (Circuit 2) and rougher-scavenger (Circuit 3) configurations each have efficiencies 1.33 times greater than the single-stage process. Note that the rougher-scavenger-cleaner (Circuit 4) configuration incorporating three stages has an efficiency that is twice that of the single-stage process.

The most common multi-stage spiral circuit used in industry today is the rougher-cleaner configuration (Circuit 5). However, unlike the circuits discussed above, the cleaner spirals are used to treat only the middlings from the rougher spirals. The clean coal streams from both spirals are combined to produce an overall clean product, while both reject streams are discarded. The circuit is normally configured so that no cleaner middlings are produced and no products are recycled. Surprisingly, circuit analysis indicates that this configuration is no more efficient than a single-stage unit. In fact, no improvement in efficiency is obtained even when both the rougher concentrate and middlings streams are passed to the cleaner spirals (Circuit 6). According to circuit analysis, the only configurations inherently capable of improving separation efficiency are those which have product streams that are recycled back to the feed of a previous stage. These recycle streams are shown as the dotted lines in Table 1.1.

Table 1.1 - Theoretical relative separation efficiencies for various circuit configurations.

Circuit	Flow Diagram	Relative Efficiency
(1) Rougher	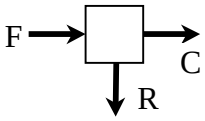	1.00
(2) Rougher Cleaner With Recycle	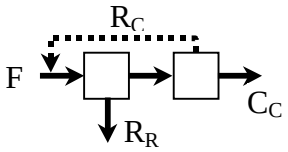	1.33
(3) Rougher Scavenger With Recycle	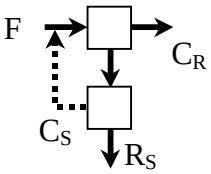	1.33
(4) Rougher Scavenger Cleaner With Recycle	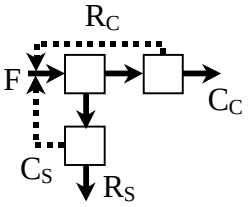	2.00
(5) Rougher Cleaner With Middlings Reclean	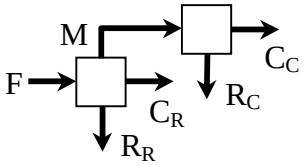	1.00
(6) Rougher Cleaner Without Recycle	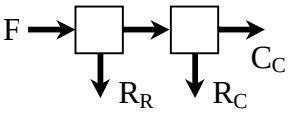	1.00
(7) Rougher Cleaner With Middlings Recycle	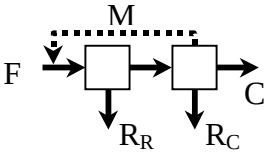	1.22

Note: F=Feed, R=Refuse, C=Clean, M=Middlings (Subscripts: R=Rougher, C=Cleaner)

The results of the linear circuit analyses should not be taken to imply that traditional multi-stage spiral circuits have no value. The primary advantage of these traditional circuits is that they provide an effective means for reducing the specific gravity cut-point (SG_{50}) below that which may be achieved using a single-stage spiral. Furthermore, the "preferred" configurations identified by circuit analysis are not practical for spiral circuits due to large circulating loads and the excessive number of spirals required.

Despite the practical shortcomings of recycle streams, the final configuration (Circuit 7) included in Table 1.1 does appear to merit further study. In this circuit, both the concentrate and middlings products from the rougher unit are passed to the cleaner unit. The clean stream from the cleaner unit is taken as final product, while the cleaner refuse is combined with the rougher refuse and discarded. The middlings stream from the cleaner spiral is recycled back to the head of the rougher unit. As shown in Table 1.1, this configuration is capable of an efficiency that is approximately 1.22 times that of the single-stage circuit. While not as efficient as a "true" rougher-cleaner circuit, this configuration substantially reduces the amount of material that must be recycled. In fact, this configuration was found to be the only practical circuit capable of simultaneously improving separation efficiency while reducing cut-point.

1.3.2 Direct Procedure to Determine Optimum Circuitry

An alternative method exists for investigating these trends not only with respect to efficiency, but also separation cut-point. Consider the popular coal spiral circuit shown in Figure 1.5. In this circuit, only the middling material is rewashed in the secondary spirals.

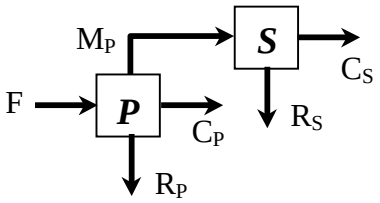

$C = C_P + C_S$
$C_P = F(P_{PC})$
$C_S = M_P(P_{SC})$
$M_P = F(P_{PR}-P_{PC})$

Figure 1.5 - Schematic of middlings reclean circuit.

Similar to the previous section, P_{PC}, P_{PR}, and P_{SC} are the dimensionless probability functions that select particles to report to a given stream. Namely, these are the partition values for the primary spiral clean product, primary spiral refuse product and secondary spiral clean product, respectively. By simple algebraic substitution described above, the overall concentrate-to-feed ratio ($C/F=P_T$) at a given specific gravity for this particular circuit can be represented as:

$$P_T = P_{PC} + P_{SC}\,(P_{PR} - P_{PC}) \qquad [1.10]$$

Once a partition expression is established for a bank of spirals, Equation [1.10] can be easily expanded by utilizing a transition function to depict the separations that occur within a bank or circuit of spirals. A sigmoid equation was used for all of the preliminary calculations, due to its symmetrical representation of an S-shaped partition (Tromp) curve that will not "flatten out" at higher specific gravities. According to the sigmoid model, the partition curve for a density separation may be represented by the following exponential transition function:

$$P = 1/(1+exp\,((SG-SG_{50})/\alpha_s)) \qquad [1.11]$$

where P is the partition factor, α_s is an empirical fitting constant, and $SG\text{-}SG_{50}$ is the specific gravity cut-point of the separation subtracted from the specific gravity of interest. A value of

0.0911 for α_s was found to provide a reasonable fit with experimental data available in the technical literature. By substituting the sigmoid partition function for each of the separations represented in Equation [1.10], the overall partition expression for this circuit now becomes:

$$P_T = 1/(1+exp\ ((SG-SG_{50_{PC}})/\alpha_s))+1/(1+exp\ ((SG-SG_{50_{SC}})/\alpha_s))* \\ [1/(1+exp\ ((SG-SG_{50_{PR}})/\alpha_s))-1/(1+exp\ ((SG-SG_{50_{PC}})/\alpha_s))] \quad [1.12]$$

where $SG_{50_{PC}}$, $SG_{50_{SC}}$, and $SG_{50_{PR}}$ are the specific gravity cut-points for the primary spiral clean coal, secondary spiral clean coal, and the primary spiral refuse products.

An example of partition data for a two-stage, middlings reclean spiral circuit is shown in Figure 1.6. This simulated data depict separations where the clean and refuse splitter positions on the primary spirals are set for specific gravity cuts of a 1.6 and 2.0 SG, respectively. The inner and outer splitter settings on the secondary spirals are set for an SG_{50} of 1.67. The fitting constant (α_s) is 0.0911.

Suppose the specific gravity in question was at a 1.75 SG. By simple substitution into Equation [1.12], the partition factor for this circuit can be calculated as 0.390. Simply stated, only 39% of the 1.75 SG material is reporting to the clean coal launder. If the overall cut-point of the circuit is needed, then it is only required to sweep through specific gravities until *P* is equal to 0.5. The cut-point for this circuit was found to be 1.715 SG. More importantly, these findings resulted independently of feed washability.

To validate this procedure for directly calculating circuit concentrate-to-feed ratios, circuit partition factors were calculated both directly and through an iterative simulation technique, which utilized feed coal washability. This was completed for the middling rewash circuit described in Figure 1.5. The results can be seen in Table 1.2. For each technique, the

primary clean coal and refuse splitters were set to make separations at 1.65 and 1.95 SG, respectively. The secondary spiral was set to make a separation at a 1.65 SG.

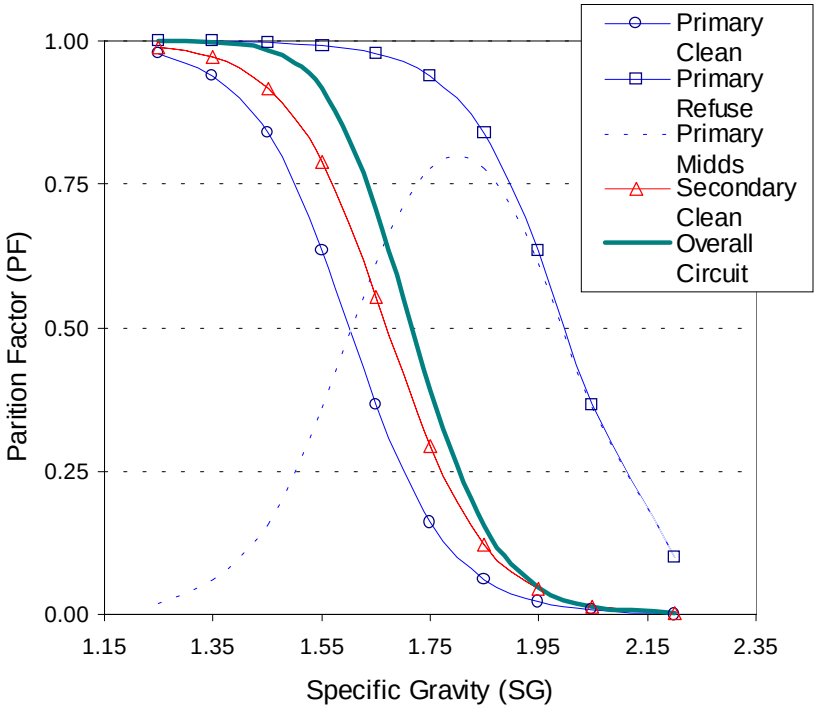

Figure 1.6 – Sigmoid partition data generated for the circuit depicted in Figure 1.5.

Table 1.2 - Comparison of simulated and directly determined partition factors.

Specific Gravity	Circuit 5	
	Direct	Simulation
1.25	0.999	0.999
1.35	0.997	0.997
1.45	0.986	0.986
1.55	0.928	0.928
1.65	0.732	0.732
1.75	0.413	0.413
1.85	0.165	0.165
1.95	0.052	0.052
2.05	0.015	0.015
2.20	0.003	0.003

Clearly, as seen in Table 1.2, this alternative method of determining circuit partition factors is mathematically equivalent to the simulation method which utilized feed coal washability. The consistency of the directly calculated and simulated partition values verifies that for any specific gravity cut-point, a circuit partition value can be calculated. This also indicates that circuit results such as SG_{25}, SG_{50}, and SG_{75} can be ascertained by simply varying the specific gravity of interest (SG in Equation [1.12]) until the indicated partition value equals 0.25, 0.50, and 0.75, respectively. More importantly, the Ecart Probable Error (*Ep*) and cut-point (SG_{50}) of the entire circuit can be determined completely independent of feed coal washability. Naturally, the results will be more accurate provided that a proper transition function is used.

It becomes obvious that Equation [1.12] would be more useful in the form:

$$SG = f(P, \alpha, SG_{50_{PC}}, SG_{50_{PR}}, SG_{50_{SC}}) \qquad [1.13]$$

where the specific gravity of interest is a function of the circuit partition factor (P), the fitting constant (α), and the specific gravity cut-points for the primary and secondary spirals, as indicated by splitter position. Unfortunately, the complexity of the ensuing mathematical expressions prevented accomplishment of this task.

Mathematica, a powerful mathematical software package, was utilized in an effort to achieve this goal. In order to derive an equation for the specific gravity of interest, the term *SG* had to be separated from the other variables present in the partition expression (i.e., *P* and α). Mathematica had great difficulty in completing this task, and was only able to successfully calculate an equation for one of the circuits discussed above. Unfortunately, the form of the exponential expressions constrained Mathematica to solve for *SG* using inverse functions. This

made solutions nearly impossible to obtain. On the occasion that Mathematica was successful in deriving an expression for *SG* as a function of the remaining variables (i.e., splitter position), the solution was not unique, and its sheer length made it impractical to use. Some calculated solutions reached several pages in length. Discussions with several mathematical authorities confirmed that a practical solution, unique or otherwise, was not possible.

1.3.2.1 Reid Equation

The sigmoid and Lynch-Rao (1975) partition functions were utilized throughout the preliminary calculations and concept validation to represent density-based separations. However, a more suitable partition model was needed to accurately depict spiral separations that, when represented as Tromp curves, tend to be asymmetrical and "flatten out" at higher specific gravity cut-points. A partition model developed by Reid (1971) was found to provide a reasonably good fit to experimental data available in the technical literature. This exponential transition function is given by:

$$C/F_{Reid} = P_{Reid} = \exp\{\ln(0.5)(SG/SG_{50})^{m}\} \qquad [1.14]$$

in which *m* is an empirical fitting constant.

The Reid transition function is plotted adjacent to actual plant data in Figure 1.7. It should be noted that the normalized data could not be well fit using either the sigmoid transition function, or the Lynch-Rao (1975) expression. This is due to the inability of the symmetrical Lynch-Rao or sigmoid models to fit asymmetrical partition data.

Using the Reid partition function, Equation [1.12] (expression for the circuit shown in Figure 1.5) can now be rewritten as:

$$P_T = (\exp(\ln(0.5)(SG/SG_{50_{PC}})^m)) + (\exp(\ln(0.5)(SG/SG_{50_{SC}})^m))*$$
$$[\exp(\ln(0.5)(SG/SG_{50_{PR}})^m) - \exp(\ln(0.5)(SG/SG_{50_{PC}})^m)] \quad [1.15]$$

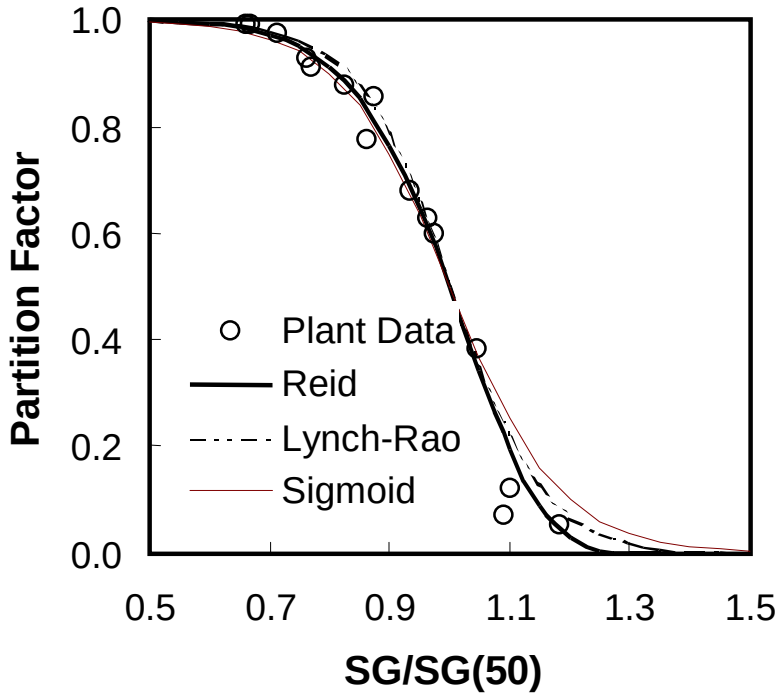

Figure 1.7 - Normalized partition data for determining best fit.

1.3.2.2 Circuit Comparison and Optimization

Water-based separators such as spirals tend to be much less efficient than dense medium devices. It is also common for single-stage spirals to suffer from high concentrate ash values due to an inherently high specific gravity cut-point. To overcome these problems, spirals are often used in two-stage circuits in which the clean coal and/or middling streams from primary spirals are rewashed using secondary spirals. Typical examples of these circuits are shown in Figures

1.8(a) and 1.8(b). When operating these two-stage circuits, plant operators must decide whether to discard the secondary middlings and sacrifice yield, or retain the middlings and accept a lower clean coal quality. The theoretical studies conducted earlier utilizing linear circuit analysis suggest that a third alternative exists for handling the middlings stream. This option involves the use of a primary-secondary spiral configuration in which the middlings from the secondary spirals are recycled back to the feed of the primary spirals. Figures 1.9(a) and 1.9(b) provide illustrations of these particular configurations.

Table 1.3 highlights key differences between these four circuits. In the case of the *traditional* circuit (Figure 1.8(a)), the secondary spirals are used to treat only the middlings product from the primary spirals. The clean coal streams from both the primary and secondary spirals are combined to produce a total clean product, while both the primary and secondary reject streams are discarded. The *traditional* circuit is normally configured so that the secondary middlings are sent to the reject stream, although it may also be diverted into the clean coal product if the quality is acceptable. The *modified traditional* circuit (Figure 1.8(b)) is similar to this configuration except that the primary clean coal is also rewashed with the primary middlings using the secondary spirals. The *modified traditional* circuit does require more secondary spirals than the *traditional* circuit, but may prove beneficial if significant amounts of high ash material are misplaced into the total clean coal product by the primary spirals. The circuits that incorporate middling recycle streams (Figures 1.9(a) and 1.9(b)) are essentially identical to the *traditional* and *modified traditional* circuits except that the secondary middlings are passed back to the primary spiral feed.

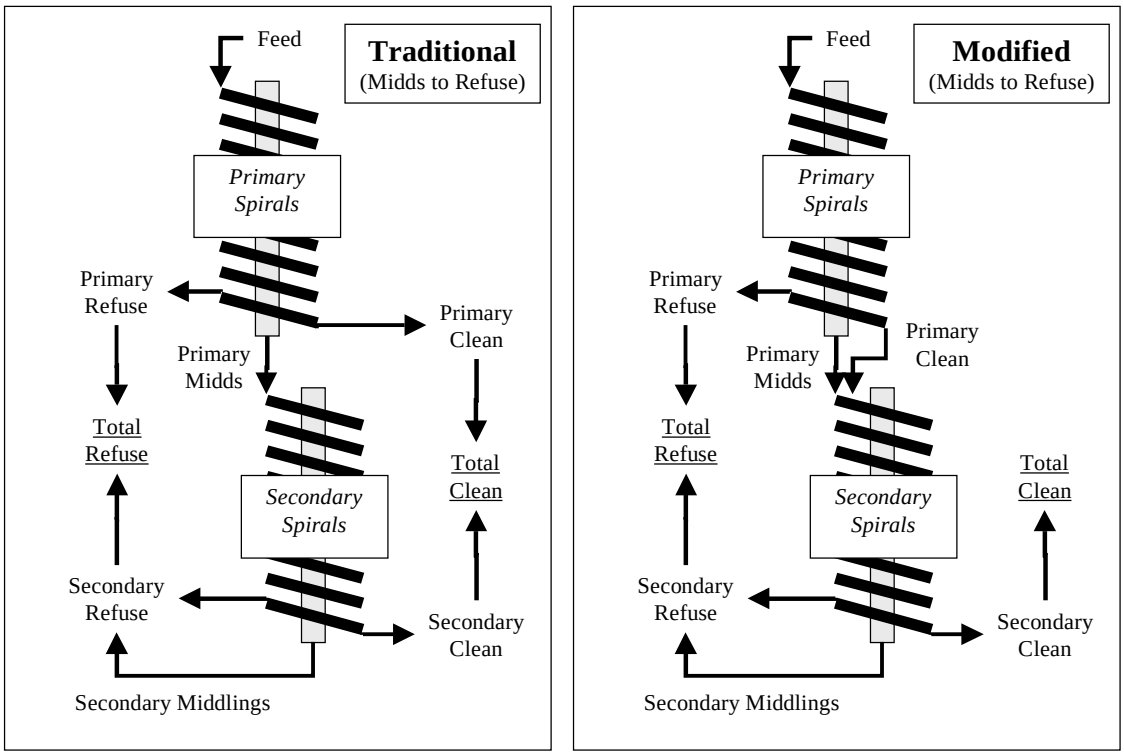

Figure 1.8 - Traditional (a) and modified traditional (b) spiral circuits without recycle.

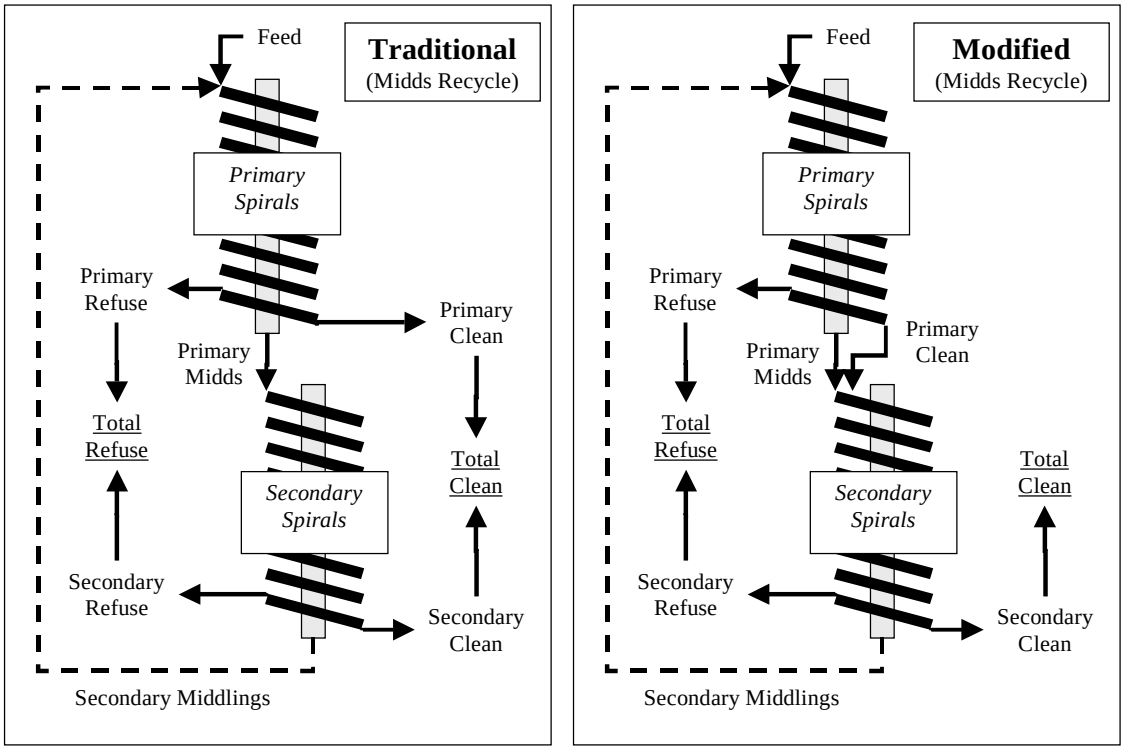

Figure 1.9 - Traditional (a) and modified traditional (b) spiral circuits with recycle.

Table 1.3 - Description of two-stage spiral circuits.

Figure	Circuit Configuration	Primary Clean	Secondary Middlings
1.8(a)	Traditional	To Clean	To Refuse (or Clean)
1.8(b)	Modified Traditional	To Secondary	To Refuse (or Clean)
1.9(a)	Traditional (with Recycle)	To Clean	To Feed
1.9(b)	Modified Traditional (with Recycle)	To Secondary	To Feed

In order to quantify the improvements gained by utilizing recycle streams, these four "popular" coal spiral circuits described above were investigated using the direct method of determining circuit partition values, as described in the previous sections. These circuits were compared in terms of overall specific gravity cut-point and separation efficiency as defined by *Ep*. Microsoft Excel, which can readily solve iterative problems, was used to carry out the comparisons in a spreadsheet based format. For each test, the primary and secondary spiral clean and refuse cut-points were varied for all SG_{50} combinations between 1.6 and 2.0 SG, inclusive. Although specific gravity cut-points approaching 1.6 SG are considerably difficult if not impossible to obtain for a given spiral in a typical operation, the theoretical results yield important insights.

To simulate a circuit with no recycle streams, the clean and refuse specific gravity cut-points for the secondary spiral ($SG_{50_{SC}}$ and $SG_{50_{SR}}$, respectively) were held equal. Because both cut-points were the same, no middlings product was created. In contrast, to simulate a recycle stream, the cut-points of the secondary unit were allowed to vary, where $SG_{50_{SC}} \leq SG_{50_{SR}}$. For each variation and circuit, the SG_{50} and *Ep* were recorded and plotted. Figures 1.10(a) and 1.10(b) show a typical example of results that were obtained for the circuit shown in Figure

1.9(b). This circuit is equivalent to Circuit 7 in Table 1.1, which incorporates both rewashing the clean and middlings stream in a secondary spiral and a recycle stream.

Figure 1.10(a) indicates that the separation efficiency for Circuit 7 is maximized when the circulating load is highest, thus giving the recycle material a higher probability of reaching the correct streams as determined by the feed washability. Allowing the primary spiral reject splitters to cut at a high specific gravity allows more material to be recleaned in the secondary spirals. Consequently, the circulating load is then maximized when the secondary spiral clean coal splitters are set to cut at the lowest specific gravity possible. The lowest specific gravity cut-point for the circuit also occurs when the secondary spiral clean coal splitters are set for a low cut-point (Figure 1.10(b)). However, unlike *Ep*, the circuit SG_{50} rises as the circulating load is increased. A higher circulating load increases the probability (through multiple passes) that middling material will now reach the clean coal streams, thereby increasing the circuit SG_{50}.

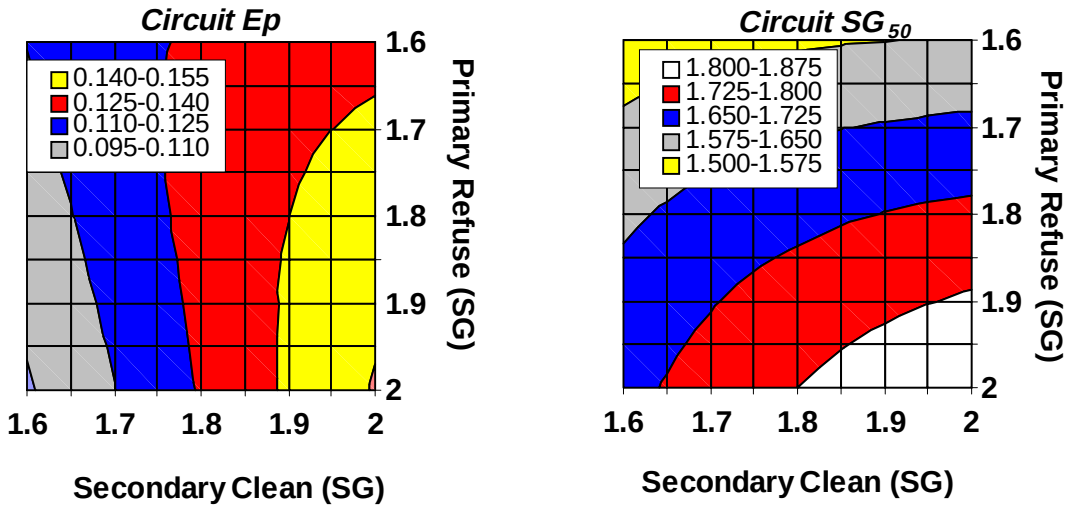

Figure 1.10 - Circuit efficiency (a) and SG_{50} (b) results for varying splitter positions.

The resultant charts for the circuits seen in Figures 1.8(a), 1.8(b), and 1.9(a) were also completed, but are not shown here. Instead, for comparison purposes, the lowest possible specific gravity cut-points and peak efficiencies for each circuit are shown in Table 1.4. It must be noted that optimization of splitter positions is necessary since the splitter positions that yield the lowest possible circuit cut-point do not necessarily maximize efficiency (i.e., minimize *Ep*). In other words, the results in Table 1.4 are independent of one another. For example, the *modified traditional* circuit with recycle is capable of achieving a minimum specific gravity cut-point of 1.53. This circuit is also capable of maintaining a minimum *Ep* of 0.094. However, these two results are generally not obtainable at the same primary refuse and secondary clean coal splitter positions.

Table 1.4 - Circuit comparisons for *Ep* and SG_{50} using the Reid partition model.

Circuit Figure	Circuit Label	Description	Min. SG_{50}	Min. Ep
1.8(a)	Traditional	Middling Rewash	1.60	0.105
1.8(b)	Modified Traditional	Clean & Midds Rewash	1.48	0.128
1.9(a)	Traditional w/Recycle	Middling Rewash w/Recycle	1.76	0.086
1.9(b)	Modified Traditional w/Recycle	Clean & Midds Rewash w/Recycle	1.53	0.094

The results recorded in Table 1.4 indicate several findings. Incorporating a recycle stream raises the maximum possible efficiency of a circuit by increasing the probability that the material being treated will report to the correct streams. By adding a recycle stream to the circuit shown in Figure 1.8(a), the *Ep* dropped from 0.105 to 0.086. By adding a recycle stream to the circuit shown in Figure 1.9(a), the *Ep* dropped from 0.128 to 0.094. These results are indicative of efficiency increases of approximately 18% and 26%, respectively. However, by adding a

recycle stream, the lowest possible specific gravity cut-point of the circuit will rise slightly due to the multiple passes of middling material in the circulating load that will now report to the concentrate.

According to linear circuit analysis, the efficiencies of the *traditional* and *modified traditional* circuits (Figures 1.8(a) and 1.8(b), respectively) should be relatively equal. However, these results indicate that the *modified traditional* circuit has a slightly lower maximum efficiency than the *traditional* circuit. This is most likely due to the increased loading of near gravity material on the secondary spiral that is more difficult to treat. Nevertheless, allowing more material to pass from the primary spiral to the secondary spiral for recleaning lowers the minimum circuit SG_{50} dramatically. For example, without any recycle streams, recleaning the concentrate and middlings (Figure 1.8(b)) from the primary unit lowered the SG_{50} of the circuit from 1.60 to 1.48 SG when compared to exclusively recleaning the middlings material (Figure 1.8(a)). This same finding holds true when recycle streams are utilized, as seen in comparing circuits shown in Figures 1.9(a) and 1.9(b). For these circuits, sending the concentrate and middlings material to the secondary spiral units yields a potential SG_{50} reduction of 23 SG points (i.e., a cut-point of 1.76 versus 1.53).

Though there are advantages to the recycle configurations that incorporate exclusive rewashing of the middlings from the primary spirals, the greatest advantage comes from utilizing recycle configurations that rewash both the concentrate and middlings from the primary spirals. These configurations lower the *Ep*, but more importantly lower the specific gravity cut-point of the entire spiral circuit. By bringing the normally high spiral circuit SG_{50} closer to the cut-points found in the plant circuits that treat coarser material at greater tonnages, plant yields and

efficiencies become maximized. In addition, the gravities in the more efficient dense medium circuits can now be incrementally raised resulting in an increase in total plant yield.

1.4 Circuit Testing

1.4.1 Site Description

The Winoc preparation plant located in southern West Virginia was identified as an ideal site for the installation of a prototype test circuit for the proposed rougher-cleaner spirals with middlings recycle. The feed coals treated at this plant contain a relatively high proportion of middlings that tend to make small improvements in efficiency highly profitable.

The plant flowsheet for the spiral circuit is shown in Figure 1.11. The circuit is fed 1 mm x 100 mesh material from a bank of 38 cm (15-inch) classifying cyclones. Cyclone underflow travels to a distributor that overflows into six sets of triple-start MDL-4 spirals. The clean coal and middlings streams from the rougher spirals flow by gravity into a cleaner feed sump. This material is then pumped up to a second distributor that feeds six sets of triple-start MDL-4 spirals located on the next floor. The clean coal from the cleaner spirals are taken as final product, while the reject streams from both the rougher and cleaner spirals are discarded. The cleaner middlings are allowed to flow by gravity back to the feed of the rougher spiral bank.

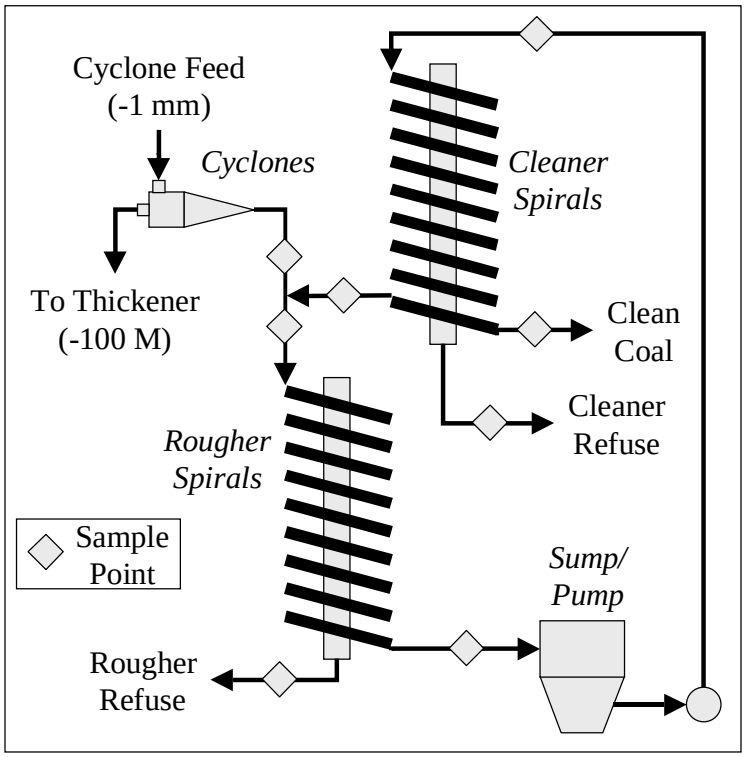

Figure 1.11 – Winoc coal preparation plant rougher-cleaner spiral circuit.

1.4.2 Test Program

Three separate sets of detailed tests were performed to evaluate the circuit. The first run (Test #1) involved the sampling of the complete rougher-cleaner circuit with partial recycle. In the second run (Test #2), the splitters on the cleaner spiral were adjusted so as to produce no middlings stream. The results obtained from this test run would be similar to those obtained from the widely used *traditional* rougher-spiral circuit. Finally, a third test run (Test #3) was performed under the same conditions as the second test run, but at a significantly reduced plant feed rate. It is well known that reducing the feed tonnage can significantly reduce the SG cut-point for spirals (Mikhail *et al*., 1988). Therefore, data from the third run was used to determine whether the SG cut-point could be more effectively reduced using (i) rougher spirals in series

with cleaner spirals or (ii) the same total number of spirals in parallel. The operating conditions for the three test runs are summarized in Tables 1.5 and 1.6.

Table 1.5 - Circuit feed rates used during spiral testing.

Run	Rougher tonne/hr (ton/hr)	Cleaner tonne/hr (ton/hr)	Middlings tonne/hr (ton/hr)
Test #1	58.9 (64.9)	40.2 (44.3)	3.9 (4.3)
Test #2	56.0 (61.7)	40.7 (44.8)	---
Test #3	30.6 (33.7)	21.0 (23.1)	---

Table 1.6 - Splitter settings used during spiral testing.

Run	Rougher Outer, cm (inch)	Cleaner Outer, cm (inch)	Cleaner Inner, cm (inch)
Test #1	27.9 (11)	34.3 (13.5)	26.7 (10.5)
Test #2	27.9 (11)	22.2 (8.75)	---
Test #3	27.9 (11)	22.2 (8.75)	---

The test program generated 22 total samples (i.e., 8 samples for Test #1 and 7 samples each for Tests #2 and #3). The diamond symbols shown in Figure 1.11 indicate the locations of the sampling points. Each sample was sized at 16 mesh and 100 mesh. The 16 x 100 mesh fraction was subjected to float-sink analysis to produce float 1.4, 1.4 x 1.6, 1.6 x 1.8, 1.8 x 2.0 and sink 2.0 gravity classes. Each class was analyzed for ash and sulfur content. The data were then analyzed using a mass-balance program to ensure that the results were reliable and self-consistent.

1.4.3 Experimental Results

Data from each test was collected and used to construct partition curves for each spiral configuration. The partition curves for Tests #1, #2, and #3 can be seen plotted in Figures 1.12, 1.13, and 1.14, respectively. Partition curves were constructed for the rougher, cleaner and combined circuit performance in each test case. The data presented in these figures indicate that the rougher bank of spirals for each configuration consistently operated at a higher cut-point than the corresponding cleaner bank of spirals. This dissimilarity was less pronounced in Test #3, where a significantly lower feed rate was utilized. This outcome is a direct result of the corresponding decrease in volumetric feed flow rate. A lower volumetric feed flow rate decreases the effect of the centrifugal force exerted on the slurry particles, resulting in a lower percentage of material reporting to the clean coal launder. This lower recovery reflects a lower cut-point.

Figures 1.12, 1.13, and 1.14 also illustrate that the overall efficiency of test circuit #1 is superior to that of test circuit #2. This is seen when comparing the relative steepness (*Ep*) of each of the corresponding combined circuit partition curves. It also appears that the overall efficiency of test circuit #3 was relatively high in comparison to both test circuit #1 and #2. Unfortunately, twice as many spirals would be required to obtain this efficiency since Test #3 was conducted at a feed rate half of that utilized in Test #1 or #2.

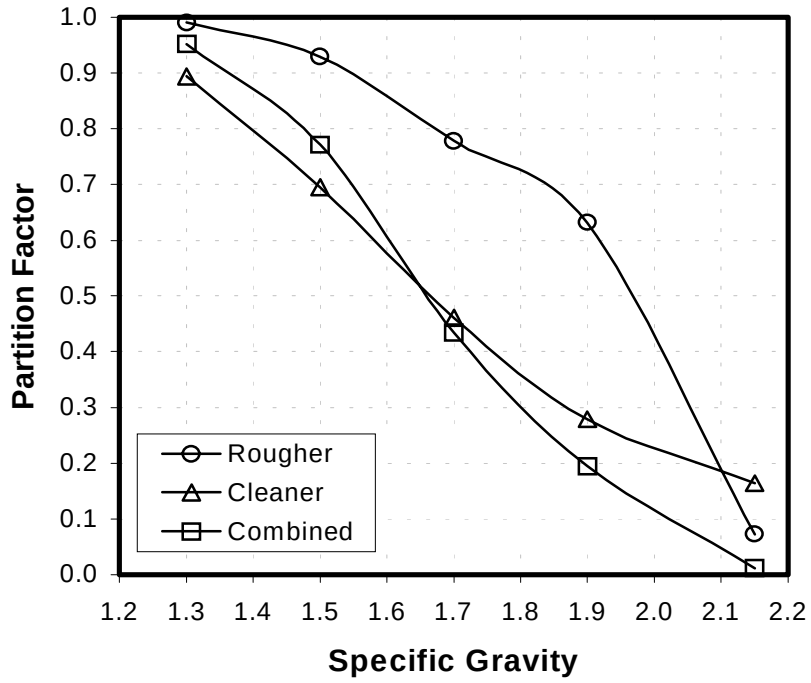

Figure 1.12 – Test #1 experimental partition data.

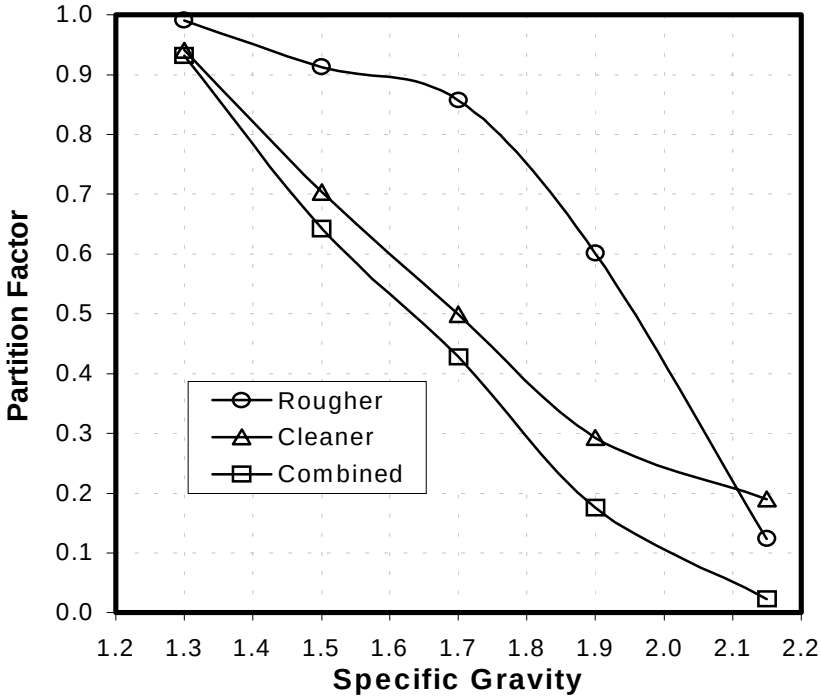

Figure 1.13 – Test #2 experimental partition data.

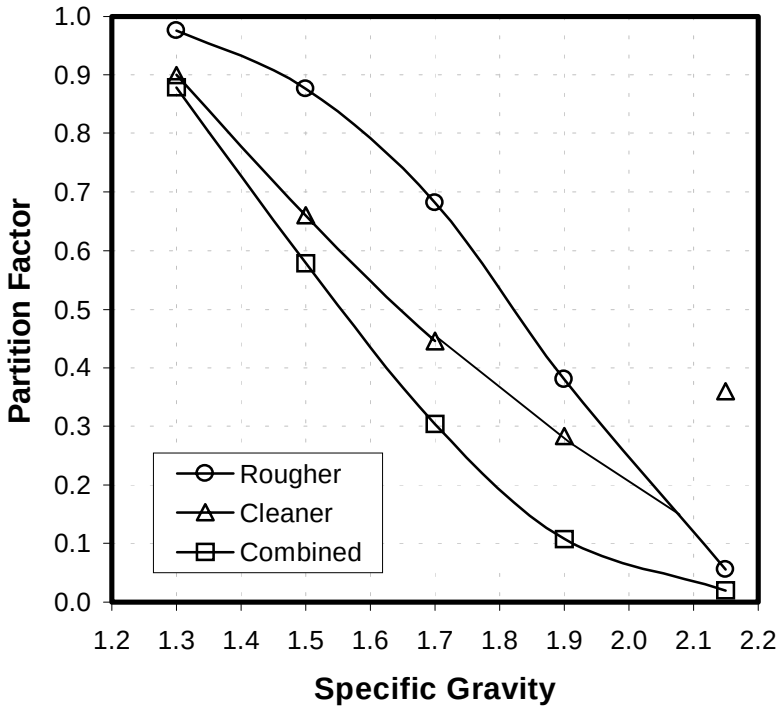

Figure 1.14 – Test #3 experimental partition data.

Tables 1.7 and 1.8 summarize the performance data seen in Figures 1.12, 1.13, and 1.14. The key comparisons are highlighted as bold numbers for each case. The data shown in the first column of Table 1.7 indicate that a reduction in feed rate (Test #3) reduced the SG_{50} for the rougher spirals from 1.95-1.97 down to 1.82. However, this cut-point was still considerably higher than the 1.63-1.65 SG values obtained using the rougher-cleaner circuits (Tests #1 and #2). It was possible to achieve SG_{50} of 1.55 for Test #3, but only at half of the feed rate (or with twice the number of spirals) used in Tests #1 and #2. These results demonstrate that a greater reduction in SG_{50} cut-point can be achieved with a rougher-cleaner circuit than with a single-stage circuit. Rougher-cleaner circuits are highly recommended for this reason.

Table 1.7 - SG_{50} values obtained from the spiral tests.

Run	Rougher	Cleaner	Overall
Test #1	1.97	1.66	**1.65**
Test #2	1.95	1.70	**1.63**
Test #3	**1.82**	1.65	1.55

Table 1.8 - *Ep* values obtained from the spiral tests.

Run	Rougher	Cleaner	Overall
Test #1	0.16	0.25	**0.16**
Test #2	0.15	0.25	**0.20**
Test #3	**0.17**	0.25	0.18

Table 1.8 shows that the *Ep* values for the rougher spirals remained relatively constant at about 0.16 $\pm$ 0.01. The *Ep* values were even more consistent for the cleaner spirals, although a worse *Ep* (i.e., *Ep*=0.25) was obtained. This suggests that the greater loading of near-gravity material adversely impacted the shape of the partition curve for the cleaner spirals. As a result, the overall *Ep* values for the traditional rougher-cleaner spiral circuit (Test #2) are worse than those obtained using single-stage spirals. Thus, a portion of the gain achieved by reducing the cut-point is lost as a result of the lower overall circuit efficiency. On the other hand, data from the modified rougher-cleaner circuit (Test #1) suggests that good efficiencies (i.e., *Ep*=0.16) can be maintained through the use of a middlings recycle stream. It is also worth noting that the ratio of the *Ep* values for Tests #1 and #2 is 1.25 (i.e., 0.20/0.16). This value is close to the theoretical ratio of 1.22 predicted by circuit analysis.

1.5 Circuit Simulations

Natural variations in the washabilities of the feed coal made it difficult to calculate the exact improvement offered by the new rougher-cleaner circuit. To overcome this limitation, a series of partition model simulations were conducted using a fixed set of "typical" washability data for the plant. This was accomplished by developing regression equations for the experimental partition curves obtained in each of the three test runs.

To properly simulate both the rougher and cleaner circuits, two different fitting expressions were required. The most adequate fitting expressions are shown as bold lines in Figures 1.15 and 1.16 for both the rougher and cleaner circuits, respectively. For the rougher spiral, the "best fit" to the rougher partition factor (P_R) was obtained using the transition function advocated by Reid (1971):

$$P_R = \exp\{-0.693\ (SG/SG_{50})^m\} \qquad [1.16]$$

in which *m* is an empirical fitting constant.

Shown in Figure 1.15 is the plant data for the rougher spiral circuit. Also shown are the "best-fit" curves for the Reid (1971) and popular Lynch-Rao (1975) equations. The rougher spiral circuit data tended to be asymmetrical. In a spiral separation, material at a lower specific gravity is efficiently partitioned to the clean coal launder; however, the slightly raised tail is an indication of how spirals tend to misplace coarse, high density material to the clean coal product stream. Since the Lynch-Rao equation is a symmetrical transition function, it did not fit the data well.

Unlike the rougher spiral circuit, the Reid (1971) equation was not an adequate fitting expression for the cleaner spiral circuit (See Figure 1.16). In this circuit, the increased amount of

near-gravity material caused an even higher lift in tail of the partition data. The near-gravity material present in the cleaner spiral circuit makes an efficient separation more difficult to obtain as evidenced by the "flatter" partition data of the cleaner spiral circuit in comparison to the rougher spiral circuit.

For the cleaner spiral, a modified version of the Reid expression had to be developed in order to obtain the "best fit" to the cleaner partition factor (P_C), , i.e.:

$$P_C = 1- \exp\{-0.693 / (SG/SG_{50})^n\} \qquad [1.17]$$

in which *n* is an empirical fitting constant. Equation [1.17] is plotted along with actual plant data in Figure 1.16. Both the Reid (1971) and Lynch-Rao (1975) equations are also plotted. It can easily be seen that neither the Lynch-Rao nor the Reid equation adequately fit the data for the cleaner spiral circuit. The modified Reid expression permits the low gravity portion of the partition curve to remain relatively steep, while allowing the tail of the partition curve to lift. Consequently, this equation accurately predicts how a coal spiral will misplace an increased amount of high gravity and/or middling particles when treating a feed material of a tight specific gravity range.

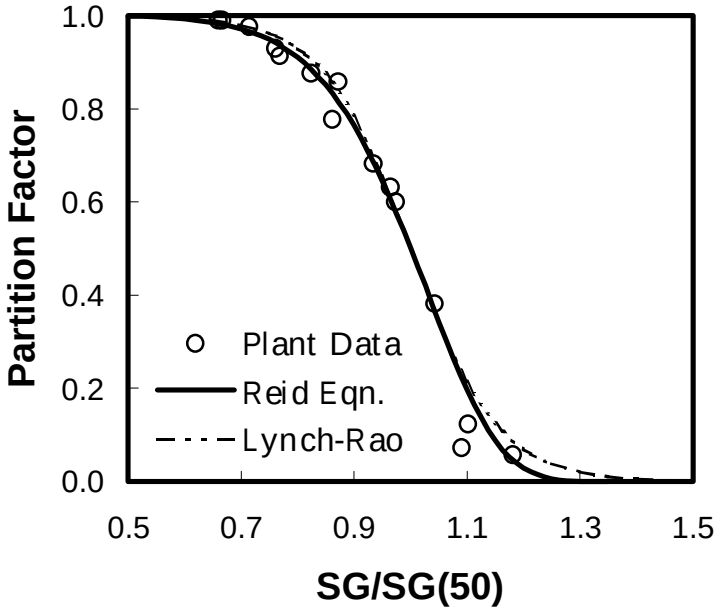

Figure 1.15 - Normalized partition curve obtained using the data from the rougher spirals.

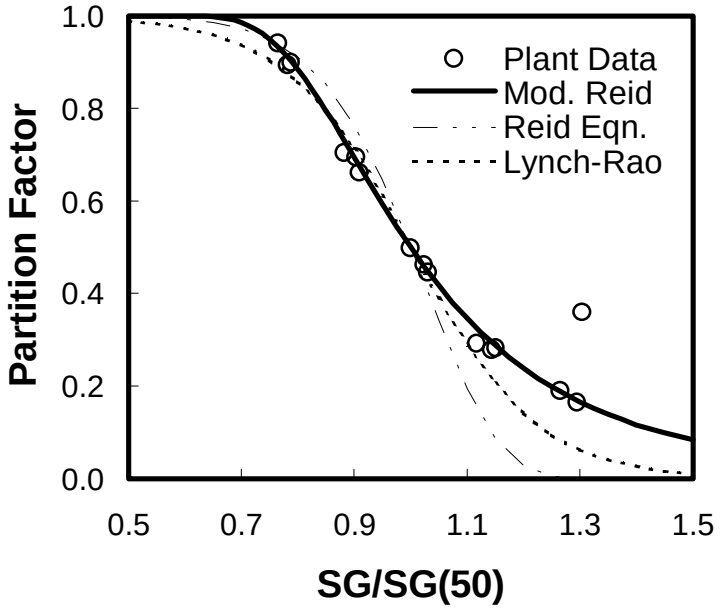

Figure 1.16 - Normalized partition curve obtained using the data from the cleaner spirals.

Circuit simulations were performed for each of the three test runs using partition factors obtained from Equations [1.16] and [1.17]. The experimental feed washability data obtained during Test #2 was used in all of the simulations. Two sets of simulations were conducted. In the first set, clean coal yield and ash was calculated using the actual SG cut-points from the experimental runs. In the second set, the SG cut-points were adjusted slightly so that a consistent product ash of 11.75% was obtained. The simulation results are summarized in Table 1.9.

Table 1.9 - Summary of simulation results.

Simulated Circuit	Yield (%)	Ash (%)	Ep	Organic Efficiency
Using Actual Cut-Points:				
Test #1	59.47	11.87	0.15	92.8
Test #2	55.27	11.66	0.19	86.2
Test #3	62.30	13.08	0.17	79.2
Using Adjusted Cut-Points:				
Test #1	59.27	11.75	0.15	92.5
Test #2	55.40	11.75	0.18	86.4
Test #3	---	---	---	---

The simulation results conducted using actual plant cut-points indicate that the rougher-cleaner circuit with middlings recycle would produce a 59.47% yield at 11.87% ash. This result compares favorably to the 55.27% yield and 11.66% ash that would be obtained using the rougher-cleaner without recycle. In contrast, the simulation of Test #3 for the rougher spiral circuit only (with no recleaning stages) operated under actual plant cut-points produced the highest yield of 62.30%, but at a relatively high ash of 13.08%. Although the organic

efficiencies for these simulation runs have been reported in Table 1.9, these values cannot be directly compared because of the variations in clean coal ash content.

In order to improve the comparisons, a second set of simulations was conducted in which the cut-points for the rougher spirals were adjusted so that a constant clean coal ash of 11.75% was obtained in each case. Unfortunately, it was not possible to achieve an ash value this low for the rougher spiral circuit only (Test #3) since it would require a substantial adjustment to the SG cut-point to a value below that which is realistically achievable. On the other hand, only minor adjustments to the SG values were necessary to achieve 11.75% ash for the rougher-cleaner configurations. As shown in Table 1.9, the circuit with the middlings recycle (Test #1) produced a yield of 59.27% at an organic efficiency of 92.8% compared to a yield of only 55.40% at an organic efficiency of 86.2% for the circuit with no middlings recycle (Test #2). This represents a yield increase of 3.87% at the same ash content. For a typical 3-shift operation with a circuit feed rate of about 40 tonne/hr (44 ton/hr), this represents a revenue increase of approximately $255,000 annually (i.e., 44 ton/hr x 3.87% x $25/ton x 6000 hr/yr = $255,000). Preliminary economic analyses show that this additional revenue would offer an attractive payback on the capital investment required to purchase additional spirals.

Finally, a few comments need to be made regarding the *Ep* values obtained from the simulation runs. According to the circuit analyses conducted in the introductory section of this chapter, the rougher-cleaner circuit with middlings recycle was expected to be 1.22 times more efficient than the same circuit without a middlings recycle stream. A comparison of the values reported in Table 1.9 for the circuit simulations shows that an *Ep* ratio of 1.20 was achieved (i.e., 0.18 / 0.15 = 1.20). The close agreement between these *Ep* ratios further supports the use of linear circuit analysis as an effective tool for evaluating spiral circuit performance. For

comparison purposes, the resultant partition curves from the simulations of the overall rougher-cleaner circuits are shown in Figure 1.17. The superior performance of the modified circuit is easily observed in this plot.

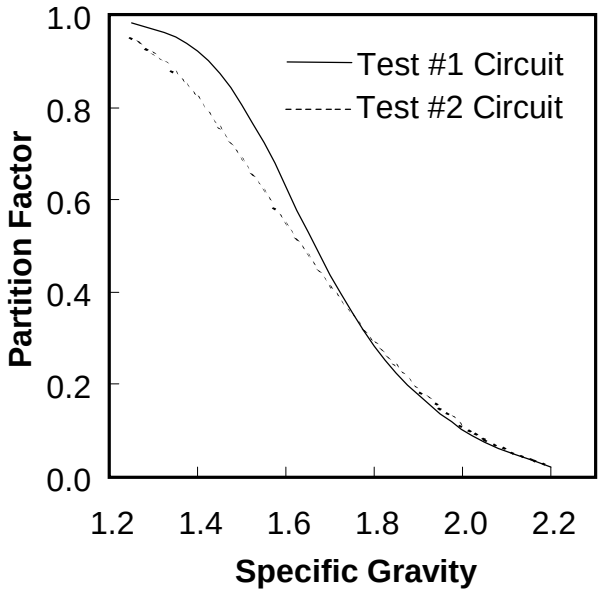

Figure 1.17 - Overall circuit partition curves for the rougher-cleaner spiral circuits with (Test #1 Circuit) and without (Test #2 Circuit) middlings recycle for simulations conducted at constant clean coal ash.

1.6 Conclusions

1. A theoretical study was conducted using linear circuit analysis to evaluate a variety of different multi-stage spiral circuits. The study suggested that a modified rougher-cleaner circuit incorporating a middlings recycle stream offered the best option for improving spiral separation efficiency while maintaining a reasonable circulating load.

2. Linear circuit analysis allowed for the derivation of an alternative method for determining the partition expression of a given spiral circuit without the requirement of a washability based simulation. Moreover and more importantly, the efficiency (*Ep*) and cut-point (SG_{50}), of a given spiral circuit can be calculated independent of washability provided a proper transition function (i.e., Reid, Lynch-Rao, and/or modified Reid expressions) is used to simulate the mineral separation.

3. A two-stage spiral test circuit was installed at the Winoc preparation plant located in southern West Virginia. The test circuit was designed so that a variety of different circuit configurations could be compared under actual plant conditions.

4. For an equivalent number of spirals, the in-plant spiral test data indicate that rougher-cleaner circuits operated in series are superior to parallel circuits for reducing the SG_{50}. This capability is needed so that the spiral circuit cut-point can be brought into line with the cut-points realized in the coarse coal dense medium circuits.

5. Test data was used to develop regression equations that were used to simulate the experimental partition curve data produced during the on-site circuit testing. While a

rougher spiral circuit separation could be simulated using an equation developed by Reid (1971), a new, modified version of this equation was developed to properly simulate cleaner spiral circuits that generally treat large amounts of near-gravity material.

6. The in-plant test results also suggest that the SG_{50} for rougher-cleaner spiral circuits operated with and without a middlings recycle are very similar (i.e., ≈1.65 SG in this case). However, the separation efficiency (as measured by *Ep*) was approximately 1.25 times higher for the circuit incorporating a middlings recycle stream. This ratio compares favorably with the theoretical ratio of 1.22 predicted by linear circuit analysis and a ratio of 1.20 obtained from partition simulations.

7. Preliminary calculations suggest that the rougher-cleaner spiral with middlings recycle is capable of increasing circuit yield by 3.86% at the same ash. For a typical plant, this would represent about $255,000 of additional revenues annually. Economic analyses suggest that this additional revenue would offer an attractive payback on the capital investment.

1.7 References

Chedgy, D.G., Placha, D.S. and Watters, L.A., "Spiral Concentrators for Fine Coal Processing," PCMIA/SME Joint Meeting, Washington, PA, November 1-2, 1990.

Edward, D., Li, M., Davis, J. and Kruitschnitt, J., "Spiral Research: Technique Development and Use," Pittston Coal Management Co., Paper B2, 1998, pp. 100-119.

Holland-Batt, A.B., "Interpretation of Spiral and Sluice Tests," Trans. Instn. Mining and Metallurgy, 1990, Vol. 99, pp. C1-C20.

Holland-Batt, A.B., "A Study of the Potential for Improved Separation of Fine Particles by Use of Rotating Spirals," Minerals Engineering, 1992, Vol. 5, Nos. 10-12, pp. 1099-1112.

Holland-Batt, A.B., "The Effect of Feed Rate on the Performance of Coal Spirals," Coal Preparation, 1994, Vol. 14, pp. 199-222.

Holland-Batt, A.B., "The Dynamics of Sluice and Spiral Separations," Minerals Engineering, 1995, Vol. 8, No. 1/2, pp. 3-21.

Holland-Batt, A.B., "Gravity Separation: A Revitalized Technology," Mining Engineering, 1998, Vol. 50, No. 9, pp. 43-48.

Kapur, P.C. and Meloy, T.P, "Spirals Observed," Inter. J. Mineral Processing, 1998, Vol. 53, pp. 15-28.

Lynch, A.J. and Rao, T.C., "Modeling and Scale-Up of Hydrocyclone Classifiers," Paper No. 9, 11th Inter. Mineral Processing Congress, Cagliari, Italy, April 21-26, 1975.

MacNamara, L., Addison, F., Miles, N.J., Bethell, P. and Davies, P., "The Application of New Configurations of Coal Spirals," Proceedings, 12th International Coal Preparation Conference and Exhibit, Lexington, Kentucky, May 2-4, 1995.

MacNamara, L., Toney T.A., Moorhead, R.G., Miles, N.J., Bethell, P. and Everitt, B., "On Site Testing of the Compound Spiral," Proceedings, 13th International Coal Preparation Conference and Exhibit, Lexington, Kentucky, April 30-May 2, 1996.

Meloy, T.P., "Analysis and Optimization of Mineral Processing and Coal-Cleaning Circuits – Circuit Analysis," Inter. J. Mineral Processing, 1983, Vol. 10, p. 61.

Mikhail, M.W., Salama, A.I.A., Parsons, I.S. and Humeniuk, O.E., "Evaluation and Application of Spirals and Water-Only Cyclones in Cleaning Fine Coal," Coal Preparation, 1988, Vol. 6, pp. 53-78.

Mills, C., "Process Design, Scale-Up and Plant Design for Gravity Concentration," Mineral Processing Plant Design, 1978, AIMME, New York.

Reid, K.J., "Derivation of an Equation for Classifier-Reduced Performance Curves," Technical Note, Canadian Metallurgical Quarterly, 1971, Vol. 10, No. 3, pp. 253-254.

Thompson, J.V. and Welker, M., "The Humphries Companies: Development and Application of Humphreys Spiral Concentrator," Skillings Mining Review, Feb. 24, pp. 4-15.

Walsh, D.E. and Kelly, E.G., "An Investigation of the Performance of a Spiral Using Radioactive Gold Tracers," Minerals and Metallurgical Processing, 1992, Vol. 9, No. 3, pp. 105-109

Weldon, W.S. and MacHunter, R.M.G., "Recent Advances in Coal Spiral Development," SME Annual Meeting, Denver, Colorado, Preprint No. 97-82, Feb. 24-27, 1997.

West, T.W. and Apodaca, L.E., "Cost Effective BTU Recovery by Fine Coal Washing Spirals," 117th Annual AIME Meeting, Proceedings, Phoenix, Arizona, Jan. 25-28, 1988.

Wills, B.A., Mineral Processing Technology, 5th Edition, 1992, pp.430-433.

CHAPTER 2

Improving Performance of Hindered-Bed Separators

2.1 Introduction

Hindered-bed hydraulic separators have been used in mineral processing applications for years. Simply stated, a hindered-bed separator is a vessel in which feed settles against an evenly distributed upward flow of water or other fluidizing medium. Typically, these devices are used for size classification, however, if the feed size distribution is within acceptable limits, hindered-bed separators can be used for the concentration of particles based on differences in density.

A simplified schematic of a typical hindered-bed separator is shown in Figure 2.1. Most hindered-bed separators utilize a downcomer to introduce feed material to the system. This material enters the feed zone and may encounter either free or hindered settling conditions, depending on the concentration of particles in the separator. The settling particles form a fluidized bed (teeter-bed) above the fluidization water injection point. Material is then segregated based on terminal, hindered-settling velocities. Slower settling material reports to the top of the teeter-bed while the faster settling particles descend to the bottom of the teeter-zone. Specifically, low density and fine material reports to the overflow, while coarse and high density material report to the underflow. Particles that settle through the teeter-bed enter a dewatering cone and are discharged through an underflow control valve. The rate of underflow discharge is regulated using a PID control loop.

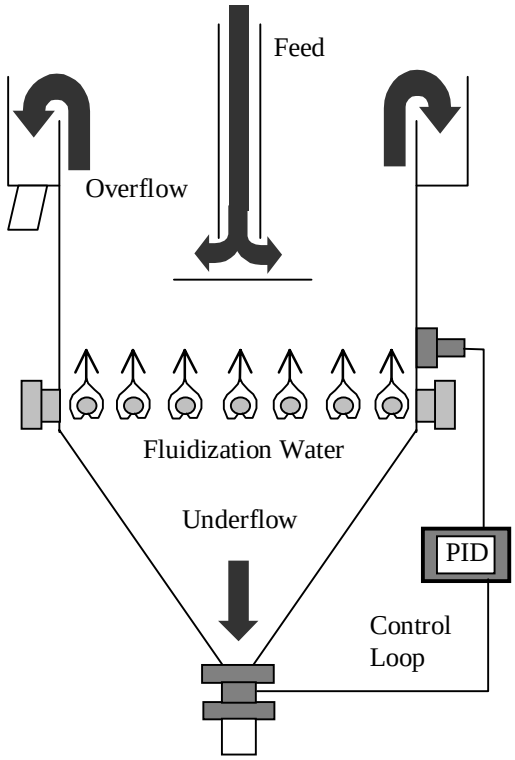

Figure 2.1 - Schematic diagram of a conventional hindered-bed separator.

More recently, a new hindered-bed classifier separator has been developed that utilizes an innovative feed presentation system. This device, which is known as the CrossFlow separator, is shown in Figure 2.2. The CrossFlow utilizes a tangential, low-velocity feed entry system that introduces slurry at the top of the classifier. This approach allows feed water to travel across the top of the unit and report to the overflow launder with minimal disturbance of the fluidization water within the separation chamber. To reduce the velocity of the feed flow, the feed stream enters a side well before flowing into the separation chamber. The feed then overflows into the top of the device. Solids settle into the separation chamber as they travel between the feed entry point and overflow launder. The result of this feed presentation system is the elimination of excess feed water in the separation chamber, which can adversely effect separation efficiency.

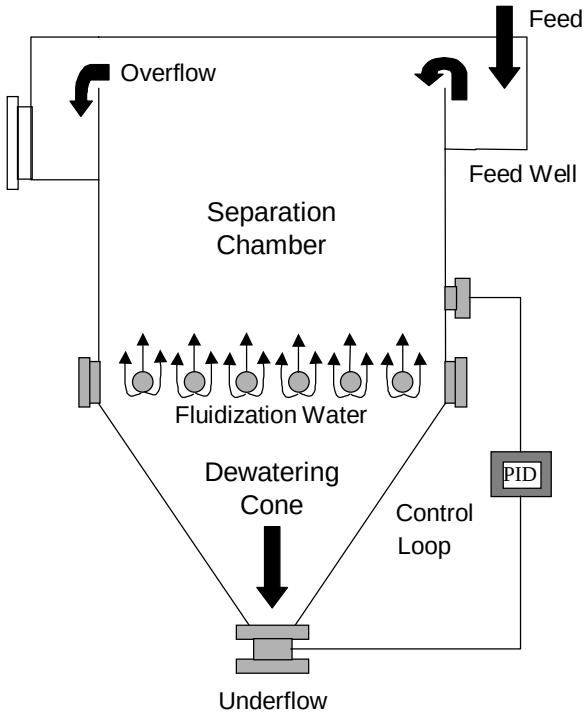

Figure 2.2 - Schematic of CrossFlow hindered-bed separator.

2.2 Literature Review

2.2.1 General

Hydraulic classifiers are primarily categorized by the method in which the coarse material is discharged from the separation zone of the unit (Heiskanen, 1993). The first category is marked by a lack of underflow (or coarse fraction) control. This causes an underflow stream of such high velocity to occur that no fluidized bed forms and no gradation of particles (by size and density) manifests. The second group of hydraulic classifiers is marked by an attempt to control the underflow discharge generally causing the appearance of a teeter-bed. Classifiers can be further subdivided into mechanical or non-mechanical categories. In mechanical classifiers, the underflow discharge is removed via mechanical means. In non-mechanical classifiers, the underflow stream is removed through mass-action and gravity.

The CrossFlow separator is a non-mechanical, hindered-settling, counter-current hydraulic classifier that utilizes a teeter-bed. There are several other classifying devices that fall under this description, including the Floatex fluidized-bed classifier (or Floatex Density Separator) and the allflux® separator. In these classifiers, the underflow rate is restricted and a teeter-column is formed by solids settling against elutriation water (teeter-water) that is fed evenly across the entire cross-section of the unit. Generally, coarse particles are graded in order of decreasing terminal velocity (Heiskanen, 1993), with the coarser particles settling through the teeter-bed, and the finer particles reporting to the overflow. The high interstitial velocities of water traveling between the particles in the teeter-bed ensure that there is little bypass of fines to the underflow. In fact, these types of classifiers often produce very clean underflows (Schwalbach, 1965).

Typically, teeter-bed classifiers are capable of separations as coarse as 800 microns and as fine as 75 microns (Littler, 1986). According to Heiskanen (1993), when the separation is coarser than 800 microns, efficiencies drop dramatically as the separator begins to act as an elutriator. When separations finer than 100 microns are conducted, low capacities become an issue. Solid capacities typically range from 10 to 40 tph/m^2 (0.85-3.40 tph/ft^2) depending on the cut-point of the separation. Generally, as separations become coarser, the solids capacity increases, and the opposite is true for finer separations.

Littler (1986) utilized a Floatex hindered-settling classifier and essentially summarized the effects on classifier performance of operating at different separation cut-points. It is stated that the Floatex separator is considered to be the most advanced commercial separator for hydraulic particle classification and is able to treat material whose size is between what would be considered optimal for either screens (coarse) or hydrocyclones (fine). A schematic of this device can be seen below in Figure 2.3. As shown, mineral slurry is introduced to the teeter chamber through a downcomer. A differential pressure cell and discharge valve controls the bed-level in the unit. According to Littler (1986), there is a discernable drop in efficiency (normally 80-90%) as the nominal mesh of the separation is increased from 140 to 16 mesh (U.S). These results reflect the response of the Floatex separator, however, the same general trend can be found in any hindered-bed classifier.

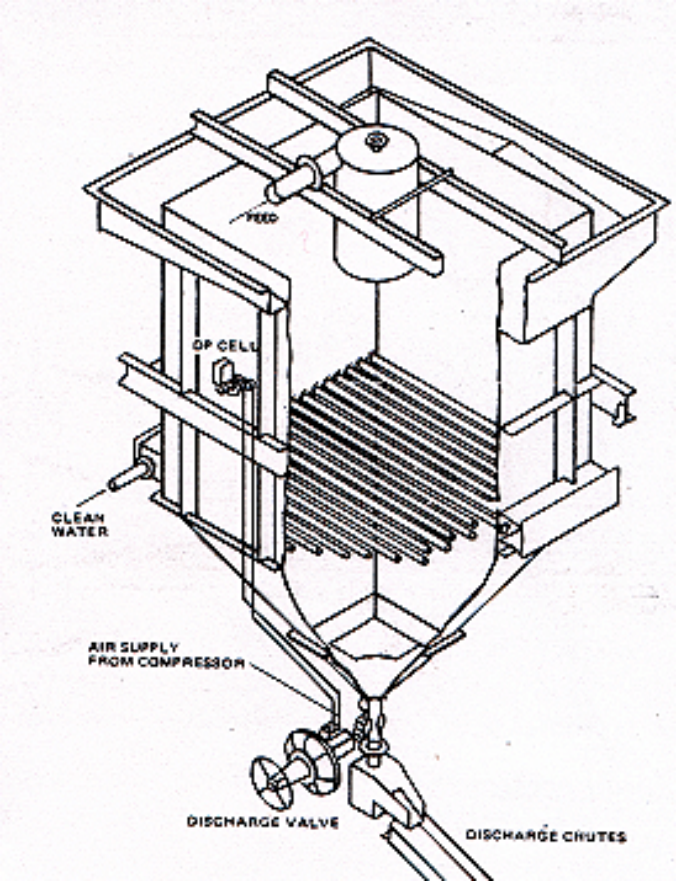

Figure 2.3 – Schematic of Floatex hindered-bed classifier (Littler, 1986).

In Littler's work, efficiency (E) is defined as:

$$E = \frac{O}{F} \times \frac{o - f}{f(100 - f)} \qquad [2.1]$$

where *O* is the separator overflow tonnage (t or %), *F* is the separator feed tonnage (t or %), *o* is the material in the overflow finer than the separation mesh (%), and *f* is the material in the feed finer than the separation mesh (%).

Improving the sharpness of classification has many benefits. The greatest of these benefits is the reduction of misplaced material to the product stream. With less misplacement, more properly sized material (an amount proportional to the total reduction of misplace material), can now report to the product launder. Littler (1986) goes on to state that improved classification can be beneficial to closed-circuit grinding, by reducing circulating load and improving the gradation of material that is treated in other downstream processes (i.e., flotation).

Since the advent of the original hydraulic classifier in 1927 by Fahrenwald (Taggart, 1950), hydraulic separators have been used most extensively in the classification of material based on hindered-settling phenomena. However, it has been shown that these devices can also be effectively applied to gravity separations provided that the size distribution of the feed is within acceptable limits, depending on the application (Heiskanen, 1993). An example of successful density applications using hindered-bed separators can be seen in fine and coarse coal processing, (Reed *et al*., 1995; Honaker, 1996) mineral sands beneficiation (Mankosa *et al*., 1995), and the recycling of chopped wire (Mankosa and Carver, 1995). Wills (1992) considers this gravity concentration component, commonly found in hindered-bed classifiers, an "added increment." According to Bethell (1988), the cleaning efficiency of a teeter-bed separator is limited to a feed size range of 6 to 1 when used as a gravity separation device. This is due to the fact that when treating wider size distributions, coarse, low density material will be misplaced to the underflow due to its net greater sizing effect. In the same way, extremely fine, high density material will report to the overflow irrespective of its overall density. This inherent disadvantage is further discussed in Chapter 3 of this dissertation.

2.2.2 Hindered-Settling

In teeter-bed applications, the free settling rates of particles are greatly reduced. This is in response to the presence of other particles that cause either particle-to-particle collisions and/or "near-misses" (Littler, 1986). As the size of the particle decreases, the reduction in the settling rate of that particle increases. According to Littler (1986), the hindered-settling phenomenon begins to take place at approximately 20% solids by mass. Classification utilizing hindered-settling is an improvement over free-settling classification due to the fact that less fine material can become entrapped by coarse particles that settle more slowly through a teeter-bed. In free-settling applications, coarse material can settle quickly enough to entrain fine particles to the underflow.

According to Zimmel (1983, 1990) five effects occur as the volume fraction of solids (ϕ) in a slurry increases. This includes a decrease in the cross sectional area available for the elutriation fluid (teeter water) which results in an increased net velocity as seen by the settling particles. The apparent viscosity of the pulp is also increased. This increase of apparent specific gravity toward the specific gravity of the particles causes a reduction of gravitational force effects on the individual particles. The last two effects include an increase of wall hindrance and the occurrence of hydrodynamic diffusion.

The apparent slurry viscosity is very important in determining the hindered-settling velocities of particles. When treating a slurry containing particles in the size ranges generally used in mineral processing classification applications, many other factors and variables can also be significant. The most important factors being the volume concentration of solids, particle size and particle shape (Heiskanen, 1993). There are various expressions available in the literature

that describes slurry viscosity. Einstein derived the following equation for apparent viscosity (η):

$$\eta = 1 + 2.5\phi \qquad [2.2]$$

where ϕ is the fraction of solids by volume. Heiskanen and Laapas (1979) and Laapas (1983) later went on to modify this formula with an empirical correction as seen below.

$$\eta = 1 + 2.5\phi + 14.1\phi^2 + 0.00273e^{16.6\phi} \qquad [2.3]$$

Rutgers (1962) derived a simple equation for pulp viscosity in the form of the Arrhenius equation as seen here:

$$\eta = \eta_w \exp(k\phi) \qquad [2.4]$$

where η_w is the viscosity of water or other fluidizing medium. The variable, *k*, is a fitting parameter which has been given values of 5 (John and Goyal, 1975) to 14 (Plitt, 1976). This equation provides values similar to the equations listed above when *k* is approximately 5.

In 1989, Swanson suggested this semi-empirical equation:

$$\eta = \eta_w \frac{2\phi_{max} + \phi}{2(\phi_{max} - \phi)} \qquad [2.5]$$

where ϕ_{max} is the highest fraction of solids by volume obtainable for a specific material. An incredible amount of work was found in the literature on determining this variable, ϕ_{max}. Disappointingly, most of the conclusions have been empirical in nature.

According to Sudduth (1993), many attempts have been made to predict the optimum size distribution for packing material, but little work has been completed on determining the exact value of the attainable maximum fraction of solids (Yu and Standish, 1993). As early as 1930, it was concluded that size ratios of particle components was an extremely important factor in determining the maximum packing of solids (Furnas, 1931; Westman and Hugill, 1930). The most definitive work was completed by McGeary (1961), nevertheless it can be considered empirical in nature, as it requires direct measurement and is only applicable for ideal spherical particle systems. However, in his work, the packed density for monosized spherical particles was approximately 62.5% that of the crystal density of the solid. Sudduth (1993) was able to match the results summarized by McGeary by utilizing the size ratios of the first to n^{th} size fraction of a dry mineral sample in determining the maximum obtainable packing of solids. Sudduth (1993) used an empirical process in choosing the proper value for *n*.

According to Low and Bhattacharya (1984), the determination of ϕ_{max} has been calculated from direct measurements and even graphical estimation. Work in estimating these values was conducted by Lewis and Nielsen (1969) who concluded that the maximum concentration of solids was far more accurately determined in air than in water. Another conclusion demonstrated was that as particles increased in aggregation, the maximum packing of solids decreased. This was a direct result of a lack of sphericity of the particles.

Other methods for determining the maximum concentration of particles include direct measurement through sedimentation (Robinson, 1957) and a least square regression of the experimental data. Essentially, most reliable means of determining ϕ_{max} are empirical in nature.

According to Yu and Standish (1993), the packing density of the system is affected by both the solids volumes as well as their particle size distribution. Yu and Standish (1988, 1991)

further demonstrate that linear models can satisfactorily predict the solids packing with the use of a discrete or simple continuous size distribution. However, recent work by Swanson (1999) in the area of hindered-settling phenomena advocates the determination of the maximum concentration of solids through the direct measurement of teeter-bed expansion when transitioning between a fully settled and fully elutriated state.

In modeling hindered-bed separations, several equations have been developed and utilized for determining the hindered-velocity of a particle (v_t). Masliyah (1979) utilizes the expression:

$$v_t = \frac{gd^2(\rho_s - \rho_f)}{18\eta_f}\alpha_f F(\alpha) \qquad [2.6]$$

where g is the force due to gravity, d is the diameter of the particle, ρ_s is the density of the solids, ρ_f is the density of the fluidizing medium, α_f is the suspension voidage (1-ϕ), and η_f is the viscosity of the fluid. The term $F(\alpha)$ describes a function that accounts for particle concentration. Usually, this function is in the form described by Richardson and Zaki (1954).

The above equation is for a laminar flow regime and can be corrected for non-stokes flow as seen below:

$$v_t = \frac{gd^2(\rho_s - \rho_{susp})}{18\eta_f\left(1+0.15\,\mathrm{Re}^{0.687}\right)}\alpha_f F(\alpha) \qquad [2.7]$$

where ρ_{susp} is the apparent density of the suspension and Re is the Reynolds number (Masliyah, 1979). Reynolds number can be calculated as:

$$Re = \frac{d\rho_f v_t \alpha_f}{\eta_{susp}} \qquad [2.8]$$

where η_{susp} is the apparent viscosity of the suspension.

Richardson and Zaki (1954) define $F(\alpha)$ as $(1-\phi)^{\beta}$ where β is an unknown function of particle size and shape. For transitional flow regimes, normally found in hindered-bed separator applications, β can be determined as seen below:

$$\beta = 4.36\ Re^{-0.03} \qquad \text{for } 0.2 < Re < 1.0 \qquad [2.9]$$

$$\beta = 4.4 / Re^{0.1} \qquad \text{for } 1.0 < Re < 500 \qquad [2.10]$$

Another accepted form of this function for transitional flow regimes comes from Barnea and Mizrahi (1973) where:

$$F(\alpha_f) = \left[1 + (1-\alpha_f)^{1/3} \exp\frac{5(1-\alpha_f)}{3\alpha_f}\right]^{-1} \qquad [2.11]$$

Mondal (1997) lists several other expressions in his work for hindered-settling velocities, including those derived by Steinour (1944) and Concha and Almendra (1979). However, these settling equations are not valid for non-transitional flows. Work has also been conducted by Brauer, *et al*. (1973) that shows the reduced (hindered) settling velocity depends on the free settling velocity of a particle in a narrow size and density class *i*, the particle size, and the distance to any other particle. According to Brauer, *et al*. the hindered settling velocity (v_{hi}) can be calculated as:

$$v_{hi} = v_{oi}\ k_{if}\ k_{ic} \qquad [2.12]$$

where the parameter k_{if} is a fluid counter flow factor which addresses the displacement of water by settling particles. The parameter k_{ic} is another factor that addresses turbulence caused by clusters of settling particles.

Recent population balance models by Mondal (1997) and Swanson (1999) each attempt to accurately simulate hindered-settling. Mondal utilizes the equation set forth by Brauer, *et al*. He was able to show significant upgrading when processing fine coal slurry using a Floatex Density Separator. Swanson, on the other hand, utilized a semi-empirical process that was self-developed and was able to show simulated consistency with 50 sets of test data. Both models demonstrate impressive results.

2.3 Comparative Studies

2.3.1 In-Plant and Laboratory Testing

The CrossFlow concept was originally investigated in the laboratory, by way of a lab-scale separator. The laboratory setup is shown in Figure 2.4. This laboratory test unit was constructed out of Plexiglas and has a cross-sectional area of 8 in^2 (0.005 m^2). The clear nature of the Plexiglas allowed for the optical determination of varying flow regimes and the presence of turbulence. A vibratory feeder was used to provide a constant feed flow rate to the separator. A control loop, consisting of a PID controller, pressure sensor, and underflow pneumatic valve was employed to maintain a constant bed level within the unit. A traditional downcomer could be installed, which would allow this lab-scale unit to operate like a conventional teeter-bed separator.

It was apparent, even at the earliest stages of experimentation, that efficiencies and capacities for applications using teeter-bed separators could be improved with the CrossFlow device. The earliest tests compared the conventional teeter-bed separator against the CrossFlow separator at relatively benign test conditions. These initial investigations were completed using either passing 14 mesh aggregate limestone or phosphate ore. Feed solids rates ranged from 1.0 to 2.3 tph/ft^2 at a feed percent solids of approximately 50%. Figure 2.5 shows the results of these initial comparative tests. For an array of separation cut-points at the solid feed rates described, it can easily be seen that the CrossFlow has a tendency to perform slightly better in terms of separation efficiency. The separation efficiency was defined as either Ecart Probable (Ep) or Imperfection as calculated in Equations [2.13] and [2.14].

$$Ep = \frac{d_{75} - d_{25}}{2} \qquad [2.13]$$

$$I = \frac{Ep}{d_{50}} \qquad [2.14]$$

where d_{75}, d_{50}, and d_{25} represent the size at which 75%, 50%, and 25% of the feed mass, respectively, reports to the underflow of the separator.

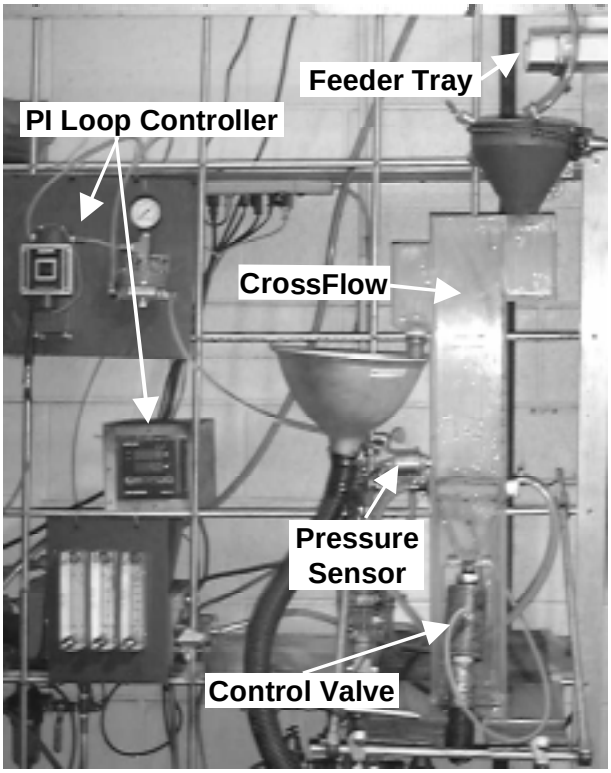

Figure 2.4 – Laboratory-scale CrossFlow separator.

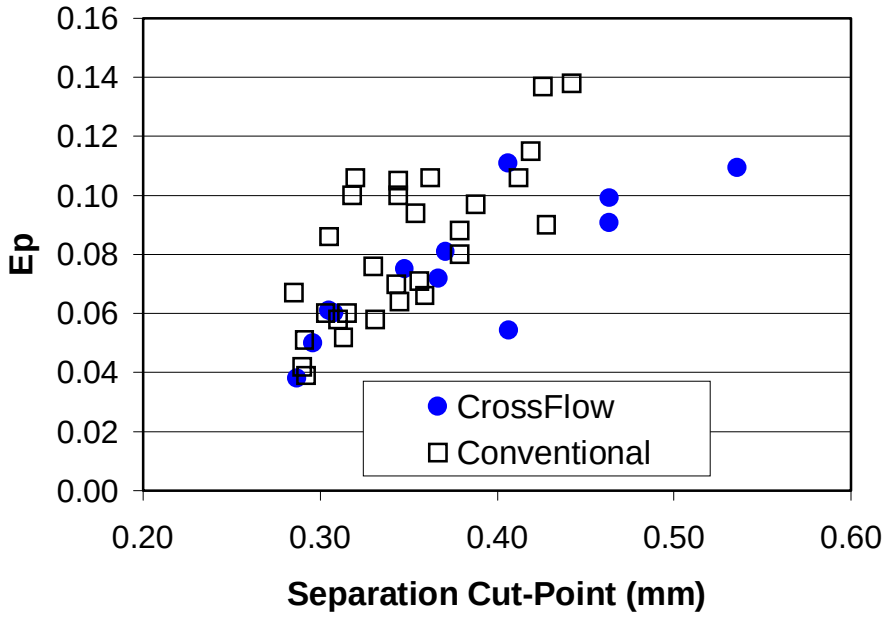

Figure 2.5 - Initial comparative test data.

The results shown in Figure 2.5 are representative of a multitude of random tests where the variables, including feed rate, elutriation water rate, bed-level, and feed percent solids are not necessarily equal. In an effort to fairly compare this data, points where these variables are consistent for both separators are graphed below in Figures 2.6 and 2.7.

Figure 2.6 reveals that for tests where all variables are equal, the CrossFlow separator repeatedly produced classification results higher in efficiency than that realized using a conventional feed system. It is also interesting to note that the separation cut-point is generally greater in the conventional separator tests, as seen in Figure 2.7. These results suggest that less feed water is entering the separation chamber of the CrossFlow unit. In a conventional feed system, the total volume of feed water is introduced directly into the separation chamber, adding velocity to the rising current of elutriation water in the upper portion of the classifier. This increase in velocity can increase the cut-point of the separation.

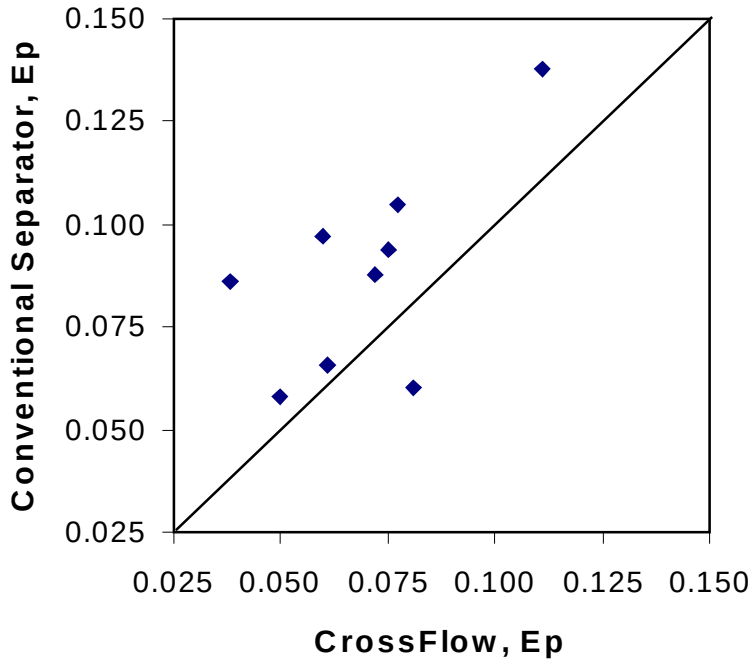

Figure 2.6 - Efficiency comparison of CrossFlow and conventional separators.

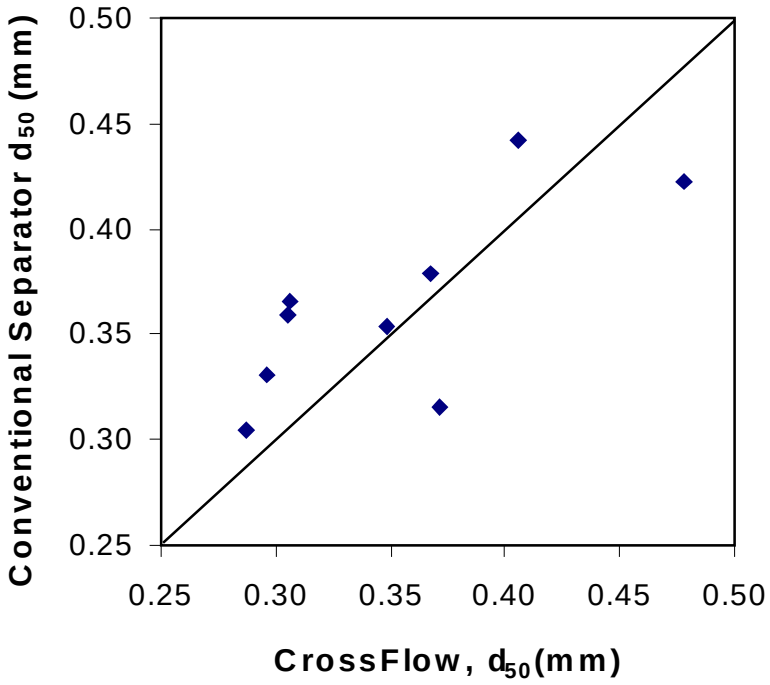

Figure 2.7 - Cut-point comparison of CrossFlow and conventional separators.

Only an incremental improvement in efficiency can be seen at the low feed rates utilized in the initial laboratory tests. Further test work was completed in a north Florida phosphate beneficiation plant where constant high rates of feed solids could be provided. For these tests, a 2 x 2 ft. (0.6 x 0.6 m) CrossFlow unit was constructed out of steel. Like the lab-scale unit, a PID controller coupled with an air-actuated underflow valve and pressure sensor was used to control bed level. In these investigations, the CrossFlow separator was compared to a Krebs Whirlsizer, which had been previously installed at the plant. Both units were fed from a bank of dewatering cyclones. Feed percent solids were highly variable, ranging from 20 to 60%.

Results for this test work can be seen in Figure 2.8. In this figure, efficiency (Imperfection) is shown as a function of solids feed rate. Much like the original laboratory tests, the CrossFlow separator demonstrated the potential for increased efficiency when compared to the Whirlsizer. More importantly, the data show that the CrossFlow is less affected by increases in feed solid rates (especially in excess of 6.0 tph/ft^2) than a more traditional water-based classifier.

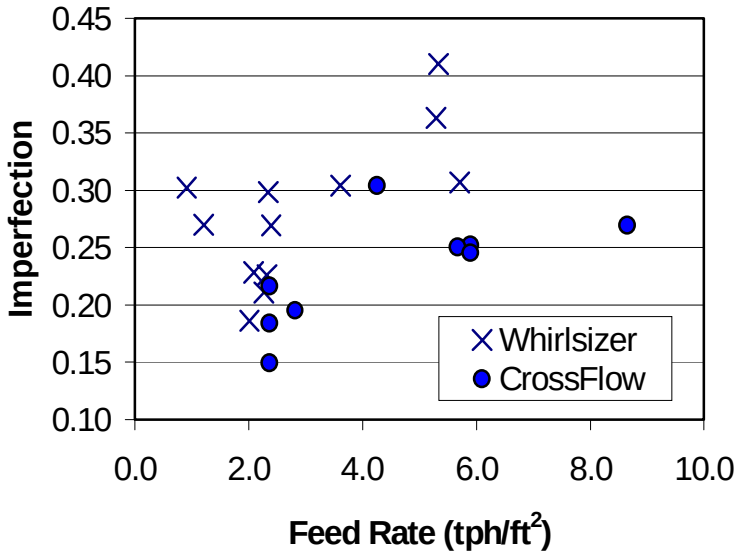

Figure 2.8 - CrossFlow and Whirlsizer solids feed rate test comparison.

A second set of solid feed rate tests, comparing the CrossFlow separator to a conventional hindered-bed separator, was completed at a Florida mineral sands plant. For this work, a 4 x 16 inch (0.1 x 0.4 m) CrossFlow unit was fabricated. This unit was constructed with a removable conventional feed pipe. This modification allowed for operation as either a conventional teeter-bed or CrossFlow separator. Typical heavy mineral concentrate, averaging 76% heavy mineral, was used for all comparative test work. It was the goal of this work to maximize heavy mineral recovery when operating as a density separator. Operating conditions were held constant for all tests with the feed rate and feed presentation being the only variables. Figure 2.9 shows the results of this testing.

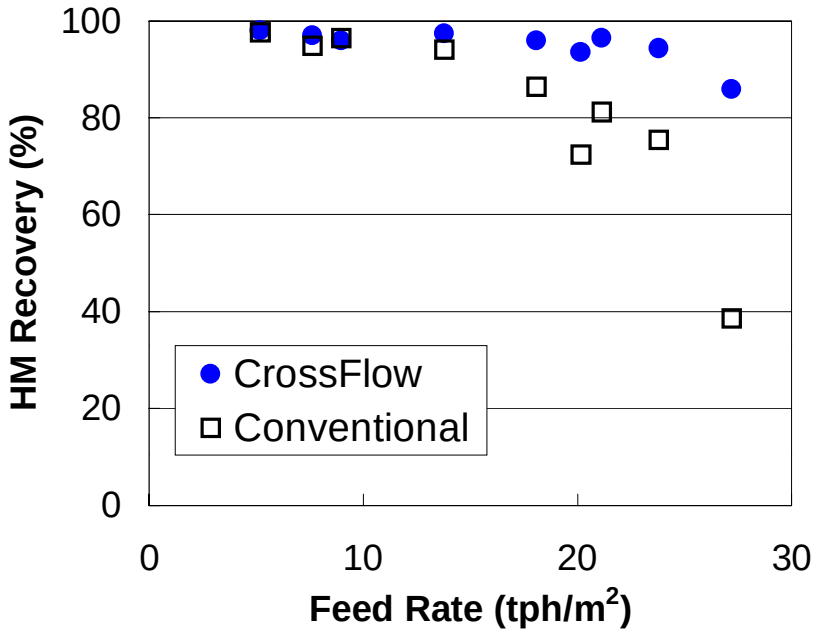

Figure 2.9 – CrossFlow and conventional teeter-bed separator solids feed rate test results.

It can be seen (Figure 2.9) that the CrossFlow unit is able to maintain high levels of heavy mineral recovery at significantly higher capacities than the identical unit with a more conventional feed introduction system. Specifically, the CrossFlow unit was able to achieve a heavy mineral recovery of 95% at a solids feed rate of 23 tph/m^2 (1.94 tph/ft^2) compared to 13 tph/m^2 (1.09 tph/ft^2) with the conventional system.

2.3.2 Tracer Studies

In an effort to explain the evident capacity and efficiency improvements of the CrossFlow feed presentation system over traditional feed systems, tracer studies were conducted. These studies investigated both the overflow and underflow streams for both "traditional" and "CrossFlow" feed configurations. The laboratory-scale separator was utilized in this effort. For comparative purposes, it was important to keep the operating conditions (i.e., solids feed rate, feed percent solids, elutriation water rate and bed-level) consistent while conducting these tests. The most important of these variables was volumetric feed rate. It was found that relatively coarse, dry silica sand could be fed at a constant rate from a vibratory feeder. This, in conjunction with make-up water flow meters, facilitated a constant volumetric feed to the separator.

Liquid residence times were calculated using the method advocated by Mankosa (1990). In this method, a conductivity probe was used to measure the salinity (conductance) of the overflow stream. Incremental samples of the stream were then taken with respect to time (seconds) and assayed for concentration (% or ppt) of tracer. The data is normally corrected for background or residual salinity, and then mathematically normalized with respect to the original tracer concentration. Plotting time versus normalized concentration yields a response curve from

which the initial tracer concentration can be calculated by summing the area under this curve. The mean residence time, τ_m, is then calculated from Equation [2.15]:

$$\tau_m = \frac{\sum C_i t_i \Delta t}{\sum C_i \Delta t} \qquad [2.15]$$

where C_i represents the concentration (salinity) at a time increment, t_i.

In order to determine the non-liquid mean residence times for a particle from the feed reporting to either the underflow or overflow stream of the separator, a modification had to be made to this procedure. In determining the mean residence time of solids from the feed that should report to the overflow, a particle had to be used, whose size and density assured its appearance in the overflow launder. Likewise, a very dense particle tracer that would settle through the teeter-bed was needed for determining the mean residence time of the feed solids that should appear in the underflow launder.

To track solids reporting to the underflow of the separator, a dense, monosized, titanium mineral sand was used as a tracer. This titanium mineral sand was dense enough to settle against the upward current of elutriation water. A spike of titanium sand (approximately 100 grams) was added to the feed stream of the separator. Samples were taken of the underflow stream with respect to time and assayed for heavy mineral content. The calculated mean residence times for particles reporting to the underflow stream are summarized in Table 2.1.

It can be seen in Table 2.1 that the mean residence time to the underflow for both the CrossFlow separator and a conventionally fed hindered-bed separator are nearly identical. Two tests were conducted for each configuration. There was some disparity between the first and second tests, which can most likely be contributed to the size of the separation chamber in conjunction with the rapidity with which the automatic control valve reacted. The PID loop

controller was extremely sensitive to variations in the feed rate, which was magnified by the small size of the separator. Consequently, as the underflow control valve responded, the internal flow regimes were altered, varying slightly differently for each test. Nevertheless, the average values of the mean residence times were relatively consistent. This finding suggests that the improved efficiency of the CrossFlow separator (i) cannot be attributed to an extended residence time in the teeter-bed and (ii) may be due to differences in how particles overflow the unit.

Table 2.1 - Mean underflow residence time for CrossFlow and conventional combinations.

Test No.	Mean Residence Time (sec)	
	CrossFlow	Conventional
1	33.05	31.23
2	29.66	34.48
Average	31.36	32.86

In order to investigate the behavior of the overflow stream, it was necessary to determine the retention time of both the water and the solids associated with the feed. This was necessary since it has been argued that the CrossFlow feed presentation system allows for the rapid removal of excess feed water from the separator without the entrainment of solids. A salt tracer (NaCl) was used to track the liquid accompanying the feed and to determine its residence time. The feed solids reporting to the overflow were tracked using a limestone tracer. The appearance of the limestone tracer in the overflow was assured due to its small size and lower density. In each test, the limestone and salt tracers were added at the same time. Similar to the process in the underflow tracer studies, incremental samples of the overflow stream were then taken with respect to time (seconds) and assayed for concentration (%).

The mean residence times of the liquid and solids from the feed that report to the overflow launder are reported in Table 2.2. The solid samples were screened at 50 mesh to provide a fine and coarse fraction. The data suggest that the CrossFlow system reduces the mean residence time of the feed water by nearly half. Upon closer examination, it can also be seen that the solids reporting to the overflow of the CrossFlow separator arrive faster than those in a conventional hindered-bed separator.

Table 2.2 - Mean overflow residence time for CrossFlow and conventional combinations.

Fraction	Mean Residence Time (sec)	
	CrossFlow	Conventional
Water (Salt Solution)	6.08	11.31
Solids (-50 mesh)	14.61	15.94
Solids (+50 mesh)	11.07	17.19

Plotting of the residence time curves for each of the separator configurations shows that each of the units acts extremely different. These residence time curves for the conventional and CrossFlow separators can be seen in Figures 2.10 and 2.11, respectively. According to Figure 2.10, feed water takes several seconds to appear in the overflow launder in a conventional configuration. The water is followed after a short time by the finest material (-50 mesh), and then the coarsest material (+50 mesh). There appears to be a distinct delay between the emergence of each tracer in the overflow stream. This suggests that in a conventional hindered-bed design, a separation is occurring to overflow material prior to its appearance in the launder.

According to the data given in Figure 2.11, there appears to be no separation between the coarse and fine material reporting to the overflow in the CrossFlow separator. As in a conventional feed system, the CrossFlow separator allows for the quick removal of liquid

associated with the feed stream. In contrast to the conventional system, the fine and coarse material reporting to the overflow exits the system at nearly the identical time and with like mixing, as indicated by the similar curves (Levenspiel, 1962). This lack of separation is providing the CrossFlow separator with an increased rate of rejection of material that should report to the overflow. This essentially increases the apparent size (volume) of the device available for separating a greater number and tighter size range of particles.

In a conventional hindered-bed unit, separator volume is being inefficiently utilized for the partitioning of material that should report to the overflow. Consequently, a wider size distribution of particles is being treated, causing an increase in particle interference and interstitial velocities. Conversely, in the CrossFlow, a greater amount of separator volume is being utilized for treating a greater number of particles closer to the cut-point of the separation. The increased amount of closely sized material in the separation chamber should decrease particle interference and the range of interstitial velocities encountered by any particle within the system. Essentially, the system becomes more homogeneous and less turbulent.

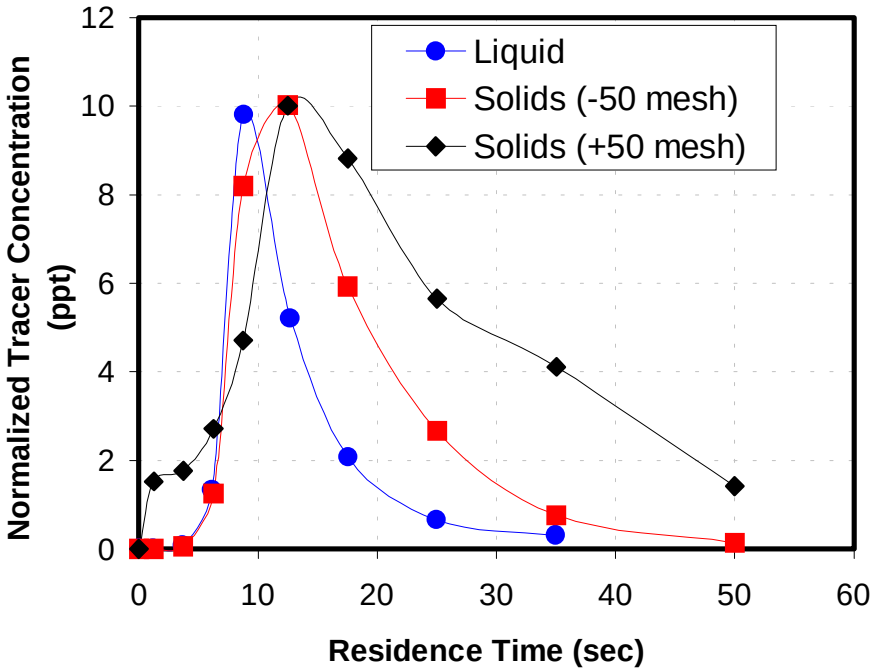

Figure 2.10 - Overflow residence time data for conventional feed system.

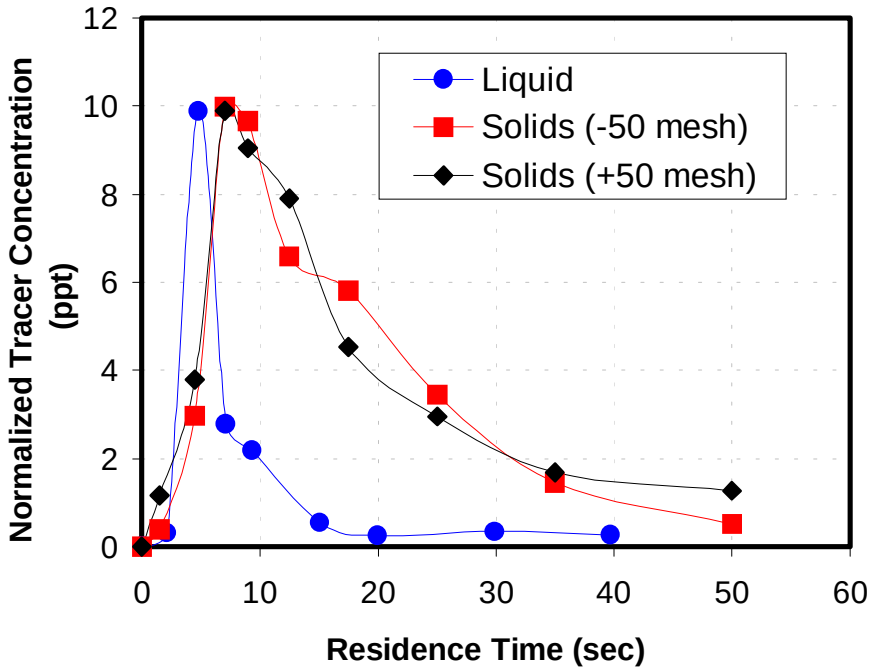

Figure 2.11 - Overflow residence time data for the CrossFlow feed system.

2.4 Population Balance Model

2.4.1 Model Description

A mathematical population balance model has been developed at Virginia Tech to help understand this new tangentially fed hindered-bed separator. This model utilizes general equations for hindered settling in transitional flow regimes to accurately predict overflow and underflow partitions, particle size distributions, and component recovery data. Input data include feed rate, percent feed solids (by mass), feed size distribution (up to 9 size fractions), density of components in the feed stream (up to 2 components), fluidization water rate, and underflow discharge rate.

The CrossFlow model was principally constructed as a series of well-mixed zones. These zones represent three distinct sections that have dissimilar mixing patterns and flow regimes. Therefore, each section must be modeled accordingly. The three primary sections include the feed inlet, teeter-bed, and underflow areas. Figure 2.12 depicts these primary sections and flows for the CrossFlow separator.

The model was constructed using the Microsoft Excel™ spreadsheet, which is a powerful engineering tool capable of performing iterative calculations (including compound iterations). Advantages of using Excel include instant graphing of results, and more importantly, ease of troubleshooting. Results of tens of thousands of calculations are readily seen in an array of spreadsheet cells where mistakes and erroneous coding errors are easily seen and corrected.

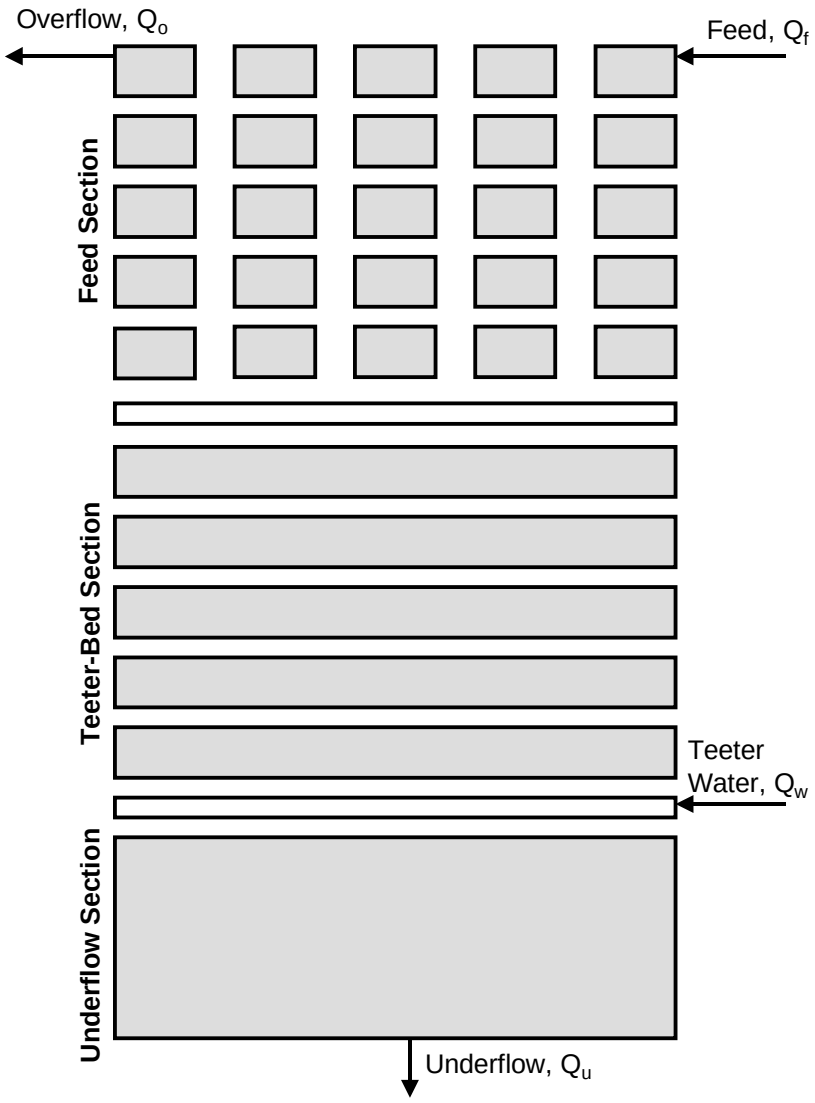

Figure 2.12 - Schematic depicting the primary divisions and flows for the CrossFlow separator.

2.4.1.1 Feed Section

Figure 2.13 shows the zone arrangement for the feed inlet area. It was necessary to divide the feed section into a series of 25 (5 x 5 configuration) zones to account for the flows induced by the cross-flowing action of the feed water, the fluidization water, and to a larger degree, the settling action of the feed solids. The settling solids are shown as dashed lines in Figure 2.13.

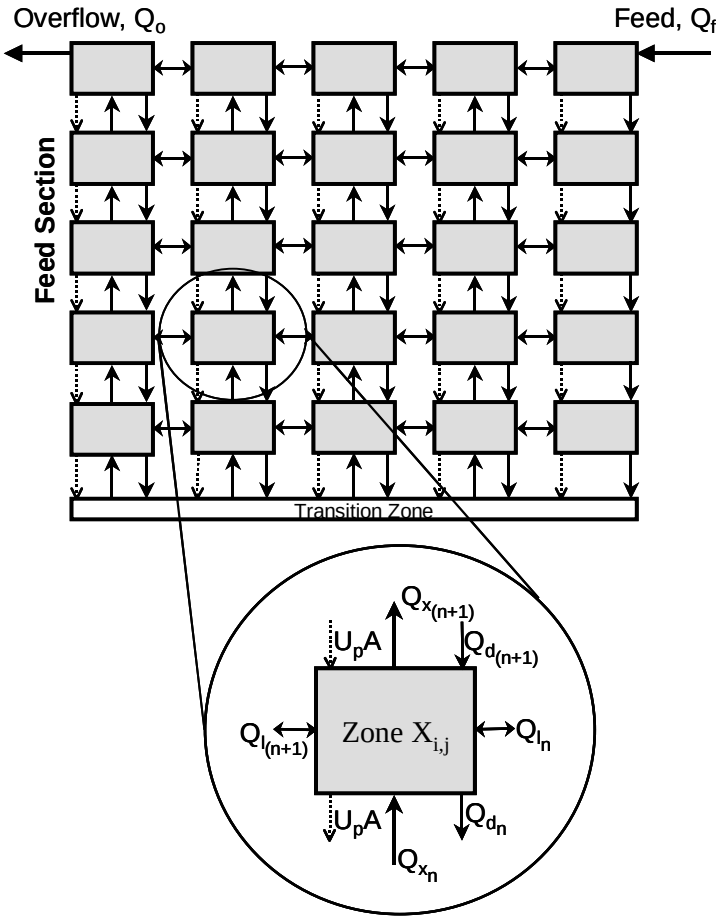

Figure 2.13 - Arrangement of zones for the feed section.

An experiment with dye was conducted to view the flow patterns in the feed section of the separator. The Plexiglas lab-scale unit, previously described, was utilized in these experiments. A photograph of one test run can be seen in Figure 2.14. From this experiment, it was determined that the feed water predominantly travels in two directions, either across the top of the classifier, or it is drawn directly down into the separator at the feed inlet point via drag. The drag created by the settling of the feed solids is responsible for the downward flow. The influx of solids and the associated liquid hinder the fluidization water from entering into the first five vertical zones of the feed section. This downward flow (Q_d) of liquid induced by the settling solids was determined to be proportional to the total volumetric concentration of settling particles within that zone as seen in Equation [2.16]. Test work to date indicates that this proportionality constant (X) has an approximate value of 12-15.

$$Q_{d(zone)} = X\,(U_p A)_{zone} \qquad [2.16]$$

where U_p = hindered settling velocity
A = area through which solids settle.

The upward flow of fluidization water that enters each zone is shown as Qx_n. This flow is counter-acted by both the flow induced by solids settling (Q_d) and by the horizontal flows (Q_l) that can move to or from adjacent cells. Material suspended within the teeter-bed acts like a distributor for the rising teeter water, evenly distributing Qx_n over the entire cross-section of the unit for each level of the feed inlet area. The horizontal flows can be calculated by conducting a flow balance for each zone within the feed section, given the elutriation water rate (Q_w), feed rate (Q_f), and the underflow discharge rate (Q_u).

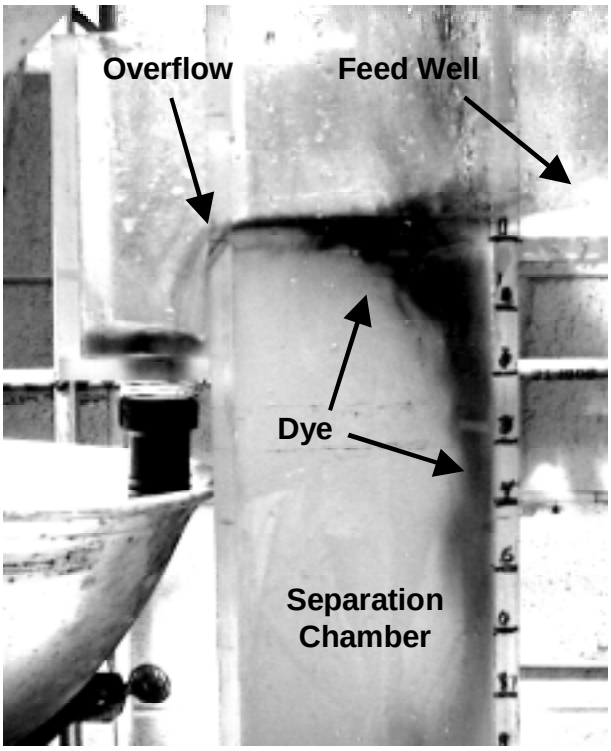

Figure 2.14 - Photo of dye experiment showing feed section flow regime.

2.4.1.2 Teeter-Bed and Underflow Sections

A schematic of the teeter-bed and underflow sections for the CrossFlow are shown in Figure 2.15. The teeter-bed section was modeled as a plug-flow device containing five zones. It is separated from the single underflow zone by a transition zone, where the fluidization water flow (Q_w) is added. It can be seen that the fluidization flow makes a split in this transition zone, with the majority of the flow rising up through the teeter-bed (Q_o). The remainder of the teeter water enters the dewatering cone and ultimately exits the system as Q_u. The underflow section was modeled as a single perfectly mixed zone. This is appropriate given that material enters by transport or settling from the above transition zone and can only exit due to mass-action through the underflow valve.

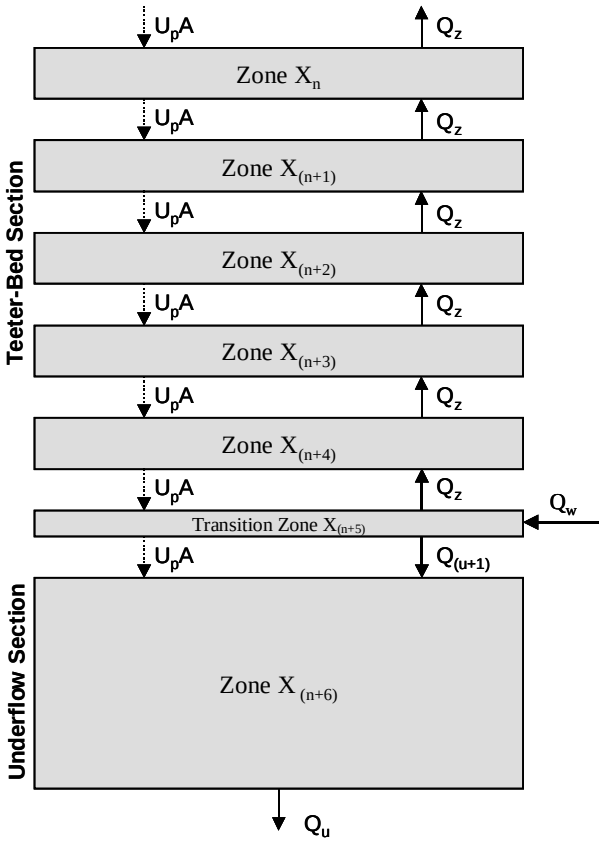

Figure 2.15 - Arrangement of zones for the teeter-bed and underflow sections.

2.4.2 Calculations

An iterative dynamic technique (i.e., finite differencing) was used to solve for the change in concentration of particles over time for each zone in the CrossFlow separator. The model was configured to allow for an array of particle sizes and densities. The volumetric flow of settling solids (U_pA) from zone to zone is shown as dotted lines in Figures 2.13 and 2.15. Using the laws of mass conservation (steady-state flow), the change in concentration for each of these cells was mass-balanced with respect to one another. To accomplish this, all volumetric flows were balanced and then multiplied by the total volumetric concentration of solids (ϕ) in the cell from which the flow originated. An iterative solution was necessary because the concentration in all

cells constantly changes until steady-state conditions are achieved. When steady-state conditions are achieved, the change in concentration of solids for all zones approaches zero.

The hindered settling velocity of particles within the CrossFlow was determined from Equation [2.17] advocated by Masliyah (1979):

$$U_p = \frac{g d_i^2 F(\alpha_f)(\rho_i - \rho_{susp})}{18\mu_f\left(1 + 0.15 Re_s^{0.687}\right)} \qquad [2.17]$$

where d_i is the particle size, ρ_i is the particle density, ρ_{susp} is the density of the suspension, and μ_f is the apparent viscosity of the fluid. As stated previously, $F(\alpha_f)$ is a function defined by Richardson and Zaki (1954) as $(1-\phi)^{\beta}$ where ϕ is the volumetric concentration of solids. Beta (β) is dependent on Reynolds number (Re) in the zone as calculated below in Equations [2.18] and [2.19].

$$\text{For } Re_s < 1 \qquad \beta = 4.36\, Re^{-0.03} \qquad [2.18]$$

$$\text{For } Re_s \geq 1 \qquad \beta = 4.4 / Re^{0.1} \qquad [2.19]$$

Substituting $F(\alpha_f)$ into Equation [2.17] yields the overall hindered settling equation seen in Equation [2.20].

$$U_p = \frac{g d_i^2 (1-\phi)^{\beta}\left(\rho_i - \rho_{susp}\right)}{18\mu_f\left(1 + 0.15 Re_s^{0.687}\right)} \qquad [2.20]$$

Reynolds number was calculated from Equation [2.21] and is dependent on the hindered settling velocity, apparent viscosity of the suspension, and concentration of particles within each

zone. The apparent viscosity of the suspension is also dependent on the total concentration of particles in each zone as seen in Equation [2.22] developed by Swanson (1989). An iterative process is needed when calculating Equations [2.20], [2.21], and [2.22] due to their interdependencies. This iterative process must be completed for each size and density class in each zone for every time step that occurs during the overall governing mass balance steady-state iteration. A flowchart illustrating the procedure necessary to complete the mathematical model is shown in Figure 2.16, while the required mass-balance equations are available in Appendix A.

$$\mathrm{Re}_s = \frac{d_i \rho_f \left| U_p \right| (1-\phi)}{\mu_{susp}} \qquad [2.21]$$

$$\mu_{susp} = \mu_{water} \frac{2\phi_{max} + \phi}{2(\phi_{max} - \phi)} \qquad [2.22]$$

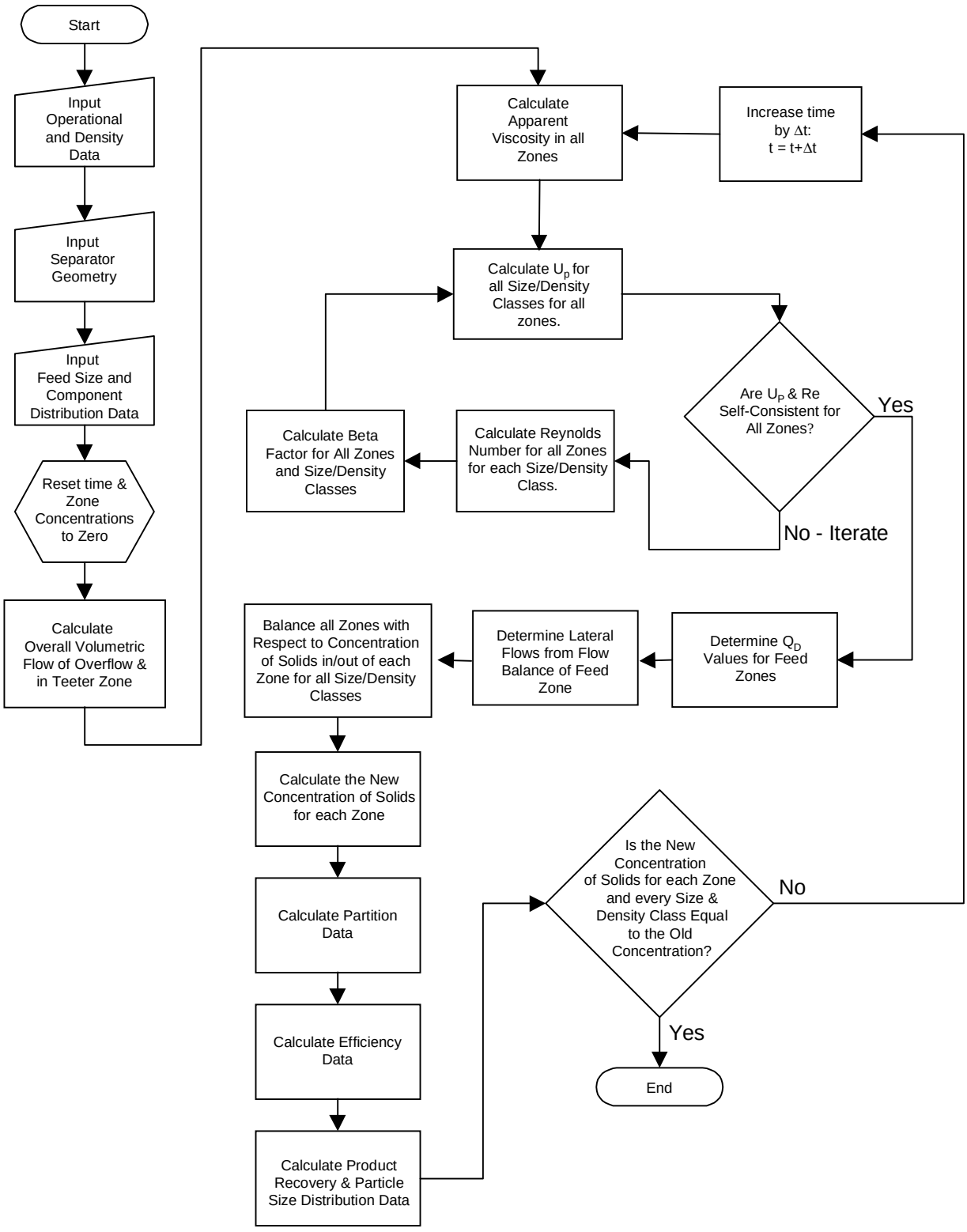

Figure 2.16 – Flowchart illustrating procedure needed to complete the population balance model.

2.4.3 Model Validation

Over sixty laboratory tests were conducted to validate the population model. A minus 1.5 mm aggregate limestone was used as the testing material. The feed size distribution is provided in Table 2.3. The validation tests were performed over a wide range of operating conditions. Feed rates generally ranged from 0.5 tph/ft^2 (5.93 tph/m^2) to over 6 tph/ft^2 (71.2 tph/m^2). Feed percent solids (by mass) ranged from 35 to 65 percent. Various cut-points were obtained by either raising or lowering bed pressure and/or fluidization water rate. Cut-points ranged from a low of 0.257 mm to a high of 0.700 mm.

Table 2.3 - Particle size distribution of limestone used in laboratory validation test work.

Particle Size (Tyler Mesh)	Mass (%)
+14	33.76
14 x 20	17.85
20 x 28	13.28
28 x 35	10.34
35 x 48	7.92
48 x 65	5.75
65 x 100	3.50
-100	7.61

It is obvious that settled material would pack closest in the dewatering cone of the CrossFlow separator where there is no elutriation. It is appropriate that as the cut-point (d_{50}) of the separation changes, so does the size distribution of the underflow stream, and hence the maximum possible concentration of particles at the underflow (ϕ_{max}). Fine material will generally fill voids that occur between coarser material, but as more fine material reports to the

overflow of a hydraulic classifier, these voids will remain proportionally empty. Yu and Standish (1993) discuss that both the fractional solid volumes and the particle size distribution affect the maximum packing density. In their work, it is stated that mathematical models are only recently relating particle size distribution to packing density; however, these linear models have been used to accurately predict the packing density of solids provided a simple continuous or discrete size distribution is available.

The maximum packing of solids was determined semi-empirically. Several laboratory tests were conducted and subsequently simulated using the CrossFlow model. The ϕ_{max} term was varied until the simulated cut-point results were consistent with the laboratory cut-point results. The d_{50}/ϕ_{max} relationship was then graphed as shown in Figure 2.17.

In general, a linear correlation was found to exist between the maximum volumetric concentration of solids (ϕ_{max}) and the target cut-point (d_{50}). A linear fit to this data yielded an R^2 value of 0.87. The three outlying data points that do not fit this data well, occurred at extremely high feed rates of over 7 tph/ft^2 (83.1 tph/m^2). It is believed that, at this feed rate, the separator is approaching its capacity limit and the necessary increase in fluidization water causes the entire teeter-bed to act as a fluid, thereby causing deviation from the linear relationship.

Due to the apparent linearity, the ϕ_{max} and d_{50} relationship can be determined by conducting as few as two laboratory control tests. One test must provide a coarse cut-point, while the other a fine cut-point. Once this relationship is known, it can be incorporated into the CrossFlow model.

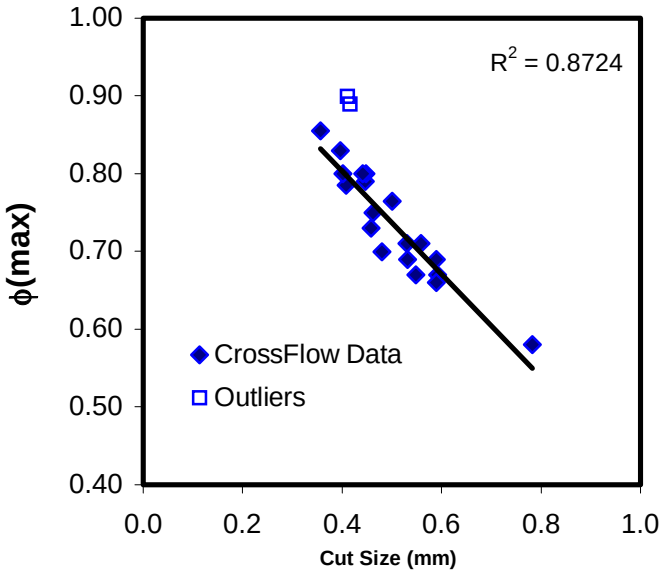

Figure 2.17 - Correlation between cut-point and maximum concentration of solids.

As stated previously, the term ϕ in Equations [2.20] and [2.21] represents the volumetric concentration of solids. As ϕ approaches unity, the term (1-ϕ) approaches zero, rendering the hindered-settling velocity (U_p) zero. However, in the case of particle classification, material can never achieve 100% solids due to particle packing constraints. The hindered-settling velocity must become zero as the volumetric concentration of particles approaches the maximum concentration of particles allowed. This maximum concentration cannot be exceeded in any zone. In view of the fact that ϕ_{max} is changing linearly with the separation cut-point, Equations [2.20] and [2.21] were transformed to:

$$U_p = \frac{g d_i^2 \left(\phi_{max} - \phi\right)^{\beta} \left(\rho_i - \rho_{susp}\right)}{18 \mu_f \left(1 + 0.15 Re_s^{0.687}\right)} \qquad [2.23]$$

$$\mathrm{Re}_s = \frac{d_i \rho_f \left| U_p \right| \left(\phi_{\max} - \phi \right)}{\mu_{susp}} \qquad [2.24]$$

where ϕ_{max} is a function of cut-size (d_{50}) and ultimately the resulting size distribution of the underflow stream.

2.4.4 Model Accuracy

Utilizing the d_{50}/ϕ_{max} relationship, the simulated results provided by the mathematical model were compared to those achieved using the laboratory-scale CrossFlow separator. The mathematical model was able to accurately predict cut-point, efficiency and the partition curves of the separations. The separation efficiency was defined as either Ecart Probable (Ep) or Imperfection as discussed previously.

Figure 2.18 shows the relationship between the actual and predicted cut-points of several tests conducted in the laboratory. The closer that the test points are to the indicated line, the better the correlation. As seen in this figure, there is evidence of a good correlation between the actual separation cut-points and those calculated via the mathematical model.

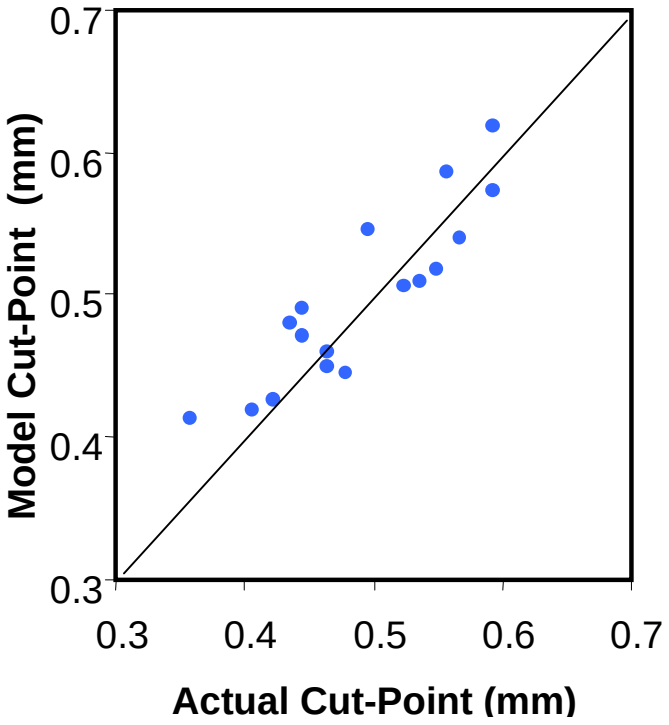

Figure 2.18 - Comparison of predicted and actual cut-points.

Figure 2.19 illustrates the accuracy of the model for predicting efficiency (i.e., Ep). The mathematical model was able to accurately predict Imperfection and *Ep*, as well as the overall partition curve of the simulated separation. Figure 2.20 shows a common result when comparing the actual and predicted partition curves for a typical laboratory validation test. In addition to cut-point and efficiency, good correlations were found between other key actual and predicted results (i.e., overflow and underflow yields and percent solids), as seen in Table 2.4.

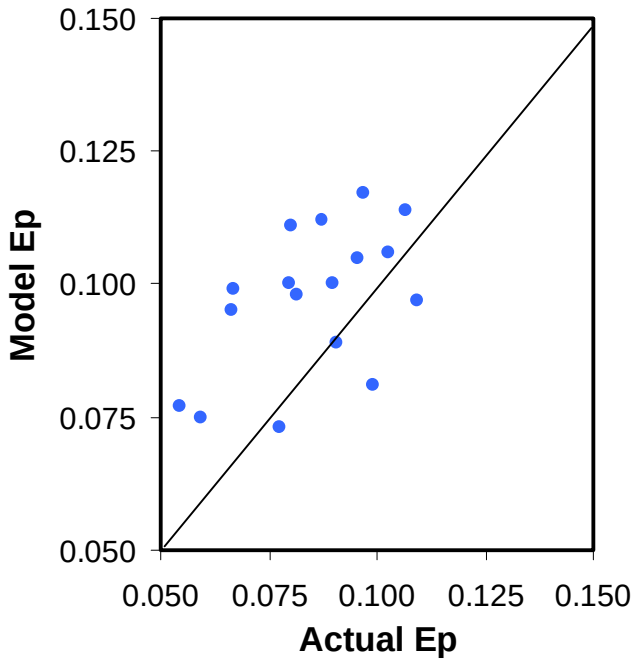

Figure 2.19 - Actual versus predicted efficiency.

Table 2.4 - Comparison of actual and predicted results.

Result	Actual	Predicted
Cut-Point (mm)	0.279	0.279
Ep	0.035	0.050
Imperfection	0.128	0.178
Underflow Yield (%)	80.31	77.87
Overflow Yield (%)	19.69	22.13
Underflow Solids (%)	55.71	50.65
Overflow Solids (%)	3.88	4.52

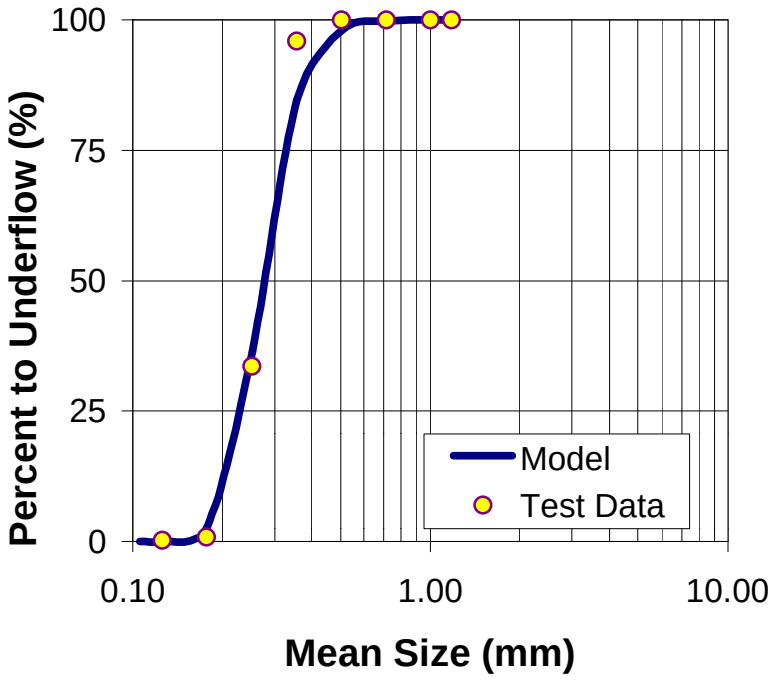

Figure 2.20 - Model predicted curve and test data.

It must be noted that efficiency is much harder to predict (i.e., in comparison to d_{50}) since there is greater error associated with sampling and size analysis when investigating either the d_{25} or d_{75} point of a separation. This is due to the fact that *Ep* and Imperfection rely on cumulative mass values for points in the overflow and underflow distributions where these values are small (Heiskanen, 1993). Discretization errors associated with the number of cells used for simulating the feed section of the separator may also cause the slight inconsistency and scatter found in Figure 2.19, which shows the prediction versus actual efficiency values for the CrossFlow separator. Nonetheless, the predicted efficiencies are generally slightly lower than the actual efficiencies, producing a conservative result.

2.4.5 Model Investigations

The impetus of the CrossFlow design was to minimize the detrimental effects of operating at low feed percent solids (by mass) and excessive overall feed rates. Therefore, investigations were completed to determine the effects of these variables on the performance (i.e., cut-point and efficiency) of the CrossFlow separator. An example of the input and output for the population balance model are available in Appendix B.

A series of feed rate simulations was conducted while maintaining a constant cut-point. The fluidization water rate and feed percent solids were held constant. The underflow volumetric flow rate was manipulated to produce the desired cut-points. Two cut-points were investigated in these feed rate tests (0.5 mm and 0.35 mm). Figures 2.21 and 2.22 illustrate the effect of feed rate on the efficiency of the CrossFlow separator in terms of *Ep* and Imperfection.

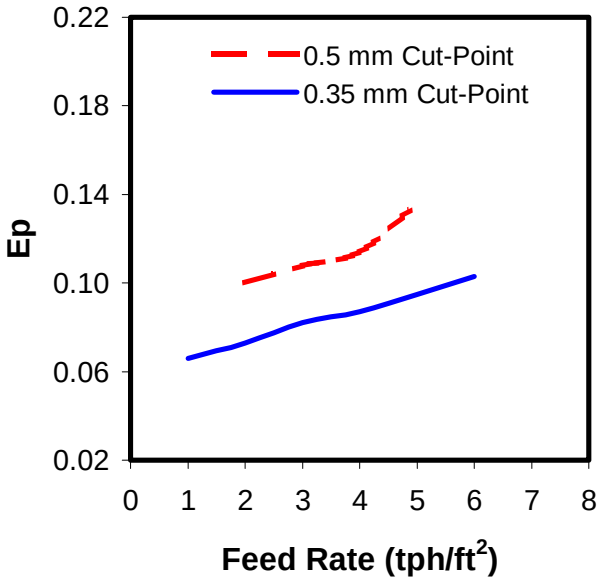

Figure 2.21 - Effect of solids feed rate on *Ep*.

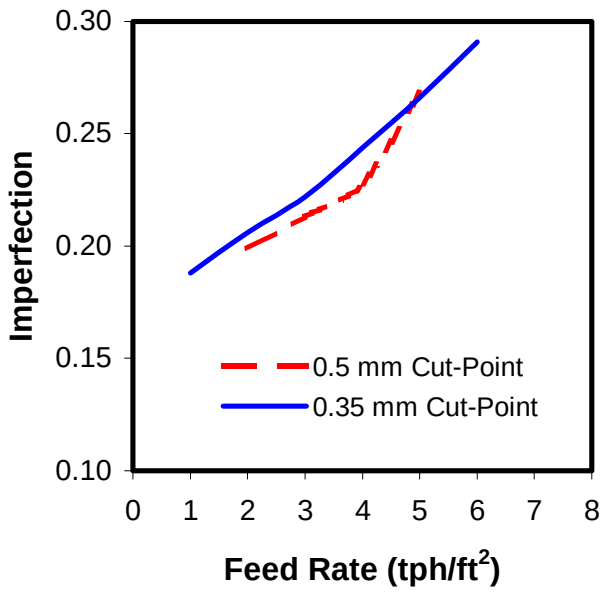

Figure 2.22 - Effect of solids feed rate on Imperfection.

Efficiency (Ep) is better for the finer separation; however, the imperfection for the coarser separation tends to be slightly superior. Nonetheless, the average imperfection of both the coarse and fine separations increases from 0.200 to 0.280 as feed rate increases from 23.76 tph/m^2 (2 tph/ft^2) to 71.2 tph/m^2 (6 tph/ft^2). Unlike other hydraulic classifiers, the CrossFlow separator is capable of high throughput capacities at acceptable efficiencies. Heiskanen (1993) states that the solids capacities for hydraulic classifiers are only typically in the range of 10 tph/m^2 to 40 tph/m^2 for fine and coarse separations, respectively.

The effect of feed percent solids (by mass) on *Ep* and cut-point was simulated at two different feed rates, 23.76 tph/m^2 (2.0 tph/ft^2) and 43.82 tph/m^2 (3.7 tph/ft^2). To complete these tests, the solids feed rate and fluidization water rate were all held constant. It was also necessary to hold the underflow volumetric flow rate constant as the feed percent solids were varied from a low of 20% to a high of 80%.

Figures 2.23 and 2.24 illustrate the effect of feed percent solids on both cut-point and efficiency, *Ep*. In these simulations, the feed solids content was varied at two different mass feed rates. While operating at 3.7 tph/ft^2 (43.82 tph/m^2), the cut-size of the separation decreased from 0.656 to 0.537 mm as the feed percent solids increased from 20 to 70% by mass (Figure 2.23). Although there was a change in cut-size, it must be noted that the greatest change in cut-point occurred between 20 and 35% solids. Once the feed reached approximately 35% solids, the separation cut-point was virtually constant and unaffected by changes in feed percent solids. At 2.0 tph/ft^2 (23.76 tph/m^2), the separation cut-point remained virtually constant (≈0.460 mm) even as feed percent solids approached 30% by mass.

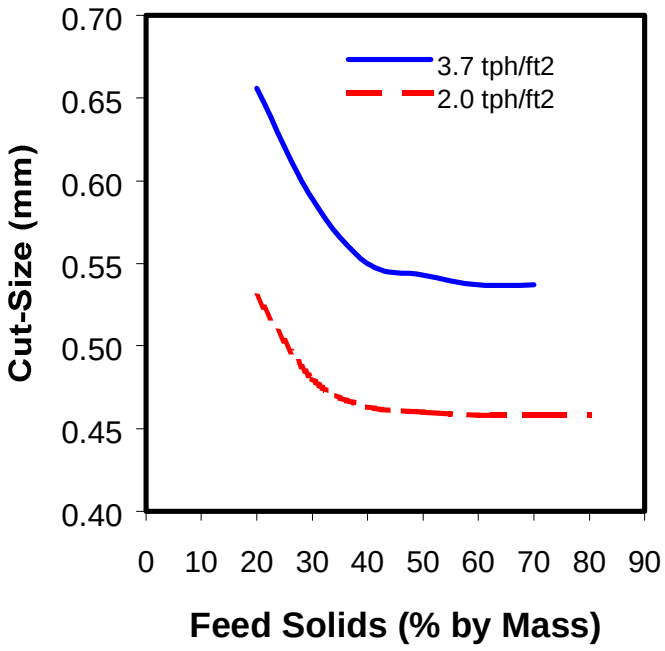

Figure 2.23 - Effect of feed percent solids on cut-point.

The effect of feed percent solids on efficiency followed the same basic trends (Figure 2.24). At the higher feed rate, the efficiency of the separation remained constant (Ep≈0.120) until the feed percent solids approached 35% by mass. At the lower feed rate, the efficiency of the separation (Ep≈0.100) remained consistent even as the feed percent solids approached 25% by mass.

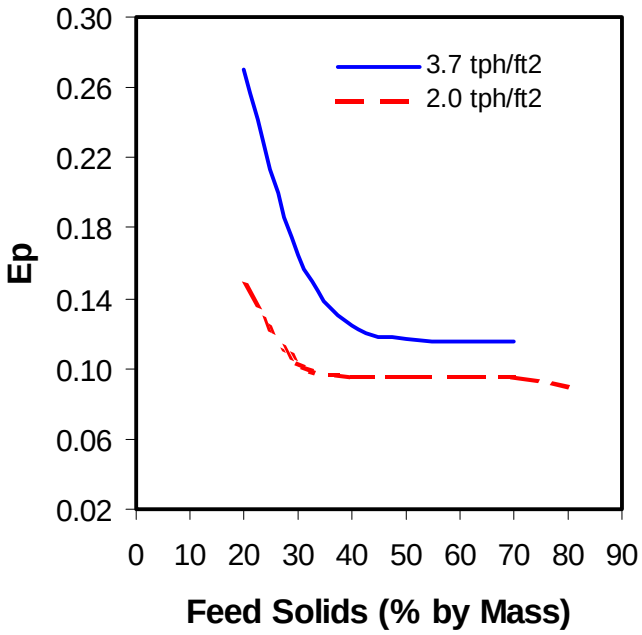

Figure 2.24 - Effect of feed percent solids on efficiency.

Lower feed percent solids generally will cause an increase in the flow velocity of the upper portion of a conventional hydraulic classifier. This increase causes some coarse material to incorrectly report to the overflow and leads to a decrease in efficiency (Heiskanen, 1993). However, the CrossFlow appears to lose very little coarse material to the overflow. The

tangential feed system allows the excess feed water to flow across the top of the separation chamber, causing only a minimal amount of vertical flow disturbance.

2.5 Conclusions

1. Comparative studies completed in the laboratory and in-plant suggested that the CrossFlow feed presentation system offers several advantages over traditional hindered-bed separator feed systems. These advantages include increased capacity and separation efficiency.

2. Solid and liquid tracer studies suggest that the unique feeding system used by the CrossFlow is capable of rapidly discharging excess feed water and fines that should report to the overflow. Comparative test work indicates that conventional teeter-bed separators are less efficient in segregating this overflow material prior to discharge.

3. A mathematical population balance model was developed to simulate the CrossFlow separator. Validation tests show a good correlation between laboratory results and model simulations. Consistent results were found for separation cut-point (d_{50}), Ecart Probable (Ep), and Imperfection.

4. A correlation between the target cut-point (d_{50}) and the maximum concentration by volume of solids (ϕ_{max}) was confirmed. This linear relationship appears to vary with material, feed size distribution, and ultimately the cut-point of the separation.

5. The mathematical model has shown that the CrossFlow separator can maintain an acceptable and less varied efficiency over a number of different operating conditions, including low feed percent solids (approaching 25% by mass) and feed solids rates in excess of 6 tph/ft^2 (71.2 tph/m^2).

2.6 References

Alexander, K.S., Dollimore, D., Tata, S.S. and Uppala, V., 1991, "A Comparison of the Coefficients in the Richardson and Zaki's and Steinour's Equations Relating to the Behavior of Concentrated Suspensions," Vol. 26, No. 6, pp. 819-829.

Austin, L.G., Lee, C.H., Concha, F. and Luckie, P.T., 1992, "Hindered Settling and Classification Partition Curves," Minerals and Metallurgical Processing, Vol. 9, No. 4, p. 161-168.

Barnea, E. and Mizrahi, J., 1973, "A Generalized Approach to the Fluid Dynamics of Particulate Systems. Part 1," Chemical Engineering Journal, Vol. 5, pp. 171-189.

Bethell, P.J., 1988, "Current and Future Processing Flowsheets," Industrial Practices of Fine Coal Processes, Chapter 30, pp. 317-329.

Brauer, H. and Thiele, H., 1973, "Bewegung von Partikel-schwarmen," Chem.-Ing.-Tech., Vol. 45, No. 13, pp. 909-912.

Cho, H. and Klima, M.S., 1994, "Application of a Batch Hindered-Settling Model to Dense-Medium Separations," Coal Preparation, Vol. 14, pp. 167-184.

Concha, F. and Almendra, E.R., 1979, "Settling Velocities of Particulate Systems – 2. Settling of Suspensions of Spherical Particles," International Journal of Minerals Processing, Vol. 6, pp. 31-41.

Furnas, C.C., 1931, "Grading Aggregates: I, Mathematical Relations for Beds of Broken Solids of Maximum Density," Ind. Eng. Chem., Vol. 23, No. 9, pp. 1052-1058.

Davis, R.H. and Gecol, H., 1994, " Hindered-Settling Function with No Empirical Parameters for Polydisperse Suspensions," AIChE Journal, Vol. 40, No. 3, pp. 570-575.

Galvin, K.P., Pratten S.J. and Nicol, S.K., 1999, "Dense Medium Separation Using a Teetered-Bed Separator," Minerals Engineering, Vol. 12, No., pp.1059-1087.

Heiskanen, K., 1993, Particle Classification, Powder Technology Series, Chapman and Hall, London, England.

Heiskanen, K. and Laapas, H., 1979, "On the Effects of Fluid Rheology and Flow Properties in the Wet Gravitational Classification," Proceedings, 13th International Mineral Processing Congress, Elsevier, Amsterdam, pp. 417-446.

Hyde, D.A., Wlliams, K.P., Morris, A.N. and Yexley, P.M., 1988, "The Beneficiation of Fine Coal Using the Hydrosizer," Mine and Quarry, Vol. 17, No. 3, pp. 50-54.

Honaker, R.Q., 1996, "Hindered Bed Classifiers for Fine Coal Cleaning," Proceedings, 13th International Coal Preparation Conference, Lexington, Kentucky, pp. 59-70.

John, P.T. and Goyal, V.K., 1975, "An Empirically Modeled Stokes Equation for Mean Particle Size from Hindered Settling Experiment at Any One Concentration," Indian Journal of Technology, Vol. 13, pp. 69-71.

Laapas, H.R., 1983, "Measurement Estimation of the Rheological Parameters of Some Mineral Slurries," DSc Thesis, Helsinki University of Technology.

Levenspiel, O., 1962, Chemical Reaction Engineering, Second Edition, John Wiley, New York.

Lewis, R.M., 1983, "Hydrosizing of Industrial Minerals," Preprint No. 83-18, SME Annual Meeting, Mar. 6-10.

Lewis, R.M., 1982, "Lewis Hydrosizer – Simple Solution to a Common Problem," Mining Congress Journal, Vol. 68, No. 4, pp. 29-32, 35-36.

Lewis, T.B. and Nielsen, L.E., 1969, Transactions of the Society of Rheology, Vol. 12., p. 421.

Littler, A., 1987, "Sand Processing, Product Optimization and Waste Treatment, Part 2 Classification," Mine and Quarry, Vol. 14, No. 8, pp. 25-31.

Littler, A., 1986, " Automatic Hindered-Settling Classifier for Hydraulic Sizing and Mineral Beneficiation," Transactions, Institute of Mining and Metallurgy, Vol. 95, pp. 133-138.

Low, G.S. and Bhattacharya, S.N., 1984, "On the Study of Maximum Solids Concentration in Suspension Rheology," The Twelfth Australian Chemical Engineering Conference, Melbourne, Australia, August 26-29, Paper 23b, pp. 805-812.

Mackie, R.I., Tucker, P. and Wells, A., 1987, "Mathematical Model of the Stokes Transactions of the Institute of Mining and Metallurgical Engineers, Vol. 96, pp. 130-136.

Mankosa, M.J. and Carver, R.M., 1995, "Processing of Chopped Wire Waste Material Using the Floatex Density Separator," Third International Symposium on Recycling of Metals and Engineered Materials, ed. P.B Queneau and R.D. Peterson, The Minerals, Metals, and Materials Society, pp. 111-120.

Mankosa, M.J., Stanley, F.L. and Honaker, R.Q., 1995, "Combining Hydraulic Classification and Spiral Concentration for Improved Efficiency in Fine Coal Recovery Circuits," High Efficiency Coal Preparation, ed. S. K. Kawatra, SME, Littleton, Colorado, pp. 99-107.

Mankosa, M.J., 1990, Scale-Up of Column Flotation, Dissertation, Virginia Polytechnic Institute and State University, Blacksburg, VA.

Masliyah, J.H., 1979, "Hindered Settling in a Multi-Species Particle System," Chemical Engineering Science, Vol. 34, pp. 1166-1168.

McGeary, R.K., 1961, "Mechanical Packing of Spherical Particles," Journal of the American Ceramic Society, Vol. 44, No. 10, pp. 513-522.

McKnight, K., Stouffer, N., Domenico, J. and Mankosa, M.J., 1996, "Recovery of Zircon and other Economic Minerals from Wet Gravity Tailings using the Floatex Density Separator," SME Annual Meeting, Phoenix, Arizona, March 11-14.

Mondal, K., 1997, A Dynamic Population Balance Model for a Hindered Bed Classifier for Fine Particle Separations, Thesis, Southern Illinois University, Carbondale, Illinois.

Plitt, L.R., 1976, "A Mathematical Model of the Hydrocyclone Classifier," CIM Bulletin, December, pp. 114-122.

Reed, S., Roger, R., Honaker, R.Q. and Mankosa, M.J., 1995, "In-Plant Testing of the Floatex Density Separator for Fine Coal Cleaning," Proceedings, 12th International Coal Preparation Conference, Lexington, Kentucky, pp. 163-174.

Rutgers, R., 1962, "Relative Viscosity and Concentration," Rheological Acts, Vol. 2, No. 4, p. 304.

Richardson, J. and Zaki, W., 1954, "Sedimentation and Fluidization: Part I," Transactions of the Institute of Chemical Engineering, Vol. 39, pp. 35-53.

Robinson, J.V., 1957, Transactions of the Society of Rheology, Vol. 1, p. 15.

Schwalbach, W.W., 1965, "Uber die Vorgange beo der Sedimentations- und Fliessbettklassierung," Aufbereit.-Tech., Vol. 6, No. 4, pp. 209-212.

Steinour, H.H., 1944, "Rate of Sedimentation. Nonflocculated suspensions of Uniform Spheres," Ind. Eng. Chem., Vol. 36, pp. 618-624.

Sudduth, R.D., 1994, "A Generalized Model to Predict the Viscosity of Solutions with Suspended Particles. IV. Determination of Optimum Particle-by-Particle Volume Fractions," Journal of Applied Polymer Science, Vol. 52, pp. 985-996.

Sudduth, R.D., 1993, "A New Method to Predict the Maximum Packing Fraction and the Viscosity of Solutions with a Size Distribution of Suspended Particles," Journal of Applied Polymer Science, Vol. 48, pp. 37-55.

Swanson, V.F., 1999, "Settling Equation for Minerals Process Application," Minerals and Metallurgical Processing, Vol. 16, No. 3, pp. 8-13.

Swanson, V.F., 1989, "Free and Hindered Settling," Minerals and Metallurgical Processing, Nov., pp. 190-196.

Taggart, A.F., 1950, Handbook of Mineral Dressing, John Wiley, New York.

Westman A.E.R. and Hugill, H.R., 1930, "Packing of Particles," Journal of the American Ceramic Society, Vol. 13, No. 10, pp. 767-779.

Wills, B.A., Mineral Processing Technology, 5th Edition, 1992, pp.407-450.

Yianatos, J.B., Finch, J.A. and Laplante, A.R., 1986, "Apparent Hindered-Settling in a Gas-Liquid-Solid Countercurrent Column," International Journal of Mineral Processing, Vol. 18, pp. 155-165.

Yu, A.B. and Standish, N., 1993, "A Study of the Packing of Particles with a Mixture Size Distribution," Powder Technology, Vol. 76, pp. 113-124.

Yu, A.B. and Standish, N., 1991, Industrial Engineering and Chemical Resources, Vol. 30, p. 1372.

Yu, A.B. and Standish, N., 1988, "An Analytical-Parametric Theory of the Random Packing of Particles," Powder Technology, Vol. 55, p. 171.

Zimmels, Y., 1990, "Hydrodynamic Diffusion of Particulates in Sedimentation Systems," Powder Technology, Vol. 61, pp. 131-141.

Zimmels, Y., 1983, "Hindered Motion of Particulate System in Newtonian Fluids. Acceleration and Steady Regimes," Powder Technology, Vol. 34, pp. 191-202.

CHAPTER 3

Improving Coarse Particle Recovery in Hindered-Bed Separators

3.1 Introduction

Hindered-bed separators are commonly used in the minerals industry as gravity concentration devices. These units can be employed for mineral concentration provided that the particle size range and density differences are within acceptable limits. However, these separators often suffer from the misplacement of low density coarse particles to the high density underflow. This shortcoming is due to the accumulation of coarse, low density particles that gather at the top of the teeter bed. These particles are too light to penetrate the teeter bed, but are too heavy to be carried by the rising water into the overflow launder. These particles are ultimately forced downward by mass action to the discharge as more particles accumulate at the top of the teeter bed. This inherent inefficiency can be partially corrected by increasing the teeter water velocity to convey the coarse, low density solids to the overflow. Unfortunately, the higher water rates will cause fine, high density solids to be misplaced to the overflow launder, thereby reducing the separation efficiency.

To overcome the shortcomings of traditional hindered-bed separators, a novel device known as the HydroFloat separator was developed based on flotation fundamentals. As shown in Figure 3.1, the HydroFloat unit consists of a rectangular tank subdivided into an upper separation chamber and a lower dewatering cone. The device operates much like a traditional hindered-bed separator with the feed settling against an upward current of fluidization water. The fluidization (teeter) water is supplied through a network of pipes that extend across the bottom of the entire cross-sectional area of the separation chamber. However, in the case of the

HydroFloat separator, the teeter bed is continuously aerated by injecting compressed air and a small amount of frothing agent into the fluidization water. The gas is dispersed into small air bubbles by circulating the water through a high-shear mixer in a closed-loop configuration with a centrifugal pump. The air bubbles become attached to the hydrophobic particles within the teeter bed, thereby reducing their effective density. The particles may be naturally hydrophobic or made hydrophobic through the addition of flotation collectors. The lighter bubble-particle aggregates rise to the top of the denser teeter bed and overflow the top of the separation chamber. Unlike flotation, the bubble-particle aggregates do not need to have sufficient buoyancy to rise to the top of the cell. Instead, the teetering effect of the hindered bed forces the low density agglomerates to overflow into the product launder. Hydrophilic particles that do not attach to the air bubbles continue to move down through the teeter bed and eventually settle into the dewatering cone. These particles are discharged as a high solids stream (e.g., 75% solids) through a control valve at the bottom of the separator. The valve is actuated in response to a control signal provided by a pressure transducer mounted on the side of the separation chamber. This configuration allows a constant effective density to be maintained within the teeter bed.

The HydroFloat separator can be theoretically applied to any system where differences in apparent density can be created by the selective attachment of air bubbles. Although not a requirement, the preferred mode of operation would be to make the low density component hydrophobic so that the greatest difference in specific gravity would be achieved. Compared to traditional froth flotation processes, the HydroFloat separator offers several important advantages for treating coarser material, including enhanced bubble-particle contacting, increased residence time, lower axial mixing/cell turbulence, and reduced air consumption.

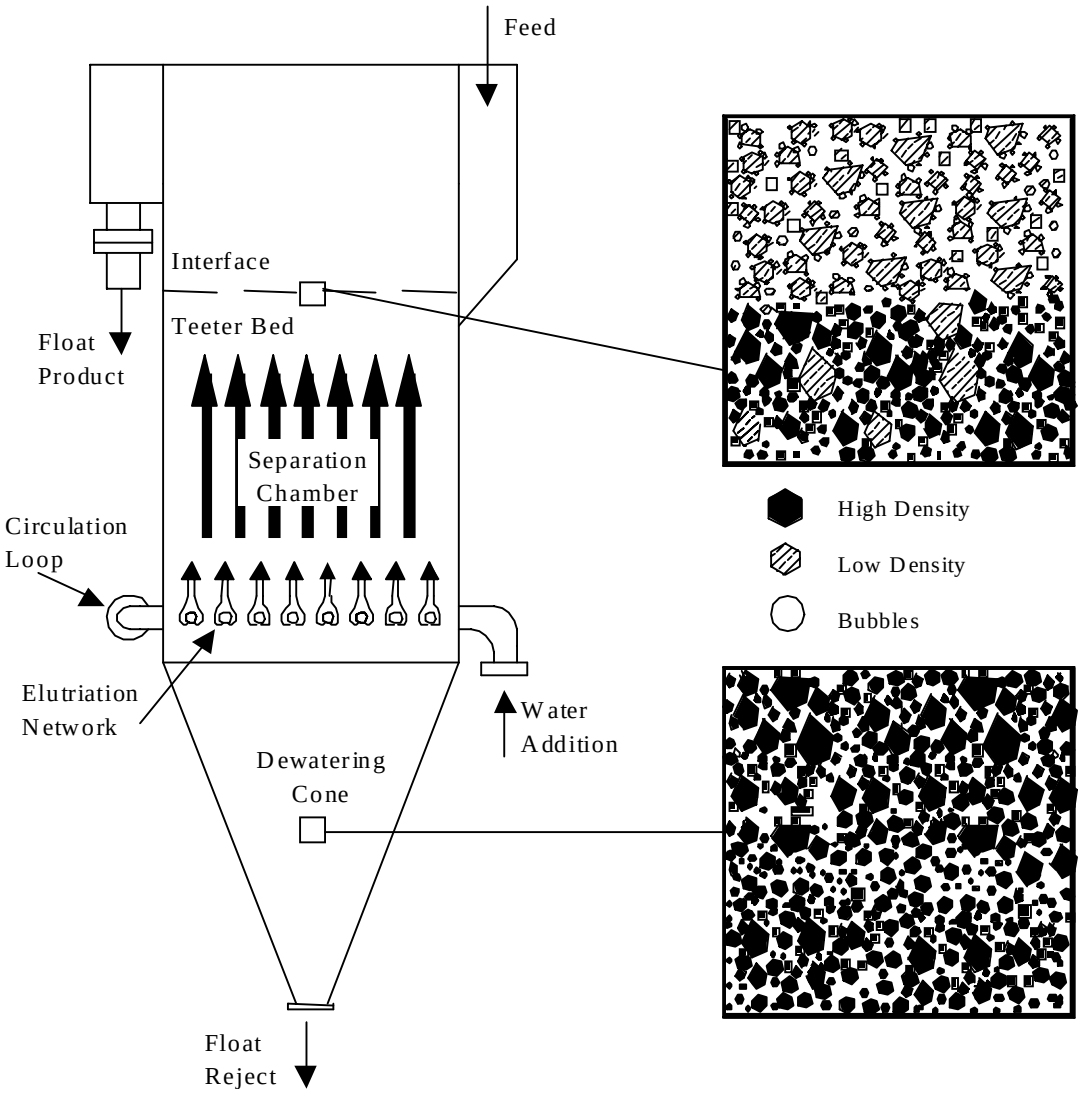

Figure 3.1 - Schematic illustration of the HydroFloat separator.

3.2 Literature Review

3.2.1 General

The improved recovery of coarse particles has long been a goal within the minerals processing industry. An array of studies has been conducted in an effort to overcome the inefficiencies found in modern processes and equipment. These studies range in scope from simple force investigation to the introduction of novel equipment. Advancements in chemistry and conditioning have also been developed and employed at a number of installations.

3.2.1.1 Recovery by Flotation

Research on the relationship between particle size and floatability began as early as 1931 with work conducted by Gaudin, *et al.* showing that coarse and extremely fine material is more difficult to treat when compared to intermediate sizes. Twenty years after this original work, Morris (1952) arrived at the same conclusion, that particle size is one of the most important factors in the recovery of ores by flotation. An illustration of this trend is seen in Figure 3.2. Generally, recovery is low for the finest particles (d_p<20μm), and is at a maximum for intermediate sized particles. A definite decrease in recovery occurs as the particle diameters continue to increase in size. This reduction in recovery on the fine and coarse ends is indicative of a reduction in the flotation rate of the particles (Jameson, 1977). It can be seen that the efficiency of the froth flotation process deteriorates rapidly when operating in the extremely fine or coarse particle size ranges. This is especially so when operating below 10μm and above 200μm. These findings might suggest that current conventional flotation practices are only fundamentally optimal for the recovery of particles smaller than 65 mesh.

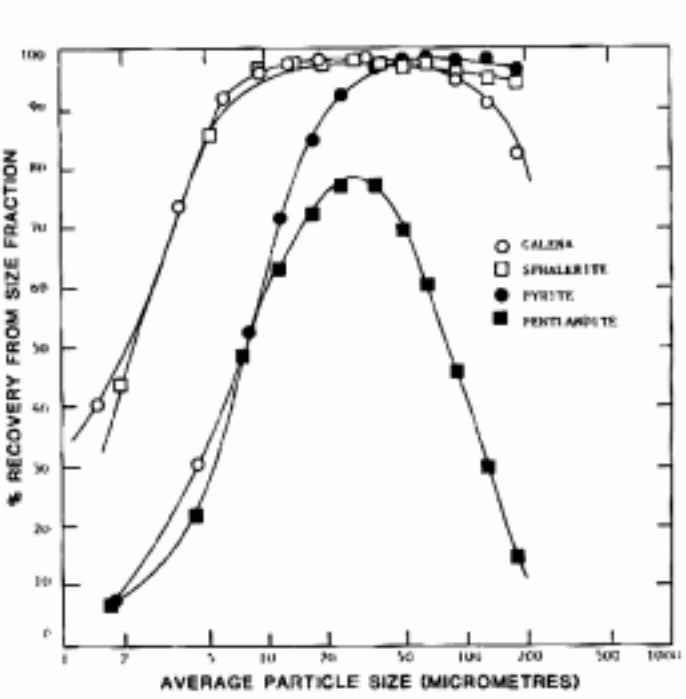

Figure 3.2 – Relationship between particle size and recovery (Ahmed and Jameson, 1989).

According to Soto and Barbery (1991), conventional flotation cells operate with two contradictory goals. A conventional cell has to provide enough agitation to maintain any particles in suspension, shear and disperse air bubbles, and promote bubble-particle collision. However, for optimal recovery, it is also required that a quiescent system be maintained to reduce detachment and misplacement of fine gangue to the overflow. To maintain these conditions when conducting coarse particle flotation is much more difficult considering that increased agitation is needed to maintain these particles in suspension. Furthermore, coarse particles are more likely to detach under these turbulent conditions. In order to compensate for this lack of recovery, some installations are using relatively small flotation devices operated at very low feed rates (Lawver, 1984). The increased high velocity, random agitation often found in large (i.e., 8.5m^3) flotation cells reduces selectivity and increases misplacement via carry-over.

Research conducted by Schulze (1977) determined that the flotation of a mineral is a resultant of forces acting on a bubble and particle in a flotation system. These forces include gravity, buoyancy, hydrostatic pressure, capillary compression, tension, and shear forces induced by the system. According to Schulze, particles in diameter of several millimeters should float (in the absence of turbulence) provided the contact angles are in excess of 50°. Later work by Schulze (1984) shows that turbulent conditions, similar to those found in mechanical flotation cells, drastically reduce the upper size limit of floatable material. Several other investigations support these findings (Bensley and Nicol, 1985; Soto, 1988). This research has demonstrated that turbulent conditions reduced the maximum floatable size to one tenth of that found in non-turbulent conditions (Ives, 1984; Ahmed and Jameson, 1989).

The recovery of fine and intermediate sized particles is a product of two phenomena, flotation and entrainment. However, coarse material is recovered solely by genuine flotation (Trahar, 1981). The low recovery of coarse particles can be attributed to several factors. Robinson (1959) observed that when coarse and fine particles are combined in one system, the result is a low surface coverage of collector on all particles in response to the magnitude of surface area generated by fine material. Generally, a lower floatability is realized for the coarser particles. Unlike fine material, coarse particles are not as capable of floating at low collector dosages. Data also suggest that when a soft mineral is attritted, overall particle surface area is substantially increased by the presence of slimes. This causes a considerable increase in reagent consumption and a reduction of floatability in some ores (Soto and Iwasaki, 1986).

Another theory is that small particles have a higher rate of flotation and, therefore, crowd out coarse particles from the air bubbles. Soto and Barbery (1991) disagree with this assessment, speculating that the poor recovery of coarse material is strictly a result of detachment. They

further advocate the use of separate circuits for fine and coarse processing in an effort to optimize the conditions necessary for increased recovery.

Several new devices have been produced and tested for the sole purpose of improving the recovery of coarse particles. Harris, *et al*. (1992) tested a hybrid mechanical flotation column, which is essentially a cross between a conventional cell and a column flotation cell. In this device, a column is mounted above an impeller type agitator. The column component offers the advantage of an upper quiescent section optimal for flotation, while the mechanical impeller offers the ability of reattachment and increased collection of any non-attached coarse material in the lower zone. When compared to a release analysis curve, this hybrid mechanical column out-performed a conventional flotation cell, but was equivalent to a traditional flotation column.

Improvements in coarse particle recovery have also been seen with the advent of non-mechanical flotation cells. Success has been observed when using column flotation (i.e., Flotair, Microcel, and CPT cells), Lang launders, Skin flotation, and the negative-bias flotation column. Column flotation offers several advantages that can be useful in any application. Barbery (1984) advocates that columns have no mechanical parts, easy automation and control, low turbulence, easy bubble size control, simple flow patterns, well-defined hydrodynamic conditions and high throughput. These advantages translate to ease of maintenance, scale-up, modeling, and a reduction of short-circuiting usually witnessed in conventional flotation.

3.2.1.2 Recovery by Gravity Concentration

Water-based gravity concentration devices are used extensively throughout the minerals industry to concentrate high density particles from a mixture of high and low density material. Although many devices have been developed over the years, a technique gaining in popularity is

hindered/fluidized-bed separators. These separators, traditionally used for classification, work reasonably well for mineral concentration if the particle size range and density difference are within acceptable limits (Bethel, 1988; Mankosa *et al*., 1995; Reed *et al*., 1995).

Separators, such as coal spirals and water-only cyclones, have been widely used in the coal preparation industry to upgrade coal feeds in the intermediate particle size range (e.g., 2 x 0.15 mm). Particles of this size are generally too small to be handled in conventional dense medium circuits and too coarse to be efficiently recovered by froth flotation circuits. Unfortunately, water-based separators often provide lower separation efficiency when compared to other plant circuits. For example, while water-only cyclones tend to misplace significant amounts of larger, low-ash coal particles to the reject stream, spirals tend to misplace coarse, high ash particles to the clean coal stream. Spiral circuits also generally suffer from high specific gravity cut-points, however they also tend to maintain high combustible recoveries. As a result, water-based separators are often used in multi-stage circuits in an attempt to deal with misplaced coal or rock (as described in Chapter 1).

A great deal of research has been devoted to the study of fluidized-beds and their use in gas/solid contacting and in liquid/solid applications. Studies describing the latter have typically focused on the classification aspects of fluidized-bed separators and less so on mineral concentration. Recent work has shown that fluidized-bed separators can be used to effectively separate mineral assemblages that have components with different densities. For instance, coal can be separated from ash forming components (Honaker, 1996), silica from iron ore, and silica from various heavy minerals such as zircon and ilmenite (McKnight *et al*., 1996). Results from these studies indicate that efficient concentration can be achieved if the particle size ratio (top size to bottom size) is less than 3 or 4 to 1 and in a range from 200 mesh to several millimeters.

Unfortunately, this is seldom the case and, as a result, separation efficiency is poor. To correct this shortcoming, the valuable component (i.e., coal, iron ore, ilmenite and zircon) frequently must be reprocessed to achieve the desired quality.

As stated previously, a hindered-bed separator is a vessel in which water is evenly introduced across the base of the separator and rises upward. The separator typically has an aspect ratio of two or more and is equipped with a means of discharging solids through the bottom of the unit. Rising water and solids flow over the top of the separator and are collected in a launder. Solids are typically introduced in the upper portion of the vessel and begin to settle at a rate defined by the particle size and density. The coarse, higher density particles settle against the rising flow of water and build a bed of teetering solids. This bed of high density solids has an apparent density much higher than the teetering fluid (i.e., water). Since particle settling velocity is driven by the density difference between the solid and liquid phase, the settling velocity of the particles is reduced by the increase in apparent density of the teetering bed. As a result, the low density component of the feed resists penetrating the bed and remains in the upper portion of the separator where it is transported to the overflow launder by the rising teeter water.

Hindered-bed separators are also well recognized as low turbulence devices. For this reason, they are used extensively for particulate processing as either gas/solid or liquid/solid contact devices (Heiskanen, 1993). The high solids concentration in the separator limits particle mobility. As a result, particles move through the separation chamber in a “plug flow” manner. Previous work has shown that this type of motion results in an increase in process recovery due to reduced back-mixing (Doby and Finch, 1990). Furthermore, particle detachment is also minimized due to a reduction in localized turbulence.

The concept of improving coarse particle recovery through the use of bubble-particle attachment in a rising current separator (flotation column) has been previously demonstrated (Laskowski, 1995; Barbery, 1989). Unfortunately, these approaches used an open-column reactor operating in the free, not hindered, settling regime. As a result, these configurations do not have the advantages associated with a teeter-bed approach. The distinctive advantage of utilizing a teeter-bed is the greatly improved hydrodynamic environment within the separator. To recognize this advantage, the fundamental difference between free and hindered-settling conditions must be examined.

Particle settling is generally recognized as falling into one of two categories: free or hindered-settling. Under free settling conditions, individual particles do not affect the settling behavior of adjacent particles and, as such, the pulp has the rheological characteristic of the fluid. Furthermore, the settling velocity is determined by particle size and particle density. Hindered-settling is fundamentally different. At high solids concentrations, adjacent particles collide with each other influencing the settling characteristics. The settling path is greatly obstructed reducing particle velocity. Additionally, the high solids concentration increases the apparent viscosity and specific gravity of the pulp, thus further reducing particle settling. As a result, the acceleration of particles becomes more important than the terminal velocity. This collision phenomenon is the most important aspect of hindered-settling and provides favorable hydrodynamic conditions that cannot be achieved in open-tank reactors, such as conventional column cells. Specifically, particle collection rate, retention time and cell turbulence are all improved.

3.2.1.3 Phosphate Recovery

The United States is the world's largest producer of phosphate rock, accounting for approximately 45 million tons of marketable product valued at more than $1.1 billion annually (United States Geological Survey, Mineral Commodity Summaries, January 1999). Approximately 83% of this production can be attributed to mines located in Florida and North Carolina. The major U.S. producers are located in Florida and include Cargill Fertilizer, Inc., CF Industries, Inc., IMC-Agrico, Inc., Agrifos, LCC, and PCS Phosphate, Inc. Of these, IMC-Agrico is by far the largest single producer in the state.

Prior to marketing, the run-of-mine phosphate matrix must be upgraded to separate the valuable phosphate grains from other impurities. The first stage of processing involves desliming at 150 mesh to remove fine clays. Although 20-30% of the phosphate contained in the matrix is present in the fine fraction, technologies currently do not exist that permit this material to be recovered in a cost-effective manner. The oversize material from the desliming stage is typically screened to recover a coarse (plus 14 mesh) high-grade pebble product. The remaining 14 x 150 mesh fraction is typically classified into coarse (e.g., 14 x 35 mesh) and fine (e.g., 35 x 150 mesh) fractions that are upgraded using conventional flotation machines, column flotation cells, or other novel techniques such as belt flotation (Moudgil and Gupta, 1989). The fine fraction (35 x 150 mesh) generally responds very well to upgrading and, in most cases, conventional flotation technologies can be used to produce acceptable concentrate grades with recoveries in excess of 90%. On the other hand, high recoveries are often difficult to maintain for the coarser (14 x 35 mesh) fraction. In fact, prior work has shown that the recovery of coarse particles (e.g., >30 mesh) can be less than 50% in many industrial operations (Davis and Hood, 1992). For example, Figure 3.3 illustrates the sharp reduction in recovery as particle size

increases from 0.1 mm (150 mesh) to 1 mm (16 mesh) for one northern Florida phosphate operation. In many cases, attempts by plant operators to improve coarse particle recovery often produce an undesirable side effect of diminishing flotation selectivity.

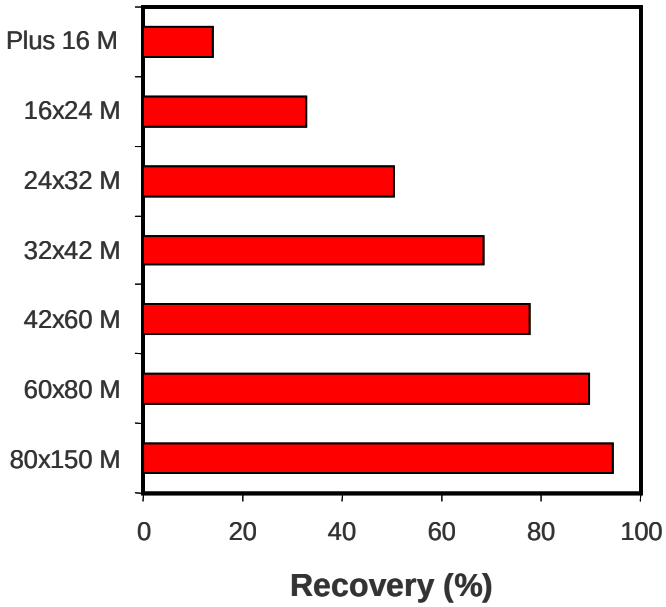

Figure 3.3 - Recovery versus size data (Mankosa *et al*., 1999).

These findings are consistent with historical data (Gaudin *et al*., 1931) from other flotation applications, which show coarse particles are more difficult to recover using traditional flotation machines. Current research indicates that coarser material is lost due to the unfavorable hydrodynamic conditions within the turbulent pulp of agitated flotation machines and/or the competition with the fines for the available bubble surface area. For this reason, a split-feed circuit arrangement is recommended when treating a wide feed particle size distribution. Furthermore, new and/or improved technologies that are more efficient in treating coarser feeds need to be developed.

Existing column cells used in the phosphate industry also have performance limitations due to mechanical design. In most cases, air is introduced using "venturi-type" aspirators that require a great deal of water. The majority of this aeration water reports to the column overflow product. This aeration water carries undesired gangue material into the froth product. Additionally, the column aeration rate is intrinsically dependent upon the aspirator water flow rate. As a result, an increase in aeration rate requires an increase in water flow rate which, in turn, can have a detrimental effect on performance. Based on these limitations, it is apparent that a flotation system is required that incorporates quiescent hydrodynamic conditions and provides for a de-coupling of the aeration system from external water supplies.

One well-known method of improving flotation performance is to classify the feed into narrow size fractions and to float each size fraction separately. This technique, which is commonly referred to as split-feed flotation, has several potential advantages such as higher throughput capacity, lower reagent requirements and improved separation efficiency. Split-feed flotation has been successfully applied to a wide variety of flotation systems including coal, phosphate, potash and industrial minerals (Soto and Barbery, 1991).

The United States Bureau of Mines (USBM) conducted one of the most comprehensive studies of the coarse particle recovery problem in the phosphate industry (Davis and Hood, 1993). This investigation involved the sampling of seven Florida phosphate operations to identify sources of phosphate losses that occur during beneficiation. According to this field survey, approximately 50 million tons of flotation tailings are discarded each year in the phosphate industry. Although the tailings contain only 4% of the matrix phosphate, more than half of the phosphate in the tailings is concentrated in the plus 28 mesh fraction. In all seven plants, the coarse fraction was higher in grade than overall feed to the flotation circuits. In some

cases, the grade of the plus 28 mesh fraction in the tailings approached 20% P_2O_5. The USBM study indicated that the flotation recovery of the plus 35 mesh fraction averaged only 60% for the seven sites included in the survey. Furthermore, the study concluded that of the seven phosphate operations, none have been successful in efficiently recovering the coarse phosphate particles.

There have been several attempts to improve the poor recovery of coarse (16 x 35 mesh) phosphate grains through the addition of improved flotation reagents. One such study, which was funded by the Florida Institute of Phosphate Research (FIPR), was completed by the University of Florida in early 1992 (FIPR Project 86-02-067). These investigators also noted that the flotation of coarse phosphate is difficult and normally yields recoveries of only 60% or less when using flotation. The goal of the FIPR study was to determine whether the recovery of coarse phosphate could be enhanced via collector emulsification and froth modification achieved by frothers and fines addition. Plant tests conducted as part of this project showed that the appropriate selection of reagents could improve the recovery of coarse phosphate (16 x 35 mesh) by up to 6 percentage points. Furthermore, plant tests conducted with emulsified collector provided recovery gains as large as 10 percent in select cases. Unfortunately, reports of follow-up work by industry which support these findings have not yet been published.

In 1988, FIPR also provided financial support (FIPR Project 02-070-098) to the Canadian Laval University to determine the mechanisms involved in coarse particle flotation and to explain the low recoveries of such particles when treated by conventional froth flotation. In light of this study, these investigators proposed the development of a modified low turbulence device for the flotation of coarse phosphate particles. Laboratory tests indicated that this approach was capable of achieving recoveries greater than 99% for coarse phosphate feeds. In addition, the investigators noted that this approach did not suffer from high reagent costs associated with other

strategies designed to overcome the coarse particle recovery problem. Although the preliminary data was extremely promising, this work was unfortunately never carried through to industrial plant trials due to problems with the sparging system and tailing discharge system.

Building on these early findings, Soto and Barbery (1991) have recently developed a negative bias flotation column that improves coarse particle recovery (Barbery, 1989). It was surmised that the only factors preventing conventional columns from being ideally suited for coarse particle recovery were wash water flow and a thick froth layer. Wash water is used in column flotation to "wash" fine gangue (i.e., clays) from the product froth. However, wash water can also propel coarse particles back into the pulp resulting in a loss of recovery. Soto and Barbery (1991) removed this wash water resulting in a negative bias flow (i.e., net flow rising upwards). An added flow of elutriation water aids in propelling coarse particles to the overflow by inducing drag on any bubble-particle in the pulp. In fact, Barbery (1989) has been able to demonstrate a four-fold improvement in coarse particle recovery when utilizing negative bias. Essentially, this device is operated in a flooded manner and in the absence of a froth zone. Several other similar devices have also been developed (i.e., Laskowski, 1995).

A number of alternative processes have been used by industry in an attempt to improve the recovery of the coarser particles. These techniques include gravitational devices such as tables, launders, spirals and belt conveyors that have been modified to perform skin-flotation (Moudgil and Barnett, 1979). Although some of these units have been successfully used in industry, they normally must be supplemented with scavenging flotation cells to maintain acceptable levels of performance (Moudgil and Barnett, 1979; Lawver *et al.*, 1984). Furthermore, these units typically require excessive maintenance, have low throughput capacities, and suffer from high operating costs. Reagent consumption can also be a major

drawback, as up to 10 lbs/ton of chemical can sometimes be needed to facilitate skin-flotation (Keating, 1999). Despite these shortcomings, the increased recovery of coarse phosphate matrix can offer several benefits.

One of the most obvious advantages of improved coarse particle recovery would be the increased production of phosphate rock from reserves currently being mined. For example, a survey of one Florida plant indicated that 7-15% of the plant feed was present in the plus 35 mesh fraction (Mankosa *et al*., 1999). At a 2,000 tph feed rate, this fraction represents 140-300 tph of flotation feed. An improvement in coarse particle recovery from 60% to 90% would represent an additional 50-100 tph of phosphate concentrate. This tonnage corresponds to an additional $7.5-15 million of corporate revenues. This incremental tonnage and income could be produced without additional mining or reserve depletion.

3.2.1.4 Carbon/Coal Recovery

In 1993, the total world coal reserves were estimated at over 1,039,182 tons, of which 23% were estimated to be in the United States alone (Kawatra, 1995). Prior to sale, run-of-mine coal is generally upgraded in order to remove ash bearing minerals and to increase the BTU value of the clean coal product. The removal of sulfur bearing minerals has also become of greater importance since the advent of the United States Clean Air Act, which restricts the emission of sulfur dioxide from coal fired power plants.

In a general flowsheet, a coal feed is crushed to a top-size of a few inches and then further classified into several size fractions. The largest of these size fractions, approximately 2 inch x 6 mesh, is predominantly treated in dense media processes. Dense medium bathes and cyclones are the most popular and most efficient; they are capable of *Ep* (efficiency) values

approaching 0.02. The 6 x 65 mesh size fraction is generally processed in coal spirals or water-only cyclones, while the passing 65 mesh size fraction is generally treated with flotation.

Coal spirals suffer from specific gravity cut-points that are typically much higher than those employed by the coarse coal dense medium circuits. This imbalance creates either a loss of clean coal or a decrease in product quality. Spirals are capable of minimizing the rejection of these coarser, low-ash particles due to the buffering action of the flowing film on particle classification. Water-only cyclones tend to misplace significant amounts of larger, low-ash coal particles to the reject stream due to the size classification within the cyclone. Because of this particle misplacement, these water-based separators tend to be much less efficient (approximately 0.16 *Ep*) than dense medium devices. Further discussion on this topic is found in Chapter 1, Sections 1.1 and 1.2.

Froth flotation is used almost exclusively for the upgrading of coal in the passing 65 mesh size range. However, the maximum floatable size of coal particles depends on several variables, including coal rank, collector addition, pulp density, cell turbulence, and retention time. In coarse particle flotation, a bubble will rise through the pulp and encounter a particle of coal and/or gangue. If the particle is hydrophobic, and if it passes within a close enough range of the bubble, the particle will adhere to the bubble. Once attached, the particle will be swept to the rear of the bubble by its relative motion through the pulp. If the force of adhesion is strong enough, the particle will remain attached to the bubble and reach the surface.

Collision efficiencies of bubble and particles should increase as the coal particle size increases. These probabilities dictate that capture and attachment should be expected to increase along with recovery. However, according to Jameson, *et al.* (1984), this does not hold true for the coarsest material. As a bubble unites with a coarse particle, attachment occurs. The bubble

and particle become a bubble-particle aggregate that has a higher buoyancy effect than that of the particle alone. Unfortunately, even after attachment, this bubble-particle aggregate may now only have an effective buoyancy and/or density equal to that of the pulp, resulting in a loss of combustible recovery. This effective buoyancy of the bubble-particle aggregate most likely sets the upper limit on the maximum floatable size. Thus, the maximum floatable particle size for a given material is anywhere between 10 and 100μm (Jameson *et al*., 1984).

Studies conducted by Sun and Zimmerman (1950) found that bituminous coal was able to float at slightly larger sizes than anthracite coal particles (6.7 mm vs. 1.17mm). However, the specific gravity of the bituminous coal was less than that of the anthracite coal, which may have contributed to this finding. Even though these coarse particles were buoyant enough to float, they were incapable of passing over the overflow weir into the clean coal launder due to their size.

In studies conducted by Crawford (1936), it was shown that fine particles are more likely to float before coarser particles. In fact, subsequent studies conducted by Brown and Smith (1954) and Rastogi and Aplan (1985) concluded that flotation rates increase with a decrease in particle size. The slower flotation rate of coarse coal leads to a loss in recovery of these generally high quality, low ash particles.

Subsequent investigations by Luttrell (2000) have demonstrated how feed rate can influence the recovery of coarse coal particles. Plotted in Figure 3.4 is the maximum floatable particle size as a function of feed rate. It can be concluded from this plot, that if effective bubble surface area remains constant as feed rate increases, the competition for this surface area also increases. As a result, bubble surface area is first covered by the finer particles, which have a higher flotation rate in comparison to the coarser particles. This phenomenon results in

unattached coarse particles. As a consequence, as feed rate increases, the maximum floatable particle size decreases as seen in this figure.

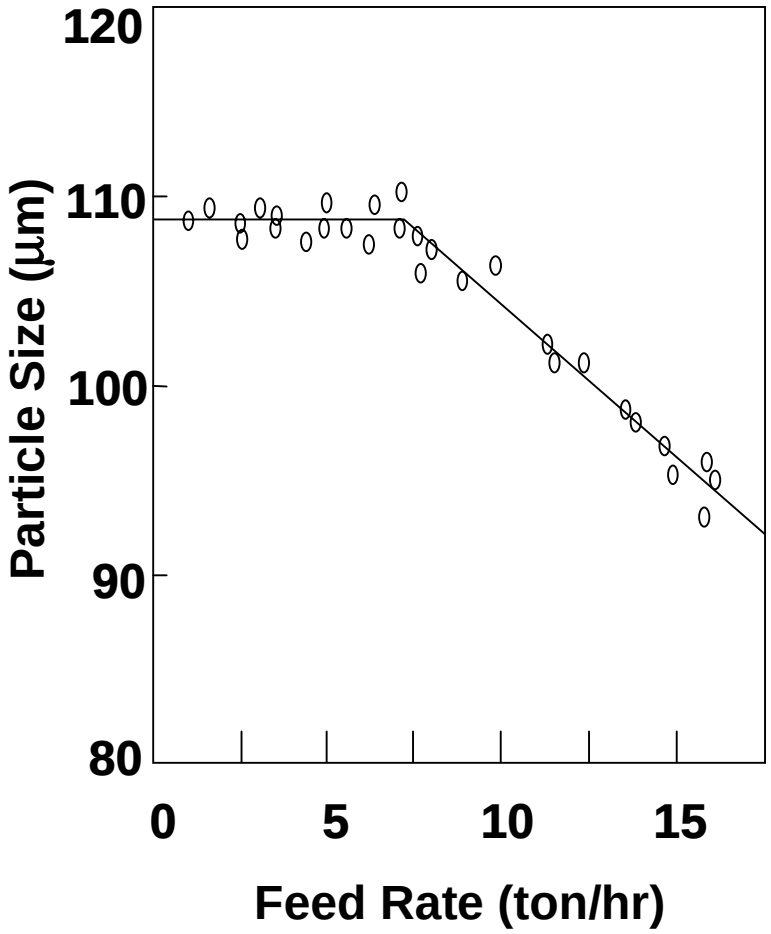

Figure 3.4 – Effect of feed rate on maximum floatable particle size (Luttrell, 2000).

Other data presented by Phillips (1998) further illustrate how this phenomenon is realized in industrial practice. Presented in Figure 3.5 are size by size recovery data for a multitude of industrial flotation feed samples. It can be seen that at smaller sizes, combustible recovery is

high for most coals (approaching 90%). However, as particle size continues to increase, there is a corresponding drop in combustible recovery. It can be concluded from this trend that coal particle recovery declines after a particle reaches an average size of approximately 65 mesh as indicated by the vertical line in this figure.

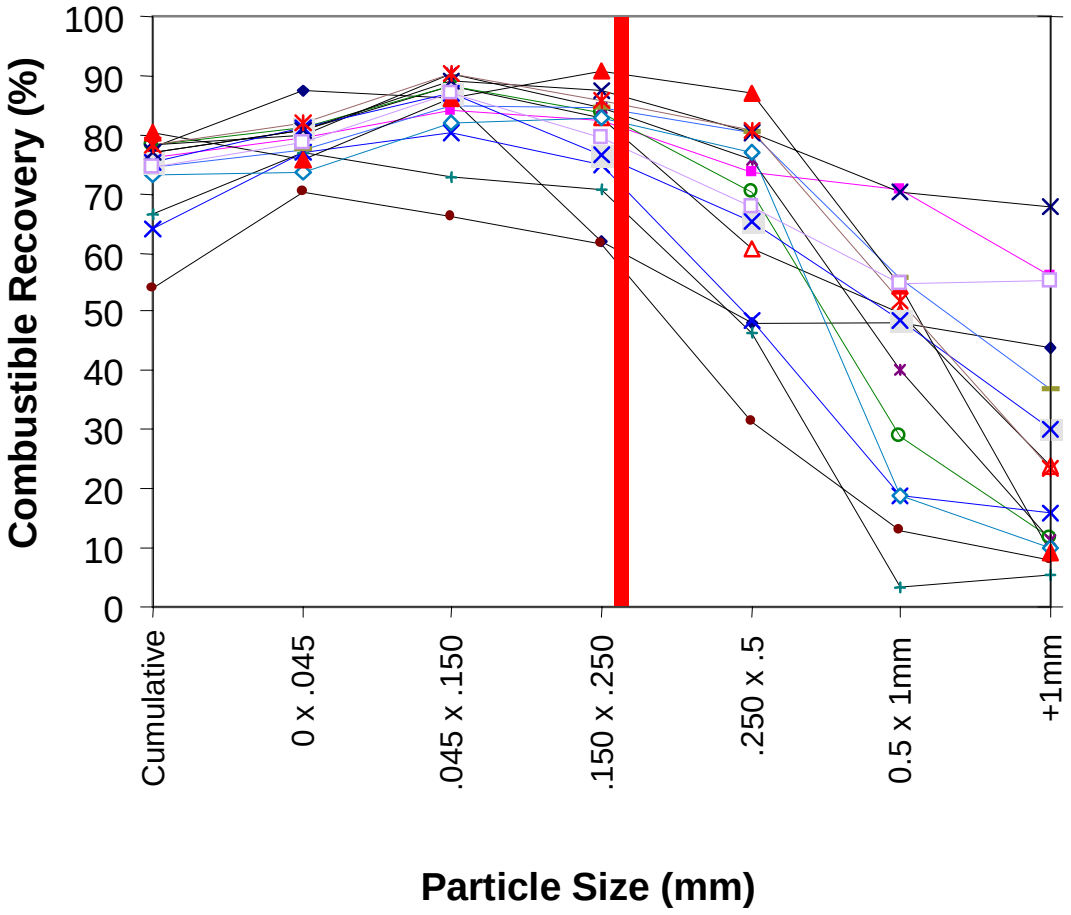

Figure 3.5 – Size by size recovery data for multiple flotation feed samples (Phillips, 1998).

As previously stated, agitation of the pulp in the flotation cell increases the flotation rate of the particles. It also has a serious effect on the particle size and rate constant relationship. A process modeled by Woodburn, *et al.* (1971) shows that a particle could be physically wrenched from a bubble to which it had adhered due to sudden acceleration. Morris (1952) also concluded that the stresses induced by turbulence were a cause for reduced recovery in the coarsest particle size fractions for flotation. With more agitation, attachment probability continues to increase due to the increased momentum of the particles within the flotation cell, but as a consequence, bubble size decreases, allowing detachment forces to play a larger role within the system. This is especially detrimental for coarse coal flotation. This is not a problem for the finer particles because their enhanced momentum will overshadow these worsening detachment forces (Ahmed *et al.*, 1989).

3.3 Theoretical Framework

3.3.1 Flotation Fundamentals

The reaction, or flotation, rate for a process is indicative of the speed at which the separation will proceed. In mineral flotation the reaction rate is controlled by several probabilities, e.g., collision, adhesion and detachment. The attachment of particles to air bubbles is the underlying principle upon which all flotation processes are based. This phenomenon takes place via bubble-particle collision followed by the selective attachment of hydrophobic particles to the bubble surface. Particles may also detach if the resultant bubble-particle aggregate is thermodynamically unstable. According to Sutherland (1948), the attachment process may be described by a series of mathematical probabilities given by:

$$P = P_c P_a (1 - P_d) \qquad [3.1]$$

in which P_c is the probability of collision, P_a the probability of adhesion, and P_d the probability of detachment. The attachment and detachment probabilities are controlled by the process surface chemistry and cell hydrodynamics, respectively. In an open (free settling) system, the collision probability is quite low due to the low particle concentration. However, at higher concentrations, the crowding effect within the hindered-bed increases the probability of collision. This phenomenon is due to the compression of the fluid streamlines around the bubbles as they rise through the teeter-bed. The increased probability of collision can result in reaction rates that are several orders of magnitude higher than found in conventional flotation.

After a particle contacts a bubble, the particle is swept over the bubble surface for a finite period of time known as the sliding time. During this period, the thin liquid film separating the bubble and particle must rupture if particle adhesion is to occur. This “sliding time” is a

reflection of the hydrodynamics of the system and is primarily a function of the particle and bubble sizes. On the contrary, the length of time required for the liquid film to thin sufficiently so that rupture occurs is a measure of the chemistry of the flotation system and is commonly referred to as the induction time. The induction time is small for hydrophobic particles (e.g., 1 msec) and may approach infinity for extremely hydrophilic particles.

Utilizing the induction time concept, Yoon and Luttrell (1989) derived an analytical expression for the probability of bubble-particle adhesion (P_a) as:

$$P_a = \sin^2\left[2\arctan\exp\left\{\frac{-BU_b t_i}{D_b(D_p/D_p+1)}\right\}\right] \qquad [3.2]$$

in which D_p is the particle diameter, D_b is the bubble diameter, t_i is the induction time, U_b is the differential velocity between the bubble and particle, and B is a constant that varies depending on the particular flow regime (as dictated by Reynolds number). In most cases, U_b is simply assumed to be the terminal rise velocity of the bubble. Since Equation [3.2] is expressed as a sine function, the calculated value of P_a will always fall between zero and unity, the correct limits for probabilities.

To illustrate the effect that particle size has on the probability of adhesion, and hence recovery, P_a was plotted as a function of particle size for different levels of induction time (hydrophobicity) as seen in Figure 3.6. As expected, P_a increases sharply as the induction time is reduced from 5 to 1 msec. It is illustrated that for a given value of t_i, P_a decreases steadily as the particle size increases. The reduced P_a value is due to the fact that larger particles tend to slide more rapidly over the bubble surface since they project further out into the high velocity region of the streamlines that pass over the bubble surface. However, it can be concluded that if

the differential velocity between the coarse particles and bubbles can be reduced, the probability of attachment will increase resulting in a corresponding increase in recovery.

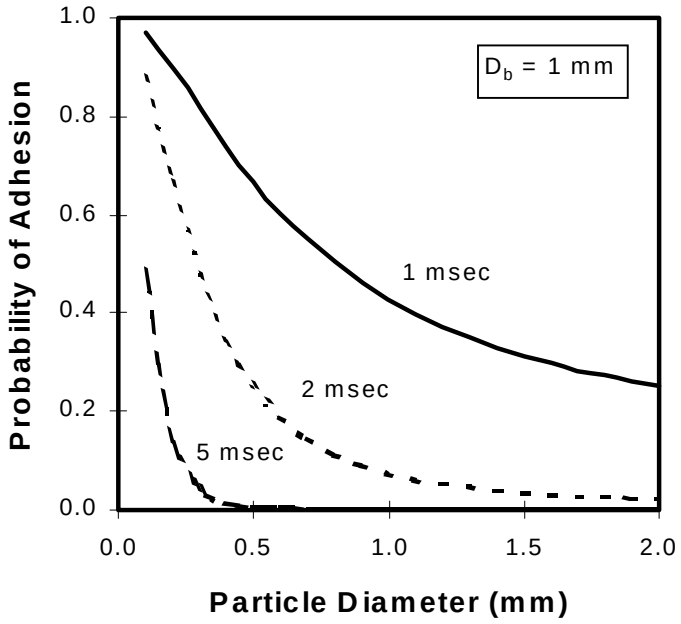

Figure 3.6 - Effect of particle size on the probability of bubble-particle adhesion for induction time values of 1, 2 and 5 msec.

Studies conducted by Woodburn, *et al*. (1971) suggest:

$$P_d = \left(D_p / D_p *\right)^x \qquad [3.3]$$

in which D_p is the particle diameter to be floated, D_p* is the maximum floatable particle diameter, and x is an experimental constant (typically 3/2). Factors that influence the magnitude of D_p* include pulp chemistry (surface tension and contact angle), physical particle properties

(size, density, composition and shape), and cell agitation intensity. Theoretical D_p* values have been calculated by Schulze (1984) from the tensile and shear stresses acting on bubble-particle aggregates under homogenous turbulence. The degree of turbulence was quantified in terms of the induced root mean square velocity (*RMSV*).

A study conducted by Schulze (1984) concluded that turbulence had a tremendous effect on the recovery of coarse particles. A typical set of results obtained by Schulze is presented in Figure 3.7. In this figure, the maximum floatable particle size is shown as a function of turbulence (RMSV) and contact angle. According to this data, the maximum size of particles that may be recovered by flotation increases by more than an order of magnitude when changing from high to low turbulence. In fact, according to Barbery (1984), the optimum conditions for coarse particle flotation occur when cell agitation intensity is reduced to a point just sufficient to maintain the particles in suspension (i.e., teeter-bed conditions).

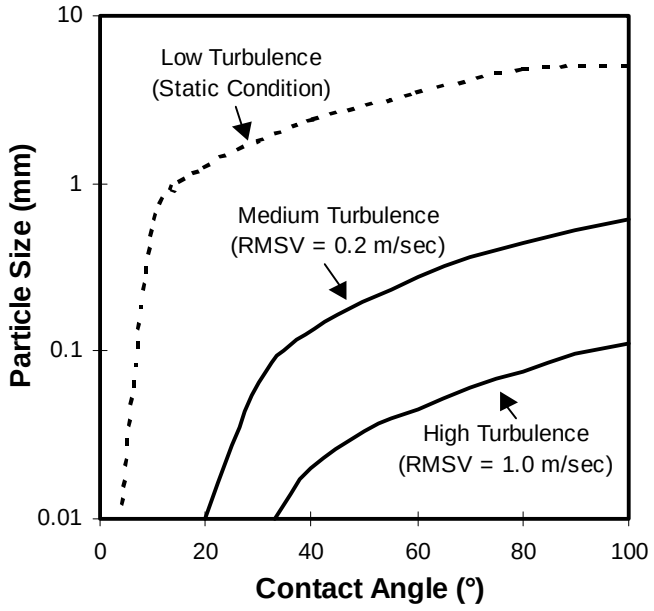

Figure 3.7 - Influence of turbulence on the maximum particle size that may be recovered by froth flotation (after Schulze, 1984).

The maximum floatable particle size is also effected by buoyancy. In froth flotation, the bubble-particle aggregate must have sufficient buoyancy to be lifted to the surface of the pulp. Mathematically, the maximum particle diameter (D_{max}) that may be floated may be estimated from:

$$D_{\max} = D_b \left(\frac{\rho_f}{\rho_p - \rho_f} \right)^{1/3} \qquad [3.4]$$

in which ρ_p and ρ_f are the densities of the particle and fluid, respectively. This expression suggests that 1 mm diameter bubbles are capable of carrying particles up to approximately 0.85 mm before the critical buoyancy limit is exceeded (ρ_p = 2.5 gm/cm^3).

Particle retention time can also greatly influence the recovery of coarse particles. The mixers-in-series model provides a convenient framework for analyzing this phenomenon (Arbiter and Harris, 1962; Bull, 1966). According to this model, the cumulative fractional recovery (R) of a given particle species can be determined using the expression:

$$R = 1 - \left(1 + k\tau_p\right)^{-n} \qquad [3.5]$$

in which k is the flotation rate constant, τ_p is the particle residence time and n is the number of equivalent mixers. Figure 3.8 shows recovery determined from Equation [3.5] for different values of n as a function of the dimensionless product $k\tau_p$. In most cases, n is assumed to be equal to the number of cells in the flotation bank. This assumption is generally valid for a cell-to-cell flotation bank. However, the magnitude of n is typically smaller for flow-through flotation banks that have a significant amount of intermixing. The appropriate value of n can be

readily estimated for any cell configuration using residence time distribution (RTD) data that have been collected using solid or liquid tracers. Details related to this procedure have been described elsewhere (Mankosa *et al*., 1992).

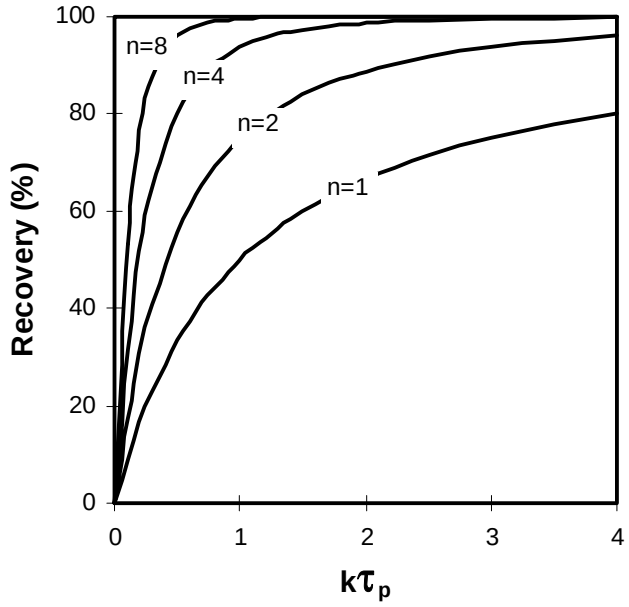

Figure 3.8 - Relationship between flotation recovery and the dimensionless quantity $k\tau_p$ for different numbers of mixers-in-series.

In column flotation, particles settle vertically through the cell either with the fluid flow (co-current) or opposite to it (counter-current). The particle residence time (τ_p) can be estimated from the liquid residence time (τ_l) using the expression:

$$\tau_p = K\tau_l = K(V / Q_s) \qquad [3.6]$$

in which V is the volume of each cell (corrected for gas holdup), Q_s is the volumetric flow rate of slurry, and K is a correction factor to account for particle settling behavior. For well-mixed cells,

K is approximately equal to one and may be ignored. For vertical flow cells such as columns, *K* may be estimated from:

$$K = \frac{Q_s}{U_p A + Q_s} \quad \{Co - Current\ Mode\} \qquad [3.7]$$

$$K = \frac{Q_s}{U_p A - Q_s} \quad \{Counter - Current\ Mode\} \qquad [3.8]$$

in which U_p is the particle settling velocity and A is the cross-sectional area of the flotation cell. In most flotation processes, feed particles move with the fluid flow towards the discharge point (co-current mode). A counter-current arrangement has obvious advantages since the settling velocity is reduced by the upward flow of liquid resulting in a higher retention time. Hindered-settling, as previously explained, provides an environment in which the particles never achieve their terminal free-fall velocity. As a result, the effective particle velocity through the cell is greatly reduced providing a significant increase in retention time as compared to a free-settling system.

Finally, the rate constant (k) is the most important term in determining flotation performance. Studies conducted by Yoon, *et al*. (1997) indicate that this parameter can be mathematically described by:

$$k = \tfrac{1}{4} P S_b \qquad [3.9]$$

in which P is the probability of bubble-particle attachment and S_b is the superficial bubble surface area rate. The latter can be calculated directly using:

$$S_b = \frac{6}{D_b}\frac{Q_g}{A_c} \qquad [3.10]$$

in which Q_g is the volumetric gas flow rate, D_b is the bubble diameter, and A_c is the cell cross-sectional area (Yoon *et al.*, 1997). Equations [3.9] and [3.10] suggest that the same flotation rate constant (k) can be maintained at a lower overall gas rate (Q_g) provided that the attachment probability (P) increases accordingly.

3.3.2 Theoretical Advantages of the HydroFloat Cell

The HydroFloat cell is a flotation device that operates much like a traditional hindered-bed separator with feed settling against an upward current of fluidization water. However, unlike a conventional teeter-bed separator, the HydroFloat cell is continuously aerated by injecting compressed air and a small amount of frothing agent into the fluidization water. As previously described, the small air bubbles are evenly dispersed into the cell and attach to the hydrophobic particles within the teeter-bed. These bubble-particle aggregates have an effective density much lower than that of the sole particle. These bubble-particle aggregates rise to the top of the denser teeter-bed and overflow from the top of the separation chamber. Hydrophilic particles that do not attach to the air bubbles continue to move down through the teeter-bed and eventually settle into the dewatering cone and are discharged. Compared to traditional froth flotation processes, the HydroFloat separator offers several important advantages for treating coarser material, including enhanced bubble-particle contacting, increased residence time, lower axial mixing/cell turbulence, and reduced air consumption.

According to Equation [3.2], the probability of attachment increases as the differential velocity between bubbles and particles (U_b) is reduced. Unlike conditions found in froth flotation where particles are allowed to settle freely opposite the direction of rising bubbles, the

hindered-settling/rise conditions realized within the teeter-bed of the HydroFloat cell slows the velocity at which bubbles and particles travel. As dictated by Equation [3.2], the reduced velocity will increase the probability of adhesion (P_a), thereby enhancing flotation recovery. As shown in Figure 3.6, this phenomenon is particularly important for coarse particles that tend to suffer from low P_a values.

Greater recovery can also be realized utilizing the HydroFloat separator due to a decrease in the probability of detachment (P_d). This decrease in detachment is a direct result of the reduction of localized turbulence generally seen in hindered-bed separators. As stated previously, the optimum conditions for coarse particle flotation occur when cell agitation intensity is reduced to a point just sufficient to maintain the particles in suspension. Thus, a teeter-bed is an ideal environment for minimizing particle detachment (Barbery, 1984).

The HydroFloat cell is both a flotation device and a density separator. The use of a teeter-bed makes it possible to achieve separations based on small differences between the density of free suspended particles and the density of bubble-particle aggregates. As a result, separations can be achieved even if the buoyancy of the bubble-particle aggregate is too small to lift the particle load. In other words, the density of the bubble-particle aggregate need only be smaller than the effective density of the teeter-bed to achieve a separation. This capability eliminates the buoyancy limitation described by Equation [3.4]. This feature is important for very large particles that are difficult to carry to the top of a conventional flotation pulp.

The HydroFloat cell also operates under nearly plug-flow conditions because of the low degree of axial mixing afforded by the uniform distribution of particles across the teeter-bed. As a result, the cell operates as if it were comprised of a large number of cells in series (i.e., high value of n). As shown in Figure 3.8, this characteristic allows a single unit to achieve the same

recovery as a multi-cell bank of conventional cells (all other conditions equal). In other words, the HydroFloat cell makes more effective use of the available cell volume than well-mixed conventional cells or open columns.

The hindered-bed environment also influences particle retention time (τ_p), and hence, particle recovery. In most flotation processes, feed particles move with the fluid flow towards the discharge point (co-current mode). In contrast, particles move in the opposite direction to the fluid flow within the HydroFloat cell (counter-current mode). As dictated by Equations [3.6] and [3.8], the fluidization water within a hindered-settling regime provides a significant increase in the particle retention time. The longer retention time allows good recoveries to be maintained without increasing cell volume.

The HydroFloat separator can be theoretically applied to any system where differences in apparent density can be created by the selective attachment of air bubbles. In summary, compared to traditional froth flotation processes, the HydroFloat separator offers several important advantages for treating coarser feed streams. These include:

- Improved Attachment: The differential velocity between bubbles and particles is greatly reduced by the hindered settling/rise conditions within the teeter-bed of the HydroFloat separator. Consequently, the reduced velocity will increase the contact time between bubbles and particles, thereby promoting the probability of adhesion and enhancing flotation recovery. This phenomenon is particularly important for coarse particles. The high solids concentration within the teeter-bed will also improve recovery by increasing the collision probability between bubbles and particles (Yoon and Luttrell, 1986).

- Reduced Turbulence: According to Barbery (1984), the optimum conditions for coarse particle flotation occur when cell agitation intensity is reduced to a point just sufficient to maintain the particles in suspension. Woodburn (1971) and Schultz (1984) have also shown that reduced cell turbulence significantly increases the maximum particle size limit for effective flotation. The use of fluidization water in the HydroFloat separator makes it possible to keep particles dispersed and in suspension without the intense random agitation required by mechanical flotation machines.

- No Buoyancy Limitation: Unlike traditional flotation processes, the HydroFloat cell is both a flotation device and a density separator. The use of a teeter-bed makes it possible to achieve separations based on small differences between the density of free suspended particles and the density of bubble-particle aggregates. As a result, separations can be achieved even if the buoyancy of the bubble-particle aggregate is too small to lift the aggregate from the surface of the teeter-bed. This capability eliminates the buoyancy limitation and is particularly important for very large particles that are difficult to carry to the top of a conventional flotation pulp.

- Plug-Flow Conditions: The HydroFloat cell operates under nearly plug-flow conditions because of the low degree of axial mixing afforded by the uniform distribution of particles across the teeter-bed. Consequently, the cell operates as if it were comprised of a large number of cells in series. Provided that all other conditions are equal, this characteristic allows a single unit to achieve the same recovery as a multi-cell bank of conventional cells (Arbiter and Harris, 1962; Mankosa *et al*., 1992). In other words, the HydroFloat cell makes

more effective use of the available cell volume than well-mixed conventional cells or open columns.

- Increased Retention Time: In most flotation processes, feed particles move with the fluid flow towards the discharge point (co-current mode). In contrast, particles move in the opposite direction to the fluid flow in the HydroFloat cell (counter-current mode). The counter-current mode has obvious advantages since the effective settling velocity of the particles is reduced by the upward flow of liquid. In addition, the hindered-settling conditions within the teeter-bed never allow the particles to achieve their terminal free-fall velocity. Therefore, the fluidization water provides a significant increase in the particle retention time. The longer retention time allows good recoveries to be maintained without increasing cell volume.

3.4 Population Balance Model

3.4.1 Model Description

A population balance model was developed and utilized in an effort to more fully understand the HydroFloat separator. Although fundamentals of flotation were used in developing the HydroFloat separator, the actual separation of particles is accomplished by gravity, based on density differences of components in the feed stream after the selective attachment of air bubbles. These bubbles change the apparent density of the hydrophobic components so that the gravity separation can be enhanced.

The HydroFloat model was constructed much like the population balance model of the CrossFlow separator developed in the previous chapter. The HydroFloat model utilizes general equations for hindered-settling in transitional flow regimes to accurately predict overflow and underflow partitions, particle size distributions, and component recovery data. Input data include feed rate, percent feed solids (by mass), feed size distribution (up to 9 size fractions), density of components in the feed stream (up to 2 components), fluidization water rate, and underflow discharge rate. The general geometry and feed characteristics of these units are nearly identical. This model was also constructed as a series of zones occurring in three distinct sections. These primary sections include the feed inlet, the teeter-bed, and the underflow area. An illustration of these primary sections has already been presented in Figure 2.12.

The Microsoft spreadsheet, Excel, was used for all calculations. This powerful software package is capable of performing the iterative calculations required to solve the steady-state equations necessary to model the HydroFloat separator.

3.4.1.1 Feed Section

The configuration of zones in the feed section of the HydroFloat separator was arranged similarly to that of the CrossFlow separator model. Again, the cross-flowing action of the feed water and solids necessitated the need for a 5 x 5 configuration as seen in Figure 2.13. If an inadequate number of zones was utilized, particles could be incorrectly partitioned and mathematically misplaced into overflow or underflow launders.

As shown in Figure 2.13, the upward flow of fluidization water that enters each zone is shown as Q_{x_n}. This flow is counteracted by both the flow induced by solids settling (Q_d) and by the horizontal flows (Q_l) that can move to or from adjacent cells. Material suspended within the teeter-bed acts like a distributor for the rising teeter water, evenly distributing Qx_n over the entire cross-section of the unit for each level of the feed inlet area. The horizontal flows can be calculated by conducting a flow balance for each zone within the feed section, given the elutriation water rate (Q_w), feed rate (Q_f), and the underflow discharge rate (Q_u).

Unlike the previous CrossFlow model, an assumption had to be made when modeling the feed section of the HydroFloat separator. In this separator, bubbles attach to hydrophobic particles creating bubble-particle aggregates. From visual inspection, it can be concluded that these agglomerates are created in the feed section of the separator and rarely penetrate the teeter-bed or underflow sections. It is not known how the attachment of air bubbles will affect the rise/sink characteristics of these agglomerates. Consequently, it was assumed that after contact and subsequent attachment of an air bubble or bubbles, the rise/sink characteristics of these agglomerates would be equal to that of a particle of equivalent apparent size and density.

3.4.1.2 Teeter-Bed and Underflow Sections

The teeter-bed and underflow sections of the HydroFloat were also arranged similarly to that of the previous CrossFlow model. This configuration can be seen in Figure 2.15. A transition zone, to which fluidization water flow is added, separates these two sections. This fluidization flow makes a split in this transition zone, with the majority of the water rising up through the teeter-bed. This fluid flow assists the activated bubble-particle aggregates in rising from the top of the teeter-bed into the overflow launder.

In the HydroFloat separator, small air bubbles are introduced into the unit along with the elutriation water. The bubbles that rise up through the teeter-bed occupy a certain fraction of volume within the separation chamber and consequently alter the apparent gravity of the teeter-bed. It can be concluded that changes in air fraction within the separation chamber can be affected by a large number of variables (i.e., average bubble size, average particle size in the teeter-bed, frother addition, elutriation water flow rate, etc.). Incorporating these variables into the general hindered-bed population balance model would add impractical complexities to the already burdensome computer code. Consequently it was assumed that the rising bubbles had no overall effect on the teeter-bed characteristics. This assumption may be inaccurate; however, conclusions drawn from trends while using this model can nevertheless provide useful insight into the advantages offered by the HydroFloat separator.

3.4.2 Calculations

Similar to the CrossFlow population balance model, an iterative dynamic technique (i.e., finite differencing) was used to solve for changes in concentration of particles over time for each zone of the HydroFloat separator. Using the general equations for hindered-settling in

transitional flow regimes presented in Chapter 2, component recovery/rejection data could be calculated. The volumetric flows and solids from each zone were mass-balanced with respect to one another using the laws of mass conservation (steady-state flow). This technique is also discussed in length in Chapter 2.

3.4.3 Modeling Insight and Investigation

In an effort to illustrate the advantages offered by the HydroFloat for recovering coarse particles, a separation of two components was simulated. Feed stream characteristics were inputted into the model. This feed consisted of two density components and was divided into nine size fractions. Both components had an equivalent and flat particle size distribution. The feed rate was assumed to be 2.5 tph/ft^2 at an elutriation water rate of 26.75 gal/ft^2. Simulations were conducted while varying the density ratio of the two components. The density of the first component was reduced (from 3.0 to 1.25 SG) while maintaining the density of the second component constant (3.0 SG).

The results of these simulations are presented in Figure 3.9. It can easily be seen that as the density ratio (ρ_1/ρ_2) decreases, the recovery of coarse particles increases. At a density ratio of 0.75, only 12% of the plus 0.71 mm material (+20 mesh) reported to the overflow. This density ratio is typically found in applications where a 2.25 SG material is being separated from a 3.00 SG material (i.e., mineral sands). However, using air bubbles, the density ratio (ρ_1/ρ_2) can be altered to 0.50. At this ratio, nearly 72% of the coarse, lower density material is now recovered to the overflow launder. These results are analogous to recovering the coarse, low density material that is typically lost in a conventional hindered-bed density separator. As presented in Figure 3.10, this change in apparent density of one component can represent an increase in total circuit recovery of nearly 22.5%. Naturally, additional improvements in overall

recovery can be realized if the apparent density of the low density component can be further altered.

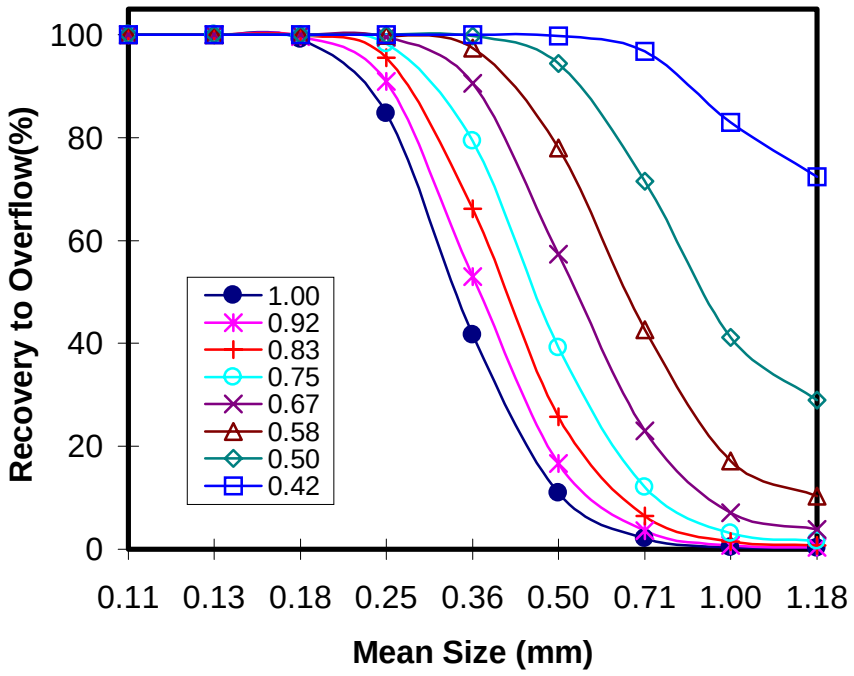

Figure 3.9 – Size by size recovery of components for varying density ratios (ρ_1/ρ_2).

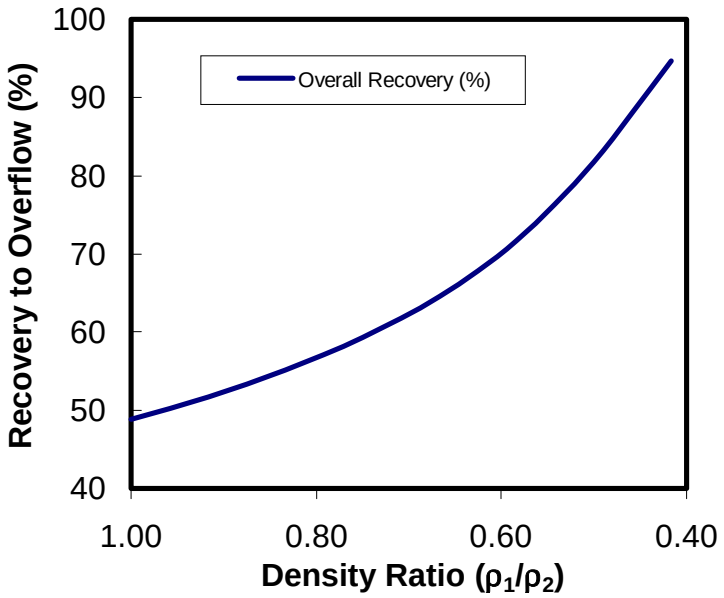

Figure 3.10 - Circuit recovery data for varying component density ratios.

3.5 Proof-of-Concept Testing

Several laboratory-scale tests were conducted to evaluate the potential of the HydroFloat separator for upgrading several types of mineral samples. These samples included mineral sands, phosphate matrix, carbonaceous slag and coal. Conventional flotation tests, whose results were used as baseline data in some investigations, were conducted using a laboratory flotation cell (Denver Model D-12). Aerated teeter-bed investigations were conducted with a laboratory-scale HydroFloat cell operated in two different modes, i.e., batch and continuous. The test unit was fabricated from Plexiglas with an open area of approximately 50 cm^2. This test unit is the same device described previously in Chapter 2 (Figure 2.4) except that a static in-line mixer was added to the elutriation water line. Using compressed air and a glycol frothing agent in conjunction with the static mixer allowed for the creation of small bubbles which were dispersed throughout the teeter-bed via the elutriation piping network.

3.5.1 Phosphate Recovery

3.5.1.1 Testing of a North Florida Phosphate Matrix

A sample of a run-of-mine north Florida phosphate matrix (5 mm x 65 mesh) was scalped at 3 mm to remove the extreme oversize and debris material. The feed ore was classified to remove the minus 35 mesh fines and conditioned with a fatty acid-diesel fuel mixture at a dosage of approximately 0.50 kg/t (active fatty acid). In all tests, ammonium hydroxide was used for pH control and a polyglycol frother was added to stabilize the bubble suspension. Batch HydroFloat tests were conducted and compared against conventional flotation results.

Figure 3.11 compares the results of the conventional flotation tests with those obtained using the HydroFloat cell operated in the batch mode. In this series of tests, the HydroFloat cell

achieved a BPL recovery of nearly 95% compared to less than 79% for the conventional cell. This represents an increase in BPL recovery of more than 20%. Although the conventional cell was floated to exhaustion, higher recoveries were not possible since many of the coarser particles remained unfloatable. Furthermore, the recovery improvement was achieved while maintaining a slighter higher concentrate grade (67.0% versus 65.7% BPL). The insol content of the HydroFloat concentrate was also lower (7.2% versus 7.7% insols). In fact, the test data show that the batch HydroFloat cell produced concentrates with a lower insol content over the entire range of BPL recoveries. The unexpected improvement in the quality of the concentrate produced by the HydroFloat cell has been attributed to the incremental recovery of very high-grade coarse particles that could not be floated by the conventional flotation technique.

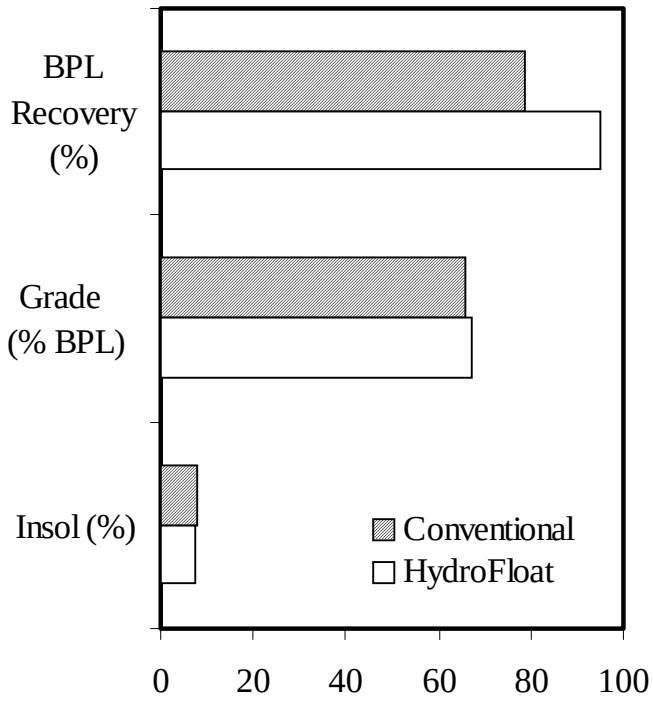

Figure 3.11 - Comparison of separation data for batch test units for a phosphate matrix.

In light of the promising results obtained in the batch tests, several follow-up experiments were conducted by operating the HydroFloat cell in the continuous mode. Several different combinations of reagent dosages, water rates, and teeter-bed levels were examined in this effort. Due to slight variations in the BPL head assay, it was necessary to compare the test results based on a concentration ratio. This parameter is mathematically defined as the ratio of the concentrate grade (%BPL) divided by the feed grade (%BPL). As shown in Figure 3.12, the continuous unit produced consistently higher BPL recoveries than the conventional cell. The average recovery for the HydroFloat was 93.8%, compared to only 78.7% for the conventional test. The best continuous HydroFloat test result provided a BPL recovery of 92.4% at a concentration ratio of 2.12.

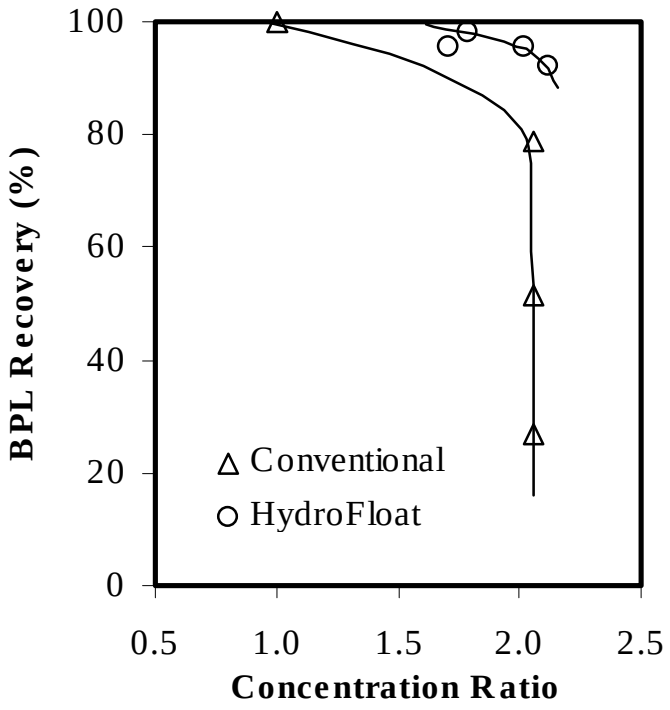

Figure 3.12 - Comparison of separation data from continuous test units for a phosphate matrix.

3.5.1.2 Testing of a Central Florida Phosphate Matrix

Considering the favorable results of the northern Florida phosphate sample, another sample of run-of-mine central Florida phosphate matrix (5 mm x 65 mesh) was investigated. It was deemed necessary in order to prove that these were not ore-specific results. Again, the feed was scalped at 3 mm to remove the extreme oversize and debris material. In this second phosphate investigation, two samples were tested. One sample was classified to remove the minus 35 mesh fines while the other was classified to remove the minus 28 mesh fines. Each sample was conditioned with a fatty acid-diesel fuel mixture at a dosage of approximately 0.50 kg/t (active fatty acid). For all tests, ammonium hydroxide was used for pH control and a polyglycol frother was added to stabilize the bubble suspension. For each feed sample, several tests were conducted in an effort to produce a grade and recovery curve.

Figure 3.13 compares the results of how each of the feeds responded to HydroFloat testing. Both the plus 35 and plus 28 mesh phosphate matrix responded extremely well to the aerated hindered-bed separator. It can be seen that the high BPL recoveries (95%) could be maintained at extremely low insol grades (5-10%). It can also be seen that the plus 28 mesh feed responded slightly better than the plus 35 mesh material as indicated by the higher separation curve. This is most likely due to the elutriation water misplacing some of the fine silica particles that were present in the finer feed sample. A lower water rate may have improved this result.

The optimum results for these tests are presented in Figure 3.14. The BPL content of the plus 28 and plus 35 mesh product were 69.5 and 68.5%, respectively. These results were produced at a BPL recovery of 93%. At these high recoveries, the HydroFloat was able to maintain low insol grades of 5.0% and 6.3% for the coarse and fine feed material, respectively.

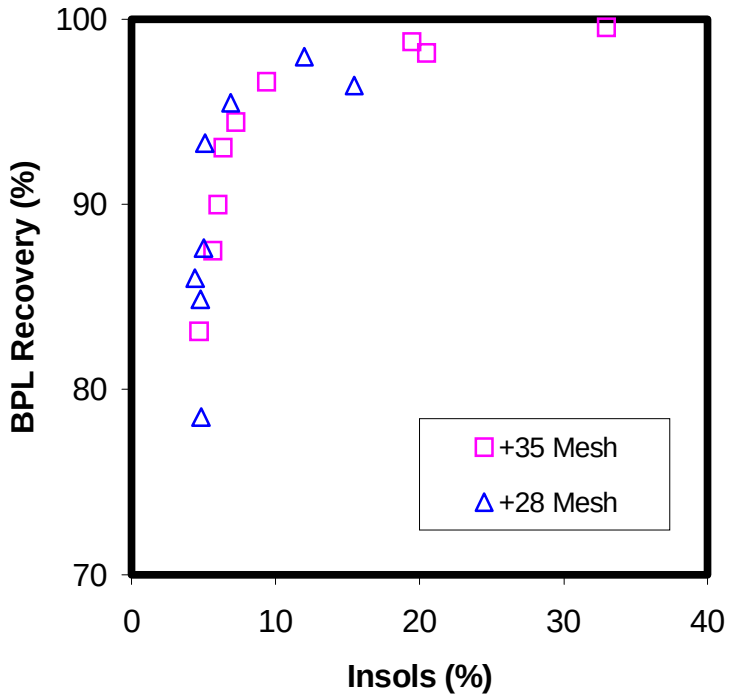

Figure 3.13 - Grade and recovery curve for central Florida phosphate sample.

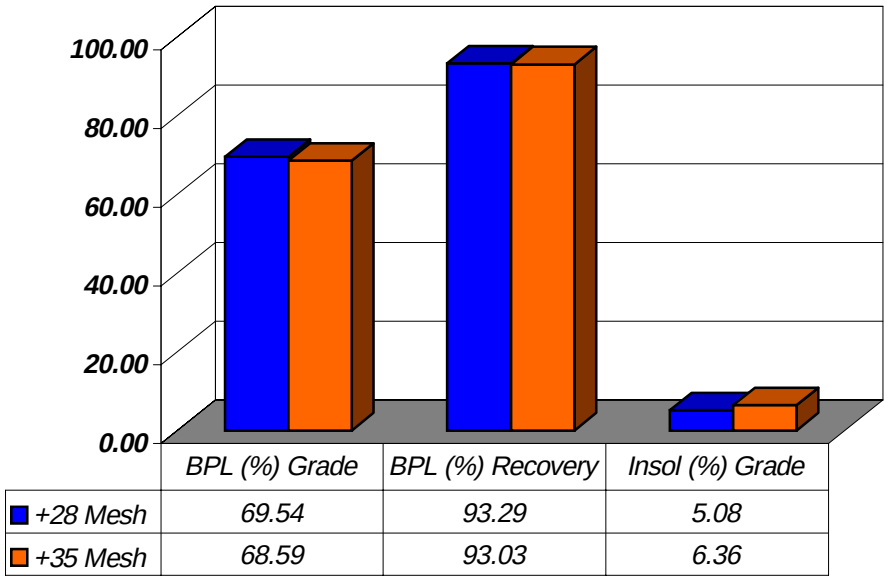

	BPL (%) Grade	BPL (%) Recovery	Insol (%) Grade
+28 Mesh	69.54	93.29	5.08
+35 Mesh	68.59	93.03	6.36

Figure 3.14 - Optimum results of HydroFloat tests on central Florida phosphate sample.

3.5.2 Coal/Carbon Recovery

3.5.2.1 Testing of Anthracite Slag

An industrial slag sample (nominally 6 mm x 200 mesh) was screened at 6.35 mm to remove oversize tramp material prior to testing. The feed sample contained ≈12% fixed carbon in the form of anthracite coal and ≈30% Fe_2O_3 and ≈26% TiO_2. This sample was ideally suited for HydroFloat treatment due to the inherent hydrophobicity of the low density component (anthracite). The objective of these tests was to recover the remaining fixed carbon at a product quality greater than 80%. Only seven tests were conducted on this sample due to the small amount of available material. Four tests were conducted utilizing the lab-scale HydroFloat with full teeter-bed aeration. Three were conducted with the HydroFloat operating as a traditional hindered-bed separator (i.e., no teeter-bed air was employed).

Figure 3.15 shows the product grade and recovery plot for the plus 28 mesh fraction of the feed material. Without aeration, the hindered-bed separator was able to make a separation, although a product quality of over 71% fixed carbon could not be achieved. In contrast, a quality of over 80% could be achieved when the teeter-bed was aerated. Aeration allowed the product recovery to be increased by an overage of 10-15%, while simultaneously improving the fixed carbon content of the product.

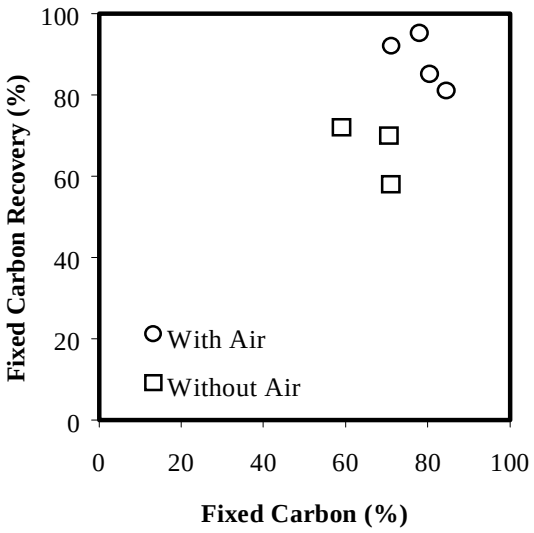

Figure 3.15 - Testing of anthracite slag using the HydroFloat separator (6.35 mm x 200 mesh).

3.5.2.2 Testing of Central Appalachian Coal

A sample of run-of-mine coal from central Appalachia was used to evaluate the effectiveness of the HydroFloat separator in treating 2 mm x 0.15 mm coal from an existing spiral circuit. The feed coal was classified to remove the minus 100 mesh fines and conditioned with approximately 0.25 kg/t of diesel fuel to enhance particle hydrophobicity. In the first series of comparison tests, the HydroFloat separator was operated without the addition of air. The separation performance achieved in this mode of operation would be identical to that obtained using a traditional hindered-bed separator. In the second series of tests, the HydroFloat was operated with air bubbles added to the teeter-bed. In this case, approximately 0.1 kg/t of polyglycol frother was injected into the teeter water to improve air dispersion and minimize bubble coalescence.

Figure 3.16 shows the recovery-ash curves comparing the performance of the HydroFloat and hindered-bed separators. For convenience, the data have been reported for both the coarse (plus 50 mesh) and fine (minus 50 mesh) size fractions. As expected, both devices achieved good recoveries (>90%) of the minus 50 mesh material. The HydroFloat separator also produced good recoveries of the plus 50 mesh material. Combustible recoveries in the range of 87-97% were readily attainable over a wide range of operating conditions. In contrast, the hindered-bed separator was not able to achieve recoveries greater than about 75% for the plus 50 mesh material. Attempts were made to improve the recovery of the plus 50 mesh particles by increasing the flow rate of the fluidization water or by raising the level of the teeter-bed. However, these attempts generally produced unacceptably high ash products due to (i) short-circuiting of mineral matter into the product launder and (ii) excessive turbulence within the teeter-bed. Since more of the feed mass resided in the plus 50 mesh fraction (approximately 60%), the overall performance of the HydroFloat was far superior to that of the hindered-bed separator in treating the overall 2 x 0.15 mm sample. As shown in Figure 3.17, the recoveries obtained for the overall feed with the addition of air were approximately 20 percentage points higher than those obtained without air injection.

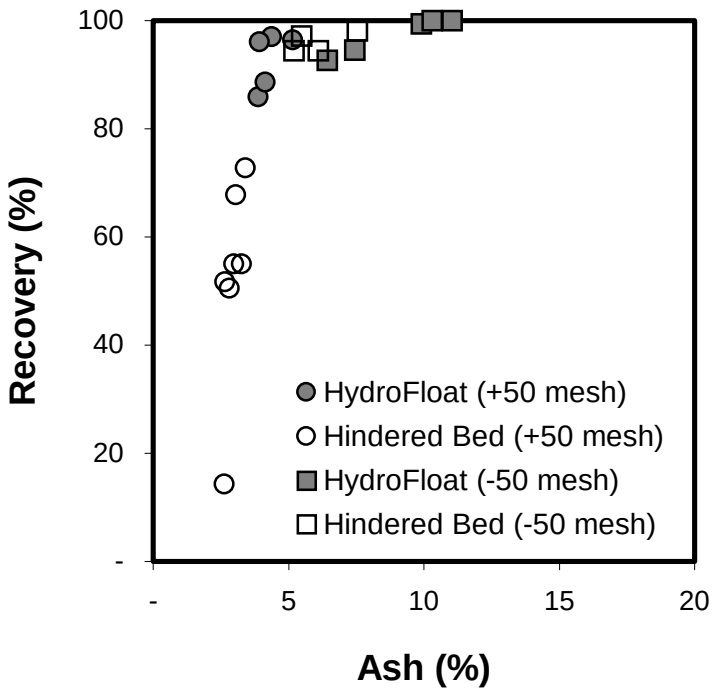

Figure 3.16 - Test results (fractionated) obtained using spiral feed from Central Appalachia.

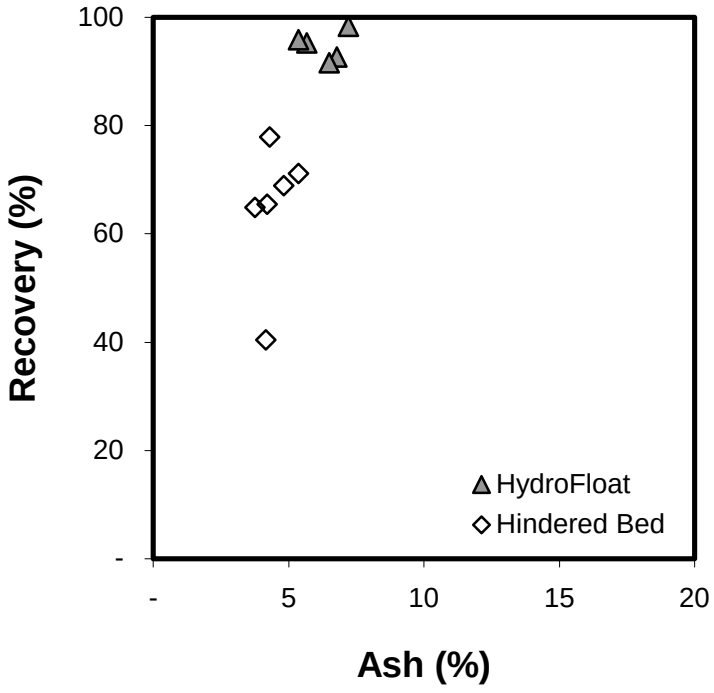

Figure 3.17 - Test results (cumulative) obtained using spiral feed from Central Appalachia.

3.5.2.3 Testing of Australian Coal

A sample of froth flotation feed from an Australian coal plant was obtained for testing in the HydroFloat separator. This sample was considered very coarse for traditional flotation processes, with over 25% of the coal greater than 0.6 mm (28 mesh). Traditionally, coal flotation suffers from low recoveries above 28 mesh. It was expected that the HydroFloat could recover the coarse feed material that was currently being lost in the froth flotation circuit. The feed to the unit was conditioned with diesel (0.25 kg/ton) and a glycol frother was used for bubble generation.

Table 3.1 provides a summary of the size-by-size recoveries and qualities obtained using the HydroFloat separator. Special attention was paid to the effect of particle size since the teeter water could easily propel fine ash particles (i.e., clay and mineral matter) into the concentrate. As shown, the preliminary data indicate the plus 28 mesh material could be cleaned to an acceptable ash content with combustible recoveries well above 90%. However, the ash content of the finer size fractions (below 65 mesh) increased sharply due to the carry-over of fine mineral matter. To overcome this problem, a second series of tests were conducted with the lab-scale HydroFloat in which the minus 65 mesh material was discarded. In this case, the HydroFloat was capable of combustible recoveries greater than 90% when air was added to the teeter-bed. In comparison, an average recovery of only 83% was achieved without the addition of air. However, the separator was capable of producing a higher quality (lower ash) product when no air was added. The higher ash values obtained using the HydroFloat can be attributed to the increased recovery of coarse high density middlings that report to the product stream when the teeter-bed is aerated.

Table 3.1 - Size-by-size HydroFloat results obtained using an Australian coal.

Sample Mesh	Yield (%)		Recovery (%)		Product Ash (%)
	Per Size Class	Cumulative	Per Size Class	Cumulative	
+16	85.0	0.5	94.4	0.8	8.4
16 x 20	80.4	8.0	93.1	12.0	13.8
20 x 28	75.8	28.2	91.7	41.6	16.5
28 x 65	61.4	61.6	86.3	83.9	21.2
-65	63.3	70.3	81.4	90.2	25.8

3.5.2.4 Testing of Heavy Mineral Sands

Two samples of heavy mineral sands were tested using the HydroFloat separator. The first sample contained unwanted carbonaceous matter as well as an undesirably high pyrite content (average 0.78% sulfur). To process this sample, the feed was first treated with sodium isopropyl Xanthate to make the pyrite hydrophobic and then passed through the HydroFloat unit. As shown in Figure 3.18, the HydroFloat separator achieved sulfur and carbon rejections of up to 80% and 55%, respectively. These rejections were maintained at a high product yield of approximately 97%. The second sample also contained an unacceptably high carbon content (average 0.92% fixed carbon). However, no Xanthate was added for this sample since the sulfur content was already within product specifications. Figure 3.19 shows that the HydroFloat separator was also effective in treating this sample. More than 81% of the carbon was removed from the feed material at a product yield of nearly 95%. The lower sulfur rejections reflect the low feed sulfur content (0.05%) of this particular sample.

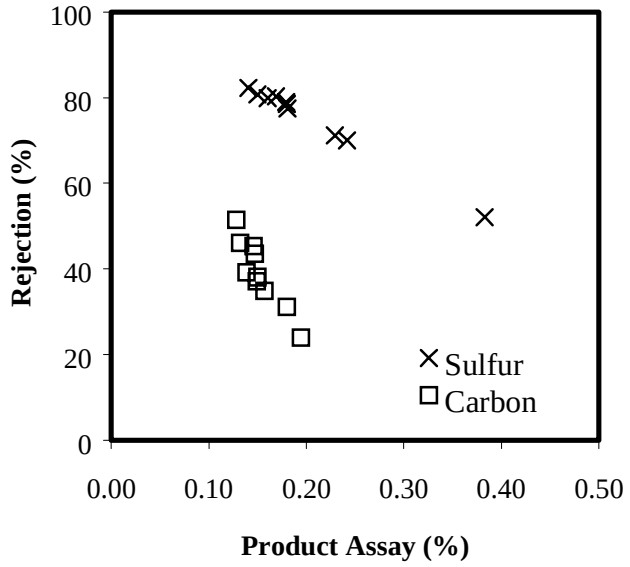

Figure 3.18 - HydroFloat results for the removal of impurities from mineral sands (Sample #1).

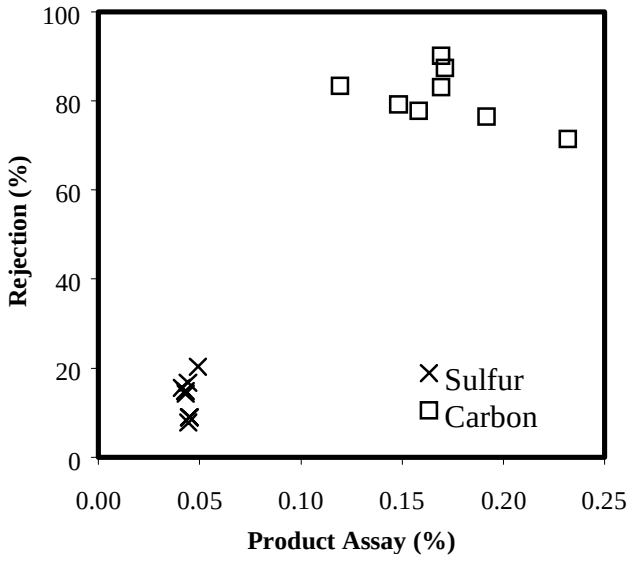

Figure 3.19 - HydroFloat results for the removal of impurities from mineral sands (Sample #2).

3.6 Pilot-Scale Testing

After the successful completion of the laboratory-scale proof-of-concept test work, sufficient data was obtained to justify pilot-scale testing of the HydroFloat separator. Pilot-scale work was carried out in two specific areas, namely, coal and phosphate. Two pilot-scale HydroFloat separators were fabricated to complete these investigations.

3.6.1 Northern Florida Phosphate Matrix

Phosphate testing was conducted at a northern Florida phosphate operation. To this end, a 0.60 m square by 2.0 m tall test unit was fabricated and installed at the processing facility. A photograph of the HydroFloat unit is provided in Figure 3.20. A flowsheet for the 10-15 tph test circuit is provided in Figure 3.21. Circuit feed was supplied from a port located in the feed line to a bank of plant dewatering cyclones used to prepare feed for existing conventional flotation cells. The feed slurry was passed through a hydroclassification circuit to produce a plus 0.6 mm underflow product. This material flowed by gravity into a bank of conditioning tanks where flotation and pH reagents were added. The operating conditions are summarized in Table 3.2. The product from the conditioners was then directed to the HydroFloat cell.

Table 3.2 - Parameters for in-plant pilot test program.

Parameter	CrossFlow	HydroFloat
Feed Rate (tph/sqft)	1-7	2-4
Feed Solids Density (%)	15-50	50-70
Water Addition Rate (gpm)	40-90	40-80
Aeration Rate (scfm)	n/a	2-5
Fatty Acid Dosage (lbs/ton)	n/a	1-3

Figure 3.20 - Photograph of the pilot-scale HydroFloat separator.

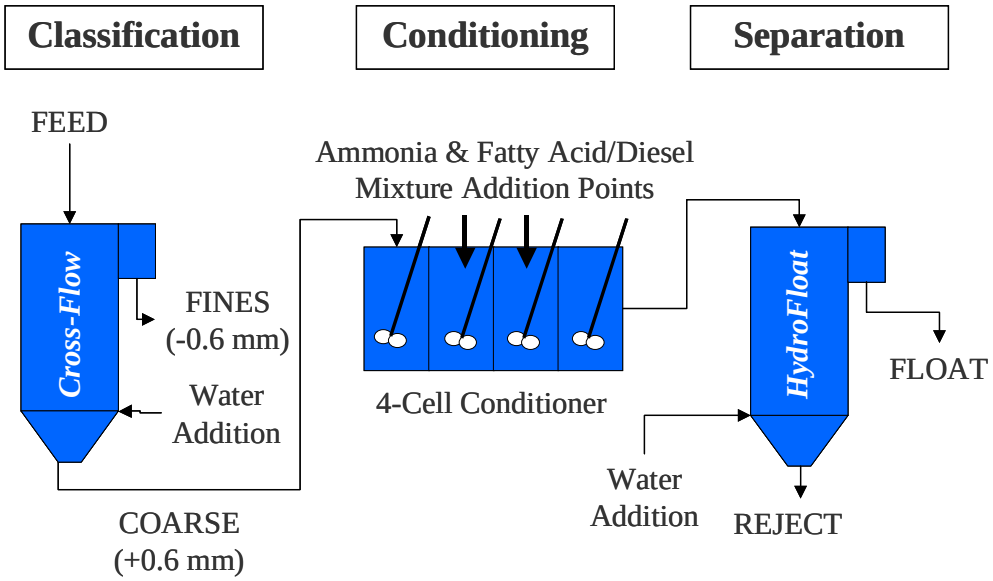

Figure 3.21 - Pilot-scale flotation circuit for phosphate investigation.

Table 3.3 provides a comparison of test data from the pilot-scale HydroFloat unit with that typically achieved by the existing full-scale conventional flotation circuit currently in operation at the phosphate plant. At present, the plant typically operates with a BPL recovery of approximately 35% for the plus 16 mesh feed and approximately 60% for the 16 x 35 mesh feed. In comparison, the HydroFloat unit achieved a BPL recovery of more than 60% for the plus 16 mesh feed and nearly 85% for the 16 x 35 mesh feed. This represents an increase in recovery of more than 40%. It is also interesting to note that the plus 16 mesh fraction had a very high BPL content (72.8% BPL) and very low insol content (4.0%). The combined (i.e., plus 35 mesh) concentrate from the HydroFloat cell represented at a total recovery of more than 80% with a BPL grade of 56.8%. This result compares very favorably with the existing plant recoveries of 80-85% normally achieved for the finer 35 x 150 mesh feed.

Table 3.3 - Comparison of typical plant data and pilot-scale HydroFloat test results.

Particle Size (mesh)	Plant Cells Recovery (%)	HydroFloat Recovery (%)	HydroFloat Grade (% BPL)
+ 16	≈ 35%	61.4%	72.8%
16 x 35	≈ 60%	84.7%	54.6%
Total	≈ 50%	80.5%	56.8%

In fact, BPL recoveries were generally higher using the HydroFloat when compared to actual plant data as seen in Figure 3.22. The data in this illustration show that the HydroFloat is capable of recovering the coarse phosphate particles that are generally lost in the conventional flotation cells. Naturally, as the particle size decreases, the performance of the HydroFloat matches that of conventional flotation. However, in the coarsest particle size range (10x16 mesh), the HydroFloat was capable of recovering nearly 70% of the available BPL, while conventional flotation only achieved a 17% BPL recovery.

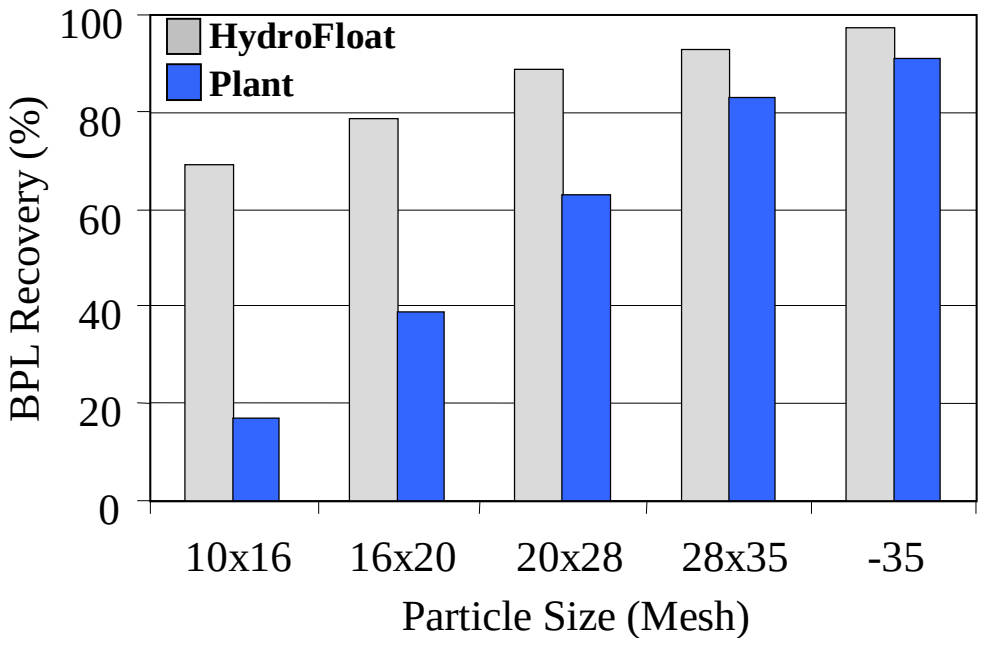

Figure 3.22 - HydroFloat and plant comparison data.

3.6.2 Appalachian Coal

The coal testing was completed at an Appalachian coal processing facility located in southwestern West Virginia. Tests were conducted using a round, 20 inch diameter HydroFloat as seen in Figure 3.23. This test unit is equipped similarly to the laboratory unit, with a PID controller, pressure sensor, and pneumatic valve. One outlet of a spiral distributor was redirected to provide constant feed (nominally 1mm x 65 mesh) to the HydroFloat. A ball valve was used to throttle the feed flow rate to the device. Feed rates generally ranged from 1-4 tph/ft^2, with diesel additions of approximately 0.25 lb/ton to enhance the recovery of the coarse middling coal. These operating conditions are summarized in Table 3.4.

Table 3.4 – Operating conditions for in-plant pilot test program.

Parameter	**HydroFloat**
Feed Rate (tph/sqft)	1-4
Feed Solids Density (%)	25-35
Water Addition Rate (gpm)	6-12
Aeration Rate (scfm)	2-5
Diesel Dosage (lbs/ton)	0.20-0.50

Figure 3.23 - Pilot-scale HydroFloat used for coal testing.

As in the laboratory coal investigation, the HydroFloat was tested with and without the addition of air bubbles in order to quantify the improvement, if any, over traditional hindered-bed separators. As seen in Figure 3.24, substantial increases in coal recovery were observed. Specifically, the recovery of the plus 28 mesh fraction of this sample was increased by nearly 40%. The 28 x 35 mesh fractional recovery increased by almost 20%. The data suggesting that the HydroFloat improved the recovery of coarse coal was further vindicated several times during this test work, as misplaced and extremely coarse coal particles in the spiral circuit arrived in the overflow launder of the HydroFloat (See Figure 3.25).

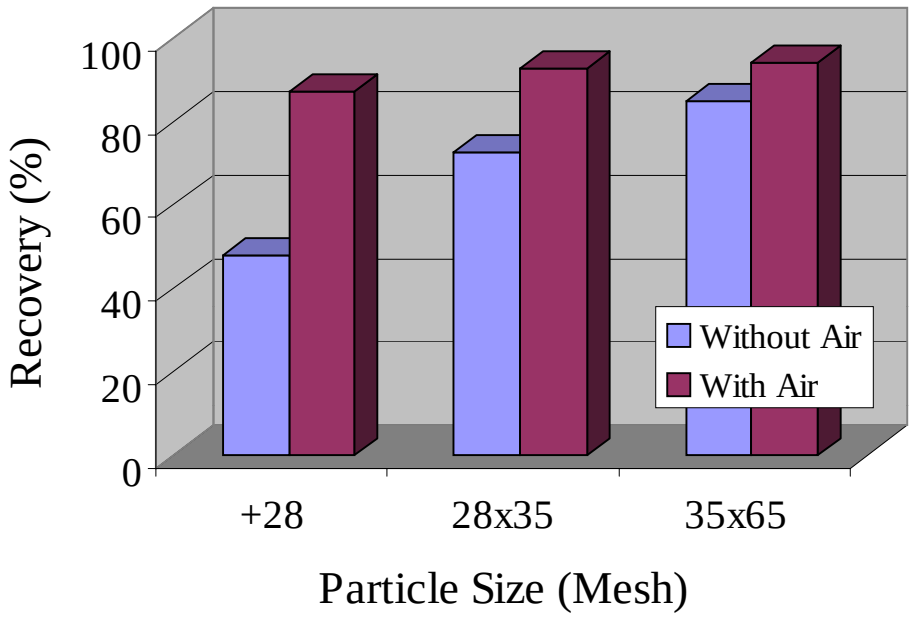

Figure 3.24 - Recovery data for the Appalachian coal tests.

Figure 3.25 - Coarse particles found in the HydroFloat product.

The HydroFloat was able to process and recover more coal without significantly increasing the ash content when compared to traditional hindered-bed separations (without air). Data presented in Figure 3.26 shows that for the plus 28 mesh fraction of coal, ash content increased by only a few percent. The ash contents of the 28x35 mesh size fractions were nearly identical. It must also be noted that the HydroFloat produced a significantly lower ash product when comparing the 35x65 mesh size fraction.

The HydroFloat was tested using feed diverted from a distributor, which was supplying feed to a bank of spirals. This bank of spirals was part of a rougher-cleaner spiral circuit with partial middlings, comparable to the spiral circuit advocated in Chapter 1 of this dissertation. Considering that the HydroFloat was treating the same material as the spiral circuit, a comparison was warranted. Data from a concurrent coal company directed, full-plant sampling endeavor were utilized in this effort. Figure 3.27 shows this data. It can be understood from this figure that the HydroFloat, operating without air, achieved recoveries far below those obtained by the existing spiral circuit. The coal spiral circuit also generally produced a higher quality (lower ash) product. However, when the HydroFloat operated with air, combustible recovery increased by nearly five percent. At optimum operating efficiency, the HydroFloat was able to slightly improve upon the product quality (ash content) produced by the coal spiral circuit.

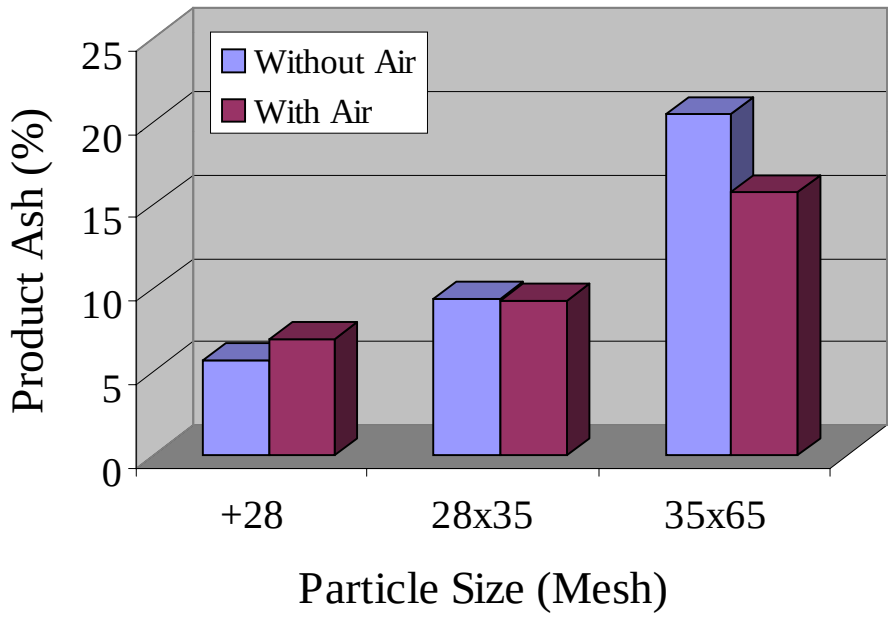

Figure 3.26 - Ash data for the Appalachian coal testing.

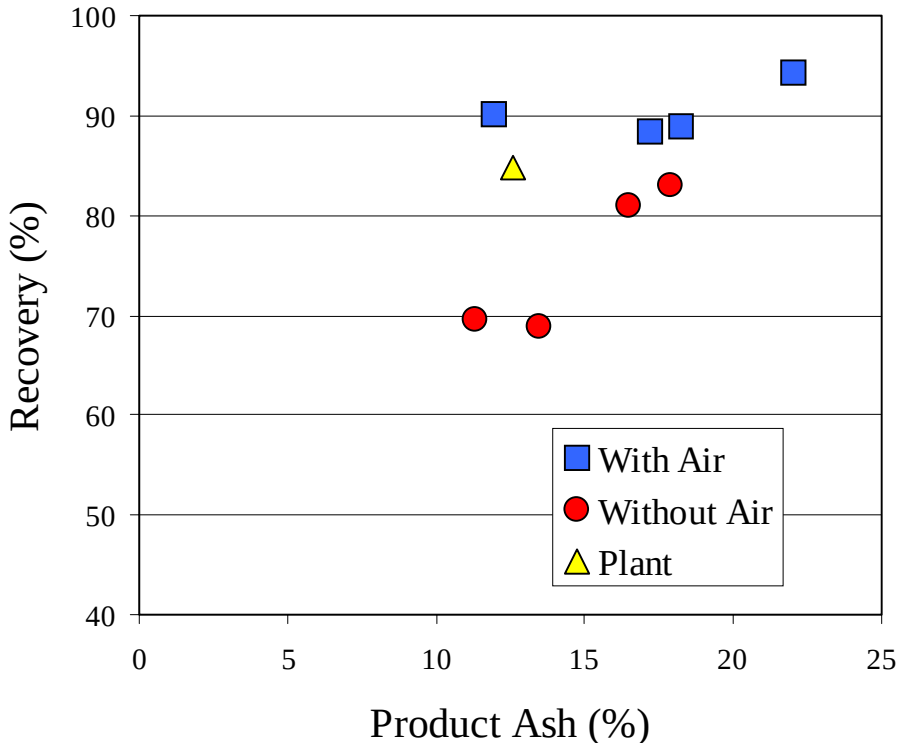

Figure 3.27 - HydroFloat and coal spiral comparative data.

3.7 Conclusions

1. A new separator, known as the HydroFloat unit, has been developed to overcome some of the shortcomings associated with traditional flotation machines in recovering coarse particles. The novel characteristic of this separator is the formation of a hindered "teeter" bed of fluidized solids into which small air bubbles are introduced. The bubbles attach to hydrophobic particles and create light bubble-particle aggregates that can be separated from hydrophilic particles based on the principle of differential density. Benefits of this new separator include enhanced bubble-particle contacting, better control of particle residence time, lower axial mixing/cell turbulence, and reduced air consumption.

2. Results from simulations conducted with a population balance model show that a decrease in the apparent specific gravity of one feed component can greatly increase the recovery of that component. If the density of a feed component can be altered through the attachment of air bubbles, the density ratio (ρ_1/ρ_2) decreases, resulting in large improvements in coarse particle recovery.

3. Laboratory tests were conducted with both batch and continuous HydroFloat cells in order to evaluate the potential of this new technology for upgrading mineral samples from various sources (e.g., phosphate matrix, coal, anthracite slag, mineral sands, etc.). The test data indicate that the HydroFloat cell is capable of increasing coarse particle recoveries by 20% over conventional flotation. Furthermore, the concentrate grades were also improved in some cases due to a reduction in coarse particle misplacement.

4. In light of promising laboratory data, a pilot-scale HydroFloat was installed at an industrial phosphate beneficiation plant. Test data obtained with this unit to date suggest that the BPL recovery of the plus 16 mesh feed can be nearly doubled (i.e., increased from approximately 35% to more than 65%) through the application of this new technology. In addition, the data suggest that the HydroFloat cell may be used to increase the BPL recovery of the 16 x 35 mesh material from about 60% to nearly 85%. As a result, the combined recovery of plus 35 mesh product from the HydroFloat cell compares very favorably with existing plant recoveries of 80-85% normally achieved for the 16 x 150 mesh feed.

5. A pilot-scale HydroFloat cell was also installed at an Appalachian coal preparation facility. Data obtained from these in-plant tests indicate increases of coarse coal (+28 mesh) recoveries of nearly 40% over traditional hindered-bed separators. Overall combustible recovery was increased by nearly 20%. Product quality and combustible recovery were consistent or better than that produced by an existing coal spiral circuit.

3.8 References

Ahmed, N. and Jameson, G.J., 1989, "Flotation Kinetics", *Mineral Processing and Extractive Metallurgy Review,* 1989, Vol. 5, pp. 77-99.

Anazia, I. and Hanna, J., 1988, "Innovative Process for Beneficiation of Dolomitic Phosphate Ores," International Journal of Mineral Processing, Vol. 23, pp. 311-314.

Anazia, I. and Hanna, J., 1987, "New Flotation Approach for Carbonate Phosphate Separation," Minerals and Metallurgical Processing, Vol. 4, No. 4, pp. 196-202.

Arbiter, N. and Steinenger, J., 1965, "Hydrodynamics of Flotation Machines," Mineral Processing, Pergamon Press, p. 595.

Arbiter, N. and Harris, C.C., 1962, "Flotation Kinetics," Froth Flotation – 50th Anniversary Volume, (D.W. Fuerstenau, Ed.), Chpt. 8, American Institute of Mining, Metallurgy and Petroleum Engineers, Inc., New York, New York, pp. 215-246.

Barbery, G., 1989, "Method for Separation of Coarse Particles", U.S. Patent No. 4,822,493.

Barbery, G., 1984, "Engineering Aspects of Flotation in the Minerals Industry: Flotation Machines, Circuits and Their Simulation," The Scientific Basis of Flotation, (K. J. Ives, Ed.), NATO Advanced Institute Services, Series E: Applied Sciences, No. 25, Martinus Nijhoff Publishers, Boston, Massachusetts, pp. 289-348.

Bensley, C.N. and Nicol, S.K., 1985, "The Effect of Mechanical Variables on the Flotation of Coarse Coal," Coal Preparation, Vol. 1, pp. 189-205.

Brown, D.J. and Smith, H.G., 1954, "The Flotation of Coal as a Rate Process," Transactions, Institution of Mining Engineers, Vol. 113, pp. 1001-1020.

Bull, W.R., 1966, "The Rates of Flotation of Mineral Particles in Sulphide Ores," Proceedings, Australian Institute of Mining and Metallurgy, No. 220, December 1966, pp. 69-78.

Crawford, R. and Ralston, J., 1988, "The Influence of Particle Size and Contact Angle in Mineral Flotation", International Journal of Mineral Processing, Vol. 23, pp. 1-24.

Crawford, J.T., 1936, "Importance of Pulp Density, Particle Size, and Feed Regulation in Flotation of Coal," Transactions of AIME, Vol. 119, pp. 150-162.

Damodaran, R.M., Fahey, M. and Moudgil, B.M., "Bench-Scale Optimization of Mixing Variables During Anionic Conditioning of Florida Phosphates," Minerals and Metallurgical Processing, February 1996.

Davis, B.E. and Hood, G.D., 1994, "Conditioning Parameter Effects on the Recovery of Coarse Phosphate," Minerals and Metallurgical Processing, Vol. 11, No. 1, pp. 50-54.

Davis, B.E. and Hood, G.D., 1993, "Improved Recovery of Coarse Florida Phosphate," Mining Engineering, Vol. 45, No. 6, pp. 596-599.

Davis, B.E. and Hood, G.D., 1992, "Conditioning Parameter Effects on the Recovery of Coarse Phosphate," Proceedings, Regional AIME/AIChE/AIPG/FIPR Phosphate Conference, Lakeland, Florida, Sept. 24-25.

El-Shall, H., Zhang, P. and Snow, R., 1996, "Comparative Analysis of Dolomite/Francolite Flotation Techniques," Minerals and Metallurgical Processing, Vol. 13, No. 3, pp. 135-140.

El-Shall, H., Moudgil, B. and Wiegel, R., "Beneficiation of Phosphate: Theory and Practice", Engineering Foundation Conference, Palm Coast, Florida, editors; December 1993.

Finch J.A. and Dobby, G.S., Column Flotation, Pergamon Press, 1990.

Florida Institute of Phosphate Research, Publication No. 01-102-112, "Defining the MgO Problem and Its Economic Impact on Phosphoric Acid Production", Prepared by Jacobs Engineering Group, Inc. and A.N. Baumann, February 1995.

Florida Institute of Phosphate Research, Publications No. 02-090-121, "Understanding the Basics of Anionic Conditioning in Phosphate Flotation," Prepared by Jacobs Engineering Group, Inc., May 1995.

Florida Institute of Phosphate Research, Publication No. 04-045-103, "An Optical Sensor for On-Line Analysis of Phosphate Minerals", Prepared by Virginia Polytechnic Institute & State University, April 1994.

Florida Institute of Phosphate Research, Publication No. 02-080-109, "On-Line Analysis of Phosphate Rock Slurry by Prompt Neutron Activation Technique", Prepared by University of Florida, July 1994.

Florida Institute of Phosphate Research, Publication No. 02-094-108, "Evaluation of Dolomite Separation Techniques", Prepared by Hassan El-Shall, Global Marketing and Consulting, October 1994.

Florida Institute of Phosphate Research, Publication No. 02-067-099, "Enhanced Recovery of Coarse Particles During Phosphate Flotation", Prepared by University of Florida, June 1992.

Florida Institute of Phosphate Research, Publication No. 02-070-098, "Development of Novel Flotation-Elutriation Method for Coarse Phosphate Beneficiation", Prepared by Laval University, June 1992.

Florida Institute of Phosphate Research, Publication No. 04-032-091, "An Investigation of Potential for Improved Efficiencies in Phosphate Rougher Flotation Through On-Line BPL Measurements", prepared by Harrison R. Cooper Systems, Inc., March 1991.

Florida Institute of Phosphate Research, Publication No. 02-063-071, "Anionic Flotation of Florida Phosphate", prepared by Zellar-Williams, Inc., February 1989.

Furey, J. and Mankosa, M.J., "Column Flotation in the Phosphate Industry", Presented to Tenth Annual Regional Phosphate Conference, Lakeland, Florida, October 1995.

Gaudin, A., Grob, J. and Henderson, H., 1931, “Effect of Particle Size in Flotation,” Technical Publication No. 414, AIME.

Harris, M.C., Franzidis, J.P., O’Conner, C.T. and Stonestreet, P., 1992, “An Evaluation of the Role of Particle Size in the Flotation of Coal Using Different Cell Technologies,” Minerals Engineering, Vol. 5, No. 10/12, pp. 1225-1238.

Heiskanen, K., Particle Classification, Chapman & Hall, 1993.

Hutwelker, J.F., “High Throughput Flotation Column Process,” U.S. Patent No. 5,307,937.

Ives, K.J., Editor, The Scientific Basis of Flotation, NATO Advanced Science Institutes Series, Martinus Nijhoff Publishers, 1984.

Jameson, G.J., Nam, S. and Young, M.M., 1984, “Physical Aspects of Fine Particle Flotation,” Principles of Mineral Flotation, Vol. 215.

Jameson, G.J., Nam, S. and Young, M.M., 1977, “Physical Factors Affecting Recovery Rates in Flotation,” Minerals Science and Engineering, Vol. 9, No. 3, pp. 103-118.

Kawatra, S.K., Editor, High Efficiency Coal Preparation: An International Symposium, SME, Littleton, CO, 1995.

Keating, J., 1999, Personal Communication, IMC-Agrico.

King, R.P., Hatton, T.A. and Hulbert, D.G., 1974, “Bubble Loading During Flotation,” Technical Note, Transactions of the Institute of Mining and Metallurgy, Section C, March, p. C9.

Laskowski, J., 1995, “Flotation Process for the Flotation of Coarse Fractions Potash Ore”, U.S. Patent No. 5,456,362.

Lawver, J.E., Bernardi, J.P., McKeraghan, G.F., Raulerson, J.D., Lynch, D. and Hearon, R.S., 1984, “New Techniques in Beneficiation of the Florida Phosphates of the Future,” Minerals and Metallurgical Processing, Vol. 1, No. 2, pp. 89-106.

Lawver, J., McClintock, W.O. and Snow, R.E., 1978, “Beneficiation of Phosphate Rock: A State of the Art Review,” Minerals Science and Engineering, Vol. 10, No. 4, pp. 278-294.

Llewllyn, T.O., Davis, B.E. and Sullivan, G.V., 1984, “Beneficiation of Florida Dolomite Phosphate Ores,” Minerals and Metallurgical Processing,” Vol. 1, No. 1, pp.43-48.

Luttrell, G.H., 2000, “Column Flotation Workshop,” conducted for CONSOL Energy, Osage, WV, Aug. 22.

Mankosa, M.J., Luttrell, G.L, Gruber, G. and Shoniker, J., 1999, “In-Plant Testing of the HydroFloat Separator for Coarse Phosphate Recovery,” Proposal to Florida Institute of Phosphate Research, FIPR #99-02-137.

Mankosa, M.J., Forrest, M.L. and Furey, J.T., “Application of the Cominco Column Cell for Coarse Phosphate Flotation, CIM 35th Annual Conference of Metallurgists, Montreal, Quebec, Canada, August 1996.

Mankosa, M.J., Luttrell, G.H., Adel, G.T. and Yoon, R.-H., 1992, "A Study of Axial Mixing in Column Flotation," International Journal of Mineral Processing, Vol. 35, pp. 51-64.

McHardy, J.C., 1983, “New Trends in Florida Phosphate Mining,” Mining Engineering, Vol. 35, No. 8, pp. 1196-1200.

McKnight, K., Stouffer, N., Domenico, J. and Mankosa, M.J., “Recovery of Zircon and Other Economic Minerals from Wet-Gravity Tailings Using the Floatex Density Separator”, SME Annual Meeting, Phoenix, Arizona, March 1996.

Morris, T.M., 1952, “Measurement and Evaluation of the Rate of Flotation as a Function of Particle Size,” Mining Engineering, Vol. 4, No. 8, pp. 794-798.

Moudgil, B.M. and Gupta, D., 1989, “Flotation of Coarse Phosphate Particles,” Advances in Coal and Mineral Processing Using Flotation, Proceedings of an Engineering Foundation Conference, Dec. 3-8, pp.164-168.

Moudgil, B.M. and Barnett, D.H., 1979, "Agglomeration Skin Flotation of Coarse Phosphate Rock," Mining Engineering, Vol. 31, No. 3, pp. 283-289.

Olsen, S.I. and Miller, H.H., 1981, "Improved Recovery of Florida Phosphate Rock by Modifying Standard 14 m^3 (500 ft^3) Wemco Cells with 28 m^3 (1000 ft^3) Cell Mechanisms," SME-AIME Fall Meeting and Exhibit, Denver, Colorado, Nov. 18-20.

Oteyaka, B. and Soto, H., 1995, "Modeling of a Negative Bias Flotation Column For Coarse Particles Flotation," Minerals Engineering, Vol. 8, No. 1/2, pp. 91-100.

Phillips, D.I., 1998, "Optimum Processing of 1mm by Zero Coal," Ph.D. Dissertation, Dept. of Mining and Minerals Engineering, Virginia Polytechnic Institute and State University, 196 pp.

Rastogi, R.C. and Aplan, F.F., 1985, "Coal Flotation as a Rate Process," Minerals and Metallurgical Processing, Vol. 2, pp. 137-147.

Robinson, A.J., 1959, "Relationship Between Particle Size and Collector Concentration," Transactions, Institution of Mining and Metallurgy, No. 69, pp. 45-62.

Schulze, H.J., 1984, "Physio-Chemical Elementary Processes in Flotation," Developments in Mineral Processing, Vol. 4, Chpt. 5, Elsevier, New York, pp. 238-253.

Schulze, H.J. and Gottschalk, 1981, Proceedings of the 13th International Mineral Processing Congress, Warsaw, Poland, June 1979, Part A, Elsevier, New York, New York, p. 63.

Schulze, H.J., 1977, "New Theoretical and Experimental Investigations on Stability of Bubble/Particle Aggregates in Flotation: A Theory on the Upper Particle Size of Floatability," International Journal of Mineral Processing, No. 4, pp. 241-259.

Schumann, R., 1942, "Flotation Kinetics, Methods for Steady-State Study of Flotation Problems," Journal of Physical Chemistry, Vol. 46, pp. 891-902.

Soto, H. and Barbery, G., 1991, "Flotation of Coarse Particles in a Counter-Current Column Cell," Minerals and Metallurgical Processing, Vol. 8, No. 1, pp. 16-21.

Soto, H., 1988, Private Report to the Florida Institute of Phosphate Research.

Soto, H. and Barbery, G., 1987, "Method and Apparatus for Separation of Coarse Particles," U.S. Patent Application No. 125-709.

Soto, H. and Iwasaki, I., 1986, "Selective Flotation of Phosphate from Dolomite Using Cationic Collectors. Part II," International Journal of Mineral Processing, No. 16, pp. 17-27.

Sun, S. and Zimmerman, R.E., 1950, "The Mechanism of Coarse Coal and Mineral Froth Flotation," Mining Engineering, Vol. 187, No. 5, pp. 616.

Sutherland, K.L., 1948, "Kinetics of the Flotation Process," Journal of Physical Chemistry, Vol. 52, pp. 394-425.

Trahar, W.J., 1981, "A Rational Interpretation of the Role of Particle Size in Flotation," International Journal of Mineral Processing, Vol. 8, pp. 289-327.

Trahar, W.J. and Warren, L.J., 1976, "The Floatability of Very Fine Particles – A Review," International Journal of Mineral Processing, Vol. 3, pp. 103-131.

United States Geological Survey, Mineral Commodity Summary, January, 1999.

Woodburn, E.T., King, R.P. and Colborn, R.P., 1971, "The Effect of Particle Size Distribution on the Performance of a Phosphate Flotation Process," Metallurgical Transactions, Vol. 2, pp. 354-362.

Yoon, R.-H. and Mao, L., 1997, "Predicting Flotation Rates Using a Rate Equation Derived from First Principles," International Journal of Mineral Processing, Vol. 51, No. 1-4, pp. 171-181.

Yoon, R.-H. and Luttrell, G.H., 1989, "The Effect of Bubble Size on Fine Particle Flotation," Mineral Processing and Extractive Metallurgy Review, Vol. 5, Gordon and Breach Science Publishers, Inc., Great Britain, pp. 101-122.

CHAPTER 4

General Summary

Mathematical analysis tools, including linear circuit analysis and population balance modeling, have been utilized to analyze and evaluate some water-based processes. The data collected from these investigations were used to make modifications and/or improvements in coal spiral circuitry, hydraulic classification and hindered-bed separation. These improvements resulted in increased separation efficiency and unit capacity. A better understanding of two novel pieces of mineral processing equipment (i.e., the CrossFlow and HydroFloat separators) were also a result of these analyses. In review, several points of summary can be identified from this work.

Improving Spiral Performance Using Circuit Analysis

1. Linear circuit analysis, a theoretical tool for comparing the relative effectiveness of various configurations of unit operations, was successfully applied to coal spiral circuitry. Early studies identified several coal spiral circuits that had the potential to improve separation efficiency. One circuit in particular, a rougher-cleaner configuration with partial middlings recycle, was capable of improving separation efficiency (*Ep*) approximately 1.22 times that of more traditional coal spiral circuits. A reduced circuit SG_{50} and reasonable circulating load were also a benefit of this modified circuit when compared to other preferred unit configurations.

2. Based on circuit analysis fundamentals, an alternative method was derived for determining the partition expressions for any given spiral circuit. This method allows for the prediction of efficiency (*Ep*), circuit cut-point or any other partition based result (i.e., SG_{25} or SG_{75}) independent of washability data, provided a proper partition function is used.

3. In-plant testing of a full-scale, two-stage spiral circuit allowed for the comparison of several alternative circuit configurations. Data obtained during the in-plant circuit evaluations indicated that for an equivalent number of spirals, rougher-cleaner circuits operated in series are far superior than parallel circuits for reducing circuit cut-point.

4. In-plant test data also indicated that although the circuit SG_{50} for rougher-cleaner coal spiral circuits operated with and without a middlings recycle are very similar (i.e., ≈ 1.65 SG), the separation efficiency increased when a middling recycle stream was utilized. In fact, separation efficiency was approximately 1.25 times higher for the circuit incorporating a middlings recycle stream.

5. Using the in-plant test data, regression equations were developed that were used to simulate alternative spiral configurations. Although a rougher spiral separation could be adequately simulated using an expression developed by Reid (1971), the increased loading of near-gravity material often found on a cleaner bank of spirals necessitated the development of an alternative expression. This expression (i.e., the modified Reid equation) accurately simulates an asymmetrical coal spiral partition in which a large amount of high gravity material is misplaced to the clean coal launder.

6. Simulations demonstrated that the rougher-cleaner coal spiral circuit incorporating a middlings recycle was capable of a separation efficiency (*Ep*) 1.20 times that of a rougher-cleaner spiral circuit without middlings recycle. This ratio compares favorably with both the theoretical ratio of 1.22 predicted by circuit analysis and the ratio of 1.25 demonstrated by actual in-plant performance.

7. The simulations further demonstrated that at a constant ash, the rougher-cleaner spiral circuit with middlings recycle is capable of increasing circuit yield by as much as 3.86%. This relatively small increase in yield translates to a growth in revenue of nearly $255,000 for the coal preparation facility at which the on-site tests were conducted. Furthermore, this increase does not reflect the additional salable coal yielded by the coarse coal dense medium circuits, which can now operate at higher effective gravities as a result of the lower overall cut-point of the spiral circuit.

Improving Performance of Hindered-Bed Separators

1. Data from comparative in-plant and laboratory studies show that the feed presentation system of the CrossFlow separator offers several advantages. Results from tests conducted with phosphate matrix, limestone aggregate and heavy mineral consistently showed an increase in capacity and separation efficiency when compared to traditional hindered-bed separators.

2. A population balance model was developed to study and understand the operation of the newly developed CrossFlow hindered-bed separator. This model was based on general hindered-settling equations for transitional flow regimes. Model input data include feed rate, feed percent solids (by mass), feed size distribution (up to 9 size fractions), density of up to two feed components, fluidization water rate, and underflow discharge rate. Output results included overflow and underflow partition data, size distributions, component recovery, and classification efficiency in terms of *Ep* or Imperfection.

3. Validation test work indicated a good correlation existed between the laboratory and model simulation results. Reliable consistency was found for separation cut-point (d_{50}) and efficiency (i.e., *Ep* or *I*). During the validation test work, a correlation between target cut-point (d_{50}) and the maximum concentration by volume of solids (ϕ_{max}) was confirmed. This linear relationship appears to vary with material, feed size distribution, and consequently, separation cut-point (d_{50}).

4. Data produced from simulations using the population balance model indicate that the cross-flow feed presentation system has several advantages when compared to those used in conventional hindered-bed separators. These benefits include increased operational stability and a unit capacity of up to 6 tph/ft^2 (71.2 tph/m^2). Simulation data also show that the CrossFlow can maintain an acceptable and less varied efficiency over a wide range of operating conditions, including low feed percent solids (i.e., approaching 24% by mass).

5. Laboratory solid and liquid tracer studies of the CrossFlow separator suggest that excess feed water and solids that should report to the overflow launder are quickly off-loaded by the cross-flowing action of the feed presentation system. This occurs without disturbing the volume of material within the separation chamber. In contrast, traditional hindered-bed separators employing downcomer technology inefficiently use separation chamber volume to manage excess feed water and segregate overflow material prior to discharge.

Improving Coarse Particle Recovery in Hindered-Bed Separators

1. A hindered-settling population balance model was developed and utilized to identify an approach to overcome the inherent disadvantages often found in conventional teeter-bed separators when used as density separation devices. A feed consisting of up to two density components and nine size fractions could be employed with this model. Output results include component partition, recovery and rejection data.

2. Results from the modeling investigations suggest that any alteration of apparent density of any one feed component can greatly effect the recovery of that component. Data showed that an increase in the recovery of coarse, low density material could be realized if the apparent specific gravity of that component could be modified (i.e., lowered). In fact, further simulation indicated that recovery could increase by up to 60%.

3. To this end, the HydroFloat separator was developed based on flotation fundamentals. This device uses an aerated teeter-bed through which bubbles can rise and attach to hydrophobic particles. The attachment of air bubbles sufficiently reduces the apparent density of the

hydrophobic particles. These low density bubble-particle aggregates are then separated from the hydrophilic particles based on the principle of differential density.

4. Data from laboratory proof-of-concept testing indicate that the HydroFloat cell was successful in upgrading various types of minerals, including phosphate matrix, coal, anthracite slag, and mineral sands. Data further indicate the HydroFloat cell is capable of increasing the recovery of coarse (2mm x 50 mesh) particles over that traditionally found in either froth flotation or conventional hindered-bed separations. Coarse particle misplacement was also reduced resulting in improved product concentrate grades.

5. In-plant testing was conducted at a north Florida phosphate beneficiation plant. Coarse phosphate recovery increased substantially using the HydroFloat cell when compared to existing conventional froth flotation cells. BPL recovery nearly doubled for the +16 mesh size fraction, and an increase of 25% was also achieved for the 16 x 35 mesh size fraction. Product quality also improved due to the increased recovery of substantially higher grade, coarse phosphate.

6. Further in-plant testing of the HydroFloat cell was conducted at an Appalachian coal processing facility. Increases of up to 40% in coarse coal recovery were realized using the HydroFloat cell when compared to a traditional hindered-bed separator. As a result, an increase of 20% in combustible recovery was also achieved. A concurrent in-plant survey showed that the HydroFloat cell was capable of achieving a product quality and combustible recovery equivalent to that of an existing coal spiral circuit.

CHAPTER 5

Recommendations for Future Work

Several suggestions for follow-up efforts are offered here. These recommendations address all aspects of this investigation as seen below.

Improving Spiral Performance Using Circuit Analysis

1. It is recommended that a plant-wide study be conducted in order to quantify the improvements seen throughout the coal preparation facility as a direct result of the reduced cut-point in the spiral circuitry. As the specific gravity cut-point of the spiral circuit becomes lower, the cut-points of other circuits in the plant should increase slightly to compensate for the decrease in product ash content. These higher cut-points should translate to increased revenue since these circuits generally treat coarser material at higher tonnages and efficiencies.

2. It is suggested that several other preferred circuit configurations be tested in plant. Several configurations as indicated by linear circuit analysis had relative efficiencies better than the rougher-cleaner configuration that incorporated middlings recycle (See Table 1.1). These were discounted due to the impracticality and added cost associated with an increased circulating load in the spiral circuit. Because the improved spiral circuit efficiency will impact the entire plant, these alternative preferred circuits with high circulating loads may be feasible when accounting for total improvement in plant performance.

Improving Performance of Hindered-Bed Separators

1. As stated in Chapter 2, the CrossFlow population balance model was capable of predicting classification cut-point with a high degree of accuracy. However, the model had some difficulty predicting efficiency, predominantly showing slightly lower efficiencies than what is seen in actuality. This is most likely caused by a discretization error found in the feed section of the population balance model. Currently, the feed section of the model is composed of 25 zones, in a 5 by 5 configuration. It is recommended that this feed section be expanded to contain a higher number of zones to minimize the discretization error. In fact, a continuous model would prove to be most useful.

2. It is also recommended that more in-plant test work be completed which directly compares the CrossFlow to other conventional hindered-bed separators under identical conditions. This test work would help to quantify the advantages offered by the CrossFlow separator.

Improving Coarse Particle Recovery in Hindered-Bed Separators

1. It is suggested that an advanced, full-scale, in-plant evaluation of the HydroFloat be undertaken. A beneficiation plant will prove to be the only location where a high rate of constant feed can be maintained for test purposes. The effect of treating coarse (1mm x 50 mesh) material with the HydroFloat can also be quantified with respect to any performance changes in the conventional flotation cells.

2. The development of a hybrid, hindered-bed/flotation-based population balance model for the HydroFloat separator is highly recommended. Although the separation of components in this

device is based on differences in apparent density, many operating characteristics are flotation based. It is important to understand the effect, if any, that bubble size, air fraction, aeration rate, etc., will have on the flotation and the recovery of coarse particles with respect to the overall performance of this device.

APPENDIX A

Mass-Balance Equations

Flow Balances

Using the overall CrossFlow zone schematic shown in Figure A1, the following overall volumetric flow balances can be written:

$$Q_F + Q_W = Q_U + Q_{L_{O_5}}$$
$$Q_Z = Q_W - Q_U$$

where Q_F, Q_W, Q_U, and Q_{LO5} are the feed, elutriation, underflow, and overflow volumetric flows, respectively. The feed, elutriation and underflow flow rates are known at time t = 0.

Using the enlarged feed zone schematic seen in Figure A2, the following flow balance can be written:

$$Q_{L_{O_5}} = Q_F + Q_{X_1}$$

where Q_{X1} is the vertical upwards flow rate exiting zone A and entering the feed zone sections.

The fluidized-bed evenly distributes all vertical flows evenly across the cross-sectional area of the separator, except for the first five vertical zones (O_1, B_1, C_1, D_1, and E_1). In these zones, it can be shown that the falling action of feed solids and associated liquid prevents little or no upward flow from entering. This assumption is valid as the cross-sectional area of these zones is minimized. Using this information, the following flow balances can be equated:

$$Q_{X_2} = Q_{X_1} + Q_{L_{B_1}} + \sum Q_{D_{C_{2-4}}} - \sum Q_{D_{B_{2-4}}}$$
$$Q_{X_3} = Q_{X_2} + Q_{L_{C_1}} + \sum Q_{D_{D_{2-4}}} - \sum Q_{D_{C_{2-4}}}$$
$$Q_{X_4} = Q_{X_3} + Q_{L_{D_1}} + \sum Q_{D_{E_{2-4}}} - \sum Q_{D_{D_{2-4}}}$$
$$Q_{X_5} = Q_{X_4} + Q_{L_{E_1}} + \sum Q_{D_{O_{2-4}}} - \sum Q_{D_{E_{2-4}}}$$

where Q_D is the is the downward volumetric flow induced by the settling action of solids in to and out of each respective zone.

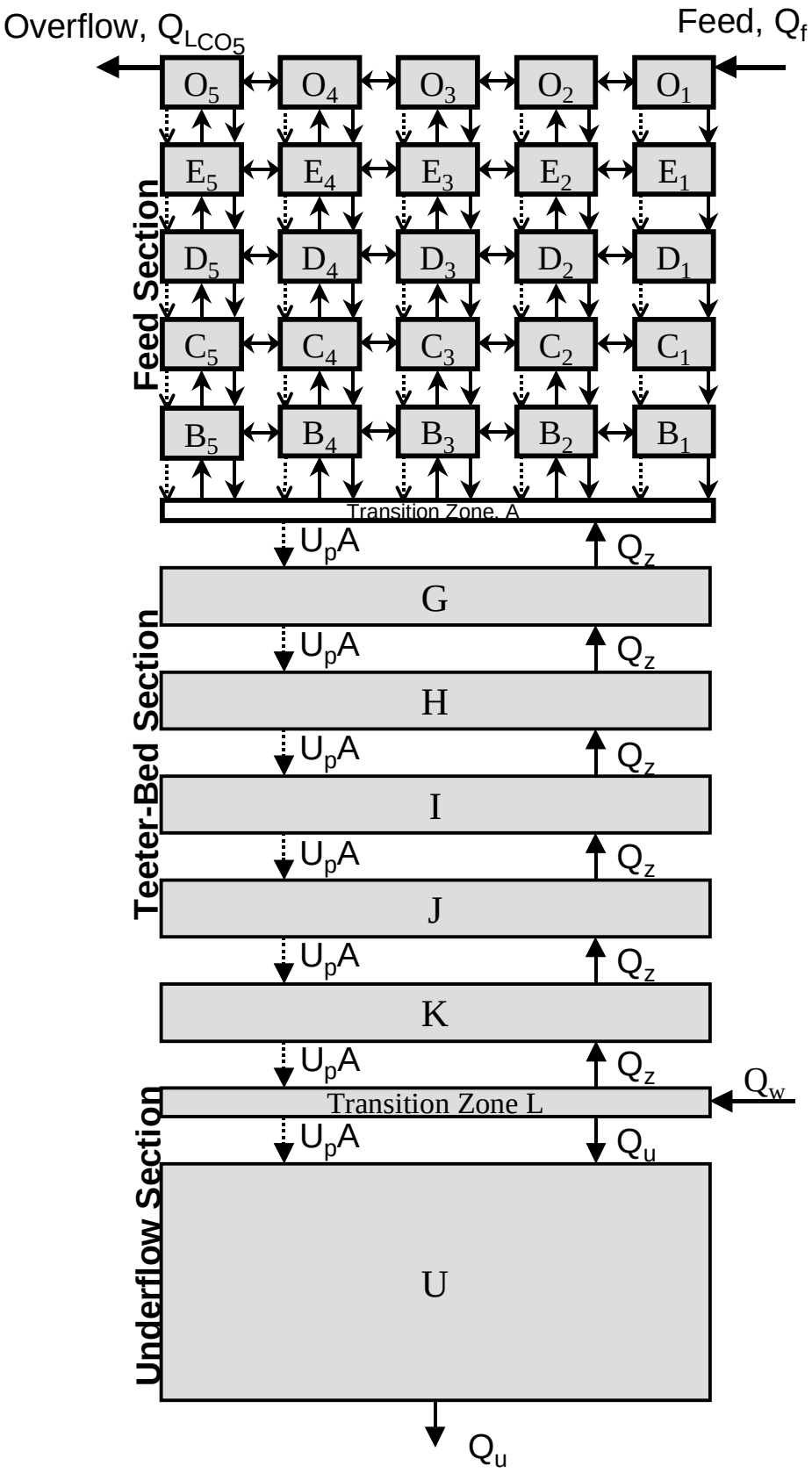

Figure A1 – Overall zones and major flows in the CrossFlow population balance model.

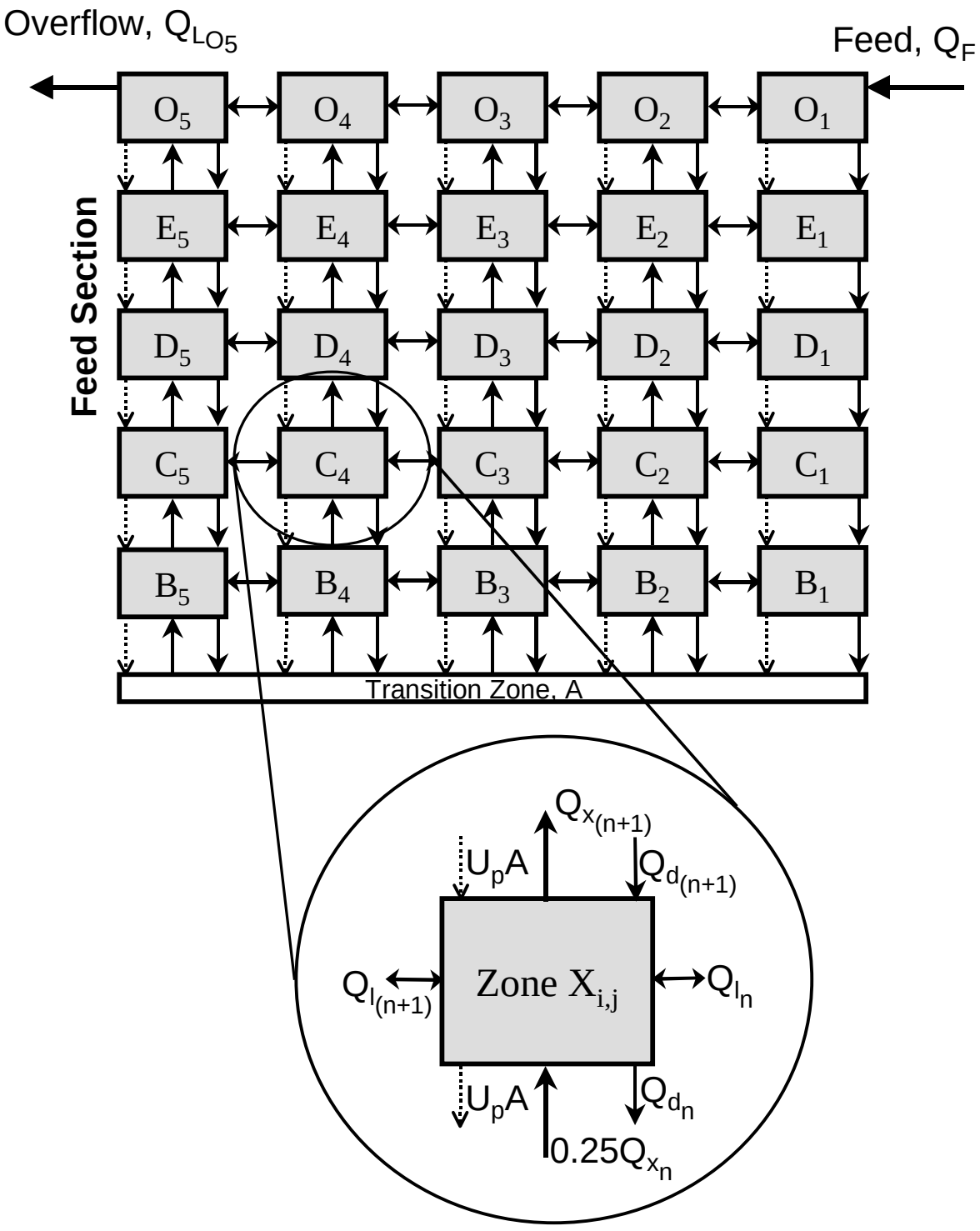

Figure A2 – Zone and flow schematic for feed section of CrossFlow model.

The horizontal flows that are found between each zone of the feed section can be determined from simple flow balances around each zone. Completing these flow balances yield the following equations:

$$Q_{L_{O_1}} = Q_F - Q_{D_{O_1}}$$
$$Q_{L_{O_2}} = 0.25 * Q_{X_5} + Q_{L_{O_1}} - Q_{D_{O_2}}$$
$$Q_{L_{O_3}} = 0.25 * Q_{X_5} + Q_{L_{O_2}} - Q_{D_{O_3}}$$
$$Q_{L_{O_4}} = 0.25 * Q_{X_5} + Q_{L_{O_3}} - Q_{D_{O_4}}$$
$$Q_{L_{O_5}} = 0.25 * Q_{X_5} + Q_{L_{O_4}} - Q_{D_{O_5}}$$

$$Q_{L_{E_1}} = Q_{D_{O_1}} - Q_{D_{E_1}}$$
$$Q_{L_{E_2}} = 0.25 * Q_{X_4} + Q_{D_{O_2}} + Q_{L_{E_1}} - 0.25 * Q_{X_5} - Q_{D_{E_2}}$$
$$Q_{L_{E_3}} = 0.25 * Q_{X_4} + Q_{D_{O_3}} + Q_{L_{E_2}} - 0.25 * Q_{X_5} - Q_{D_{E_3}}$$
$$Q_{L_{E_4}} = 0.25 * Q_{X_4} + Q_{D_{O_4}} + Q_{L_{E_3}} - 0.25 * Q_{X_5} - Q_{D_{E_4}}$$

$$Q_{L_{D_1}} = Q_{D_{E_1}} - Q_{D_{D_1}}$$
$$Q_{L_{D_2}} = 0.25 * Q_{X_3} + Q_{D_{E_2}} + Q_{L_{D_1}} - 0.25 * Q_{X_4} - Q_{D_{D_2}}$$
$$Q_{L_{D_3}} = 0.25 * Q_{X_3} + Q_{D_{E_3}} + Q_{L_{D_2}} - 0.25 * Q_{X_4} - Q_{D_{D_3}}$$
$$Q_{L_{D_4}} = 0.25 * Q_{X_3} + Q_{D_{E_3}} + Q_{L_{D_3}} - 0.25 * Q_{X_4} - Q_{D_{D_4}}$$

$$Q_{L_{C_1}} = Q_{D_{D_1}} - Q_{D_{C_1}}$$
$$Q_{L_{C_2}} = 0.25 * Q_{X_2} + Q_{D_{D_2}} + Q_{L_{C_1}} - 0.25 * Q_{X_3} - Q_{D_{C_2}}$$
$$Q_{L_{C_3}} = 0.25 * Q_{X_2} + Q_{D_{D_3}} + Q_{L_{C_2}} - 0.25 * Q_{X_3} - Q_{D_{C_3}}$$
$$Q_{L_{C_4}} = 0.25 * Q_{X_2} + Q_{D_{D_4}} + Q_{L_{C_3}} - 0.25 * Q_{X_3} - Q_{D_{C_4}}$$

$$Q_{L_{B_1}} = Q_{D_{C_1}} - Q_{D_{B_1}}$$
$$Q_{L_{B_2}} = 0.25 * Q_{X_1} + Q_{D_{C_2}} + Q_{L_{B_1}} - 0.25 * Q_{X_2} - Q_{D_{B_2}}$$
$$Q_{L_{B_3}} = 0.25 * Q_{X_1} + Q_{D_{C_3}} + Q_{L_{B_2}} - 0.25 * Q_{X_2} - Q_{D_{B_3}}$$
$$Q_{L_{B_4}} = 0.25 * Q_{X_1} + Q_{D_{C_4}} + Q_{L_{B_3}} - 0.25 * Q_{X_2} - Q_{D_{B_4}}$$

Mass Balances

Utilizing the law of mass conservation, mass balance equations were written for each zone in the dynamic population balance model (mass in = mass out). For each zone and for each size class, all flows were balanced and multiplied by the concentration of solids (C_{zone}) present in the zone from which the flow emanated. This was completed for increments of time as small as 1/10000th of one second. For each time increment (iteration), a new concentration for each zone could be calculated and mathematically added to the concentration from the previous iteration. The term U_pA represents the volume of settling solids in a particular zone as defined by the hindered-settling equations presented in the body of this work.

Using Figure A2, the following equations can be written:

$$C_{O_{1NEW}} = C_{O_1} + (Q_F C_F - C_{O_1}(Q_{L_{CO_1}} + Q_{D_{CO_1}} + U_P A))\Delta t$$
$$C_{O_{2NEW}} = C_{O_2} + (Q_{L_{CO_1}} C_{O_1} + 0.25 * Q_{X_5} C_{E_2} - C_{O_2}(Q_{L_{CO_2}} + Q_{D_{CO_2}} + U_P A))\Delta t$$
$$C_{O_{3NEW}} = C_{O_3} + (Q_{L_{CO_2}} C_{O_2} + 0.25 * Q_{X_5} C_{E_3} - C_{O_3}(Q_{L_{CO_3}} + Q_{D_{CO_3}} + U_P A))\Delta t$$
$$C_{O_{4NEW}} = C_{O_4} + (Q_{L_{CO_3}} C_{O_3} + 0.25 * Q_{X_5} C_{E_4} - C_{O_4}(Q_{L_{CO_4}} + Q_{D_{CO_4}} + U_P A))\Delta t$$
$$C_{O_{5NEW}} = C_{O_5} + (Q_{L_{CO_4}} C_{O_4} + 0.25 * Q_{X_5} C_{E_5} - C_{O_5}(Q_{L_{CO_5}} + Q_{D_{CO_5}} + U_P A))\Delta t$$

$$C_{E_{1NEW}} = C_{E_1} + (Q_{D_{O_1}} C_{O_1} - C_{E_1}(Q_{L_{E_1}} + Q_{D_{E_1}} + U_P A))\Delta t$$
$$C_{E_{2NEW}} = C_{E_2} + (Q_{L_{E_1}} C_{E_1} + 0.25 * Q_{X_4} C_{D_2} + Q_{D_{O_2}} C_{O_2} - C_{E_2}(0.25 * Q_{X_5} + Q_{L_{E_2}} + Q_{D_{E_2}} + U_P A))\Delta t$$
$$C_{E_{3NEW}} = C_{E_3} + (Q_{L_{E_2}} C_{E_2} + 0.25 * Q_{X_4} C_{D_3} + Q_{D_{O_3}} C_{O_3} - C_{E_3}(0.25 * Q_{X_5} + Q_{L_{E_3}} + Q_{D_{E_3}} + U_P A))\Delta t$$
$$C_{E_{4NEW}} = C_{E_4} + (Q_{L_{E_3}} C_{E_3} + 0.25 * Q_{X_4} C_{D_4} + Q_{D_{O_4}} C_{O_4} - C_{E_4}(0.25 * Q_{X_5} + Q_{L_{E_4}} + Q_{D_{E_4}} + U_P A))\Delta t$$
$$C_{E_{5NEW}} = C_{E_5} + (Q_{L_{E_4}} C_{E_4} + 0.25 * Q_{X_4} C_{D_5} + Q_{D_{O_5}} C_{O_5} - C_{E_5}(0.25 * Q_{X_5} + Q_{L_{E_5}} + Q_{D_{E_5}} + U_P A))\Delta t$$

$$C_{D_{1NEW}} = C_{D_1} + (Q_{D_{E_1}} C_{E_1} - C_{D_1}(Q_{L_{D_1}} + Q_{D_{D_1}} + U_P A))\Delta t$$
$$C_{D_{2NEW}} = C_{D_2} + (Q_{L_{D_1}} C_{D_1} + 0.25 * Q_{X_3} C_{C_2} + Q_{D_{E_2}} C_{E_2} - C_{D_2}(0.25 * Q_{X_4} + Q_{L_{D_2}} + Q_{D_{D_2}} + U_P A))\Delta t$$
$$C_{D_{3NEW}} = C_{D_3} + (Q_{L_{D_2}} C_{D_2} + 0.25 * Q_{X_3} C_{C_3} + Q_{D_{E_3}} C_{E_3} - C_{D_3}(0.25 * Q_{X_4} + Q_{L_{D_3}} + Q_{D_{D_3}} + U_P A))\Delta t$$
$$C_{D_{4NEW}} = C_{D_4} + (Q_{L_{D_3}} C_{D_3} + 0.25 * Q_{X_3} C_{C_4} + Q_{D_{E_4}} C_{E_4} - C_{D_4}(0.25 * Q_{X_4} + Q_{L_{D_4}} + Q_{D_{D_4}} + U_P A))\Delta t$$
$$C_{D_{5NEW}} = C_{D_5} + (Q_{L_{D_4}} C_{D_4} + 0.25 * Q_{X_3} C_{C_5} + Q_{D_{E_5}} C_{E_5} - C_{D_5}(0.25 * Q_{X_4} + Q_{L_{D_5}} + Q_{D_{D_5}} + U_P A))\Delta t$$

$$C_{C_{1NEW}} = C_{C_1} + (Q_{D_{D_1}} C_{D_1} - C_{C_1}(Q_{L_{C_1}} + Q_{D_{C_1}} + U_P A))\Delta t$$
$$C_{C_{2NEW}} = C_{C_2} + (Q_{L_{C_1}} C_{C_1} + 0.25 * Q_{X_2} C_{B_2} + Q_{D_{D_2}} C_{D_2} - C_{C_2}(0.25 * Q_{X_3} + Q_{L_{C_2}} + Q_{D_{C_2}} + U_P A))\Delta t$$
$$C_{C_{3NEW}} = C_{C_3} + (Q_{L_{C_2}} C_{C_2} + 0.25 * Q_{X_2} C_{B_3} + Q_{D_{D_3}} C_{D_3} - C_{C_3}(0.25 * Q_{X_3} + Q_{L_{C_3}} + Q_{D_{C_3}} + U_P A))\Delta t$$
$$C_{C_{4NEW}} = C_{C_4} + (Q_{L_{C_3}} C_{C_3} + 0.25 * Q_{X_2} C_{B_4} + Q_{D_{D_4}} C_{D_4} - C_{C_4}(0.25 * Q_{X_3} + Q_{L_{C_4}} + Q_{D_{C_4}} + U_P A))\Delta t$$
$$C_{C_{5NEW}} = C_{C_5} + (Q_{L_{C_4}} C_{C_4} + 0.25 * Q_{X_2} C_{B_5} + Q_{D_{D_5}} C_{D_5} - C_{C_5}(0.25 * Q_{X_3} + Q_{L_{C_5}} + Q_{D_{C_5}} + U_P A))\Delta t$$

$$C_{B_{1NEW}} = C_{B_1} + (Q_{D_{B_1}} C_{C_1} - C_{B_1}(Q_{L_{B_1}} + Q_{D_{B_1}} + U_P A))\Delta t$$
$$C_{B_{2NEW}} = C_{B_2} + (Q_{L_{B_1}} C_{B_1} + 0.25 * Q_{X_1} C_A + Q_{D_{C_2}} C_{C_2} - C_{B_2}(0.25 * Q_{X_2} + Q_{L_{B_2}} + Q_{D_{B_2}} + U_P A))\Delta t$$
$$C_{B_{3NEW}} = C_{B_3} + (Q_{L_{B_2}} C_{B_2} + 0.25 * Q_{X_1} C_A + Q_{D_{C_3}} C_{C_3} - C_{B_3}(0.25 * Q_{X_2} + Q_{L_{B_3}} + Q_{D_{B_3}} + U_P A))\Delta t$$
$$C_{B_{4NEW}} = C_{B_4} + (Q_{L_{B_3}} C_{B_3} + 0.25 * Q_{X_1} C_A + Q_{D_{C_4}} C_{C_4} - C_{B_4}(0.25 * Q_{X_2} + Q_{L_{B_4}} + Q_{D_{B_4}} + U_P A))\Delta t$$
$$C_{B_{5NEW}} = C_{B_5} + (Q_{L_{B_4}} C_{B_4} + 0.25 * Q_{X_1} C_A + Q_{D_{C_5}} C_{C_5} - C_{B_5}(0.25 * Q_{X_2} + Q_{L_{B_5}} + Q_{D_{B_5}} + U_P A))\Delta t$$

$$C_{A_{New}} = C_A + (Q_F C_F + U_P A * C_B + Q_Z C_G - C_A(Q_{X_1} + U_P A))\Delta t$$

Using Figure A3, the following equations can be written:

$$C_{G_{New}} = C_G + (Q_Z C_H + U_P A C_A - C_G(Q_Z + U_P A))\Delta t$$
$$C_{H_{New}} = C_H + (Q_Z C_I + U_P A C_G - C_H(Q_Z + U_P A))\Delta t$$
$$C_{I_{New}} = C_I + (Q_Z C_J + U_P A C_H - C_I(Q_Z + U_P A))\Delta t$$
$$C_{J_{New}} = C_J + (Q_Z C_K + U_P A C_I - C_J(Q_Z + U_P A))\Delta t$$
$$C_{K_{New}} = C_K + (Q_Z C_L + U_P A C_J - C_K(Q_Z + U_P A))\Delta t$$

$$C_{L_{New}} = C_L + (U_P A C_K - C_L(Q_Z + Q_U + U_P A))\Delta t$$

$$C_{U_{New}} = C_U + (C_P(Q_U + U_P A) - C_U Q_U)\Delta t$$

These equations were solved continuously until the change in concentration for each and every zone in the population balance model was equivalent to zero or $C_{ZONE(new)}$ is equal to C_{ZONE}. Steady-state conditions are realized when the change in concentration for the entire separator is equal to zero.

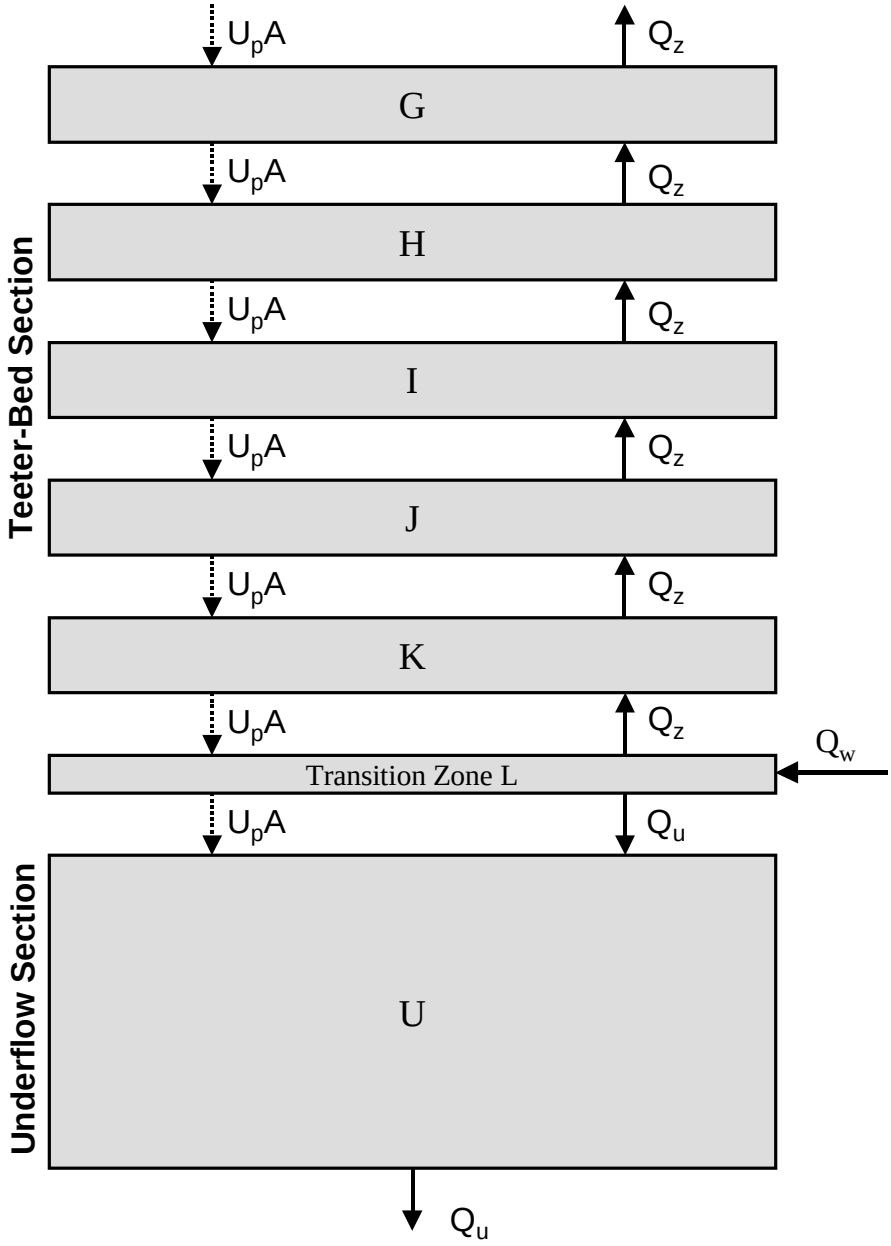

Figure A3 – Zone and flow schematic for teeter and underflow sections of the CrossFlow model.

APPENDIX B

Model Input/Output Examples

Operational Input (user input in bold font):

Feed Tonnage Data						
Solids Feed Rate					Slurry Feed Rate	
(tph/ft^2)	(tph/m^2)	tph	kg/hr	kg/s	kg/s	m^3/s
2.5	26.91	0.139	126.0	0.0350	0.070	0.00005

Feed Input Data					Water Rates		
Feed Concentration					Elutriation Water Rate		
Solids (%)	Slurry ρ	Density 1	Density 2	Overall	(gpm)	ft^3/s	m^3/s
50	1.45	**2.65**	**3.50**	2.65	**1.00**	0.0022	0.00006

Starting Values (m^3/s)		Starting Values (kg/m^3)		Starting Values (m^3/m^3)	
Qf	0.00005	Cf	726.03	ϕf	0.2740
Qw	0.00006	Cw	0.0000	ϕw	0.0000
Qo	0.00004	Co	0.0000	ϕo	0.0000
Qu	0.00002	Cu	0.0000	ϕu	0.0000
Qz	0.00004	Ca-Cp	0.0000	ϕa-ϕp	0.0000

Qu (lpm)
1.22

Reset
1

Time Limits			
Lower Time Step (sec)	**0.0001**	Starting Delta Time (sec)	**0.00001**
Higher Time Step (sec)	**0.075**	Total Time (sec)	10800
Current Time Step (sec)	0.0819	Total Time (min)	**180**

Target D_{50}
0.3
0.869

Unit Size Input (user input in bold font):

Cell Geometry								
Number of Zones (#):			13	Total Volume (m^3)			2.13E-03	
Separation Chamber Area			Vessel Outlet Area				Cell Depth	
(in^2)	(ft^2)	(m^2)	Dia. (in)	(in^2)	(ft^2)	(m^2)	(in)	(m)
8.0	0.056	0.0052	**0.5**	0.196	0.00136	0.00013	**2**	0.0508

Horizontal Sectioning						
Cell	C5	C4	C3	C2	C1	Check
Length	0.75	0.75	0.75	0.75	**1**	4
Area	0.0010	0.0010	0.0010	0.0010	0.0013	0.0052

Vertical Sectioning					
Zone (#)	Zone Depth (in)	Zone Depth (m)	Volume (m^3)	Area (m^2)	Comments
O5	**2.00**	0.0508	4.92E-05	0.0010	Overflow Zone
O4	2.00	0.0508	4.92E-05	0.0010	
O3	2.00	0.0508	4.92E-05	0.0010	
O2	2.00	0.0508	4.92E-05	0.0010	
O1	2.00	0.0508	6.55E-05	0.0013	Feed Inlet
E5	**1.00**	0.0254	2.46E-05	0.0010	
E4	1.00	0.0254	2.46E-05	0.0010	
E3	1.00	0.0254	2.46E-05	0.0010	
E2	1.00	0.0254	2.46E-05	0.0010	
E1	1.00	0.0254	3.28E-05	0.0013	
D5	**1.00**	0.0254	2.46E-05	0.0010	
D4	1.00	0.0254	2.46E-05	0.0010	
D3	1.00	0.0254	2.46E-05	0.0010	
D2	1.00	0.0254	2.46E-05	0.0010	
D1	1.00	0.0254	3.28E-05	0.0013	
C5	**1.00**	0.0254	2.46E-05	0.0010	
C4	1.00	0.0254	2.46E-05	0.0010	
C3	1.00	0.0254	2.46E-05	0.0010	
C2	1.00	0.0254	2.46E-05	0.0010	
C1	1.00	0.0254	3.28E-05	0.0013	
B5	**0.50**	0.0127	1.23E-05	0.0010	
B4	0.50	0.0127	1.23E-05	0.0010	
B3	0.50	0.0127	1.23E-05	0.0010	
B2	0.50	0.0127	1.23E-05	0.0010	
B1	0.50	0.0127	1.64E-05	0.0013	
A	**1.00**	0.0254	1.31E-04	0.0052	Transition Zone
G	**1.00**	0.0254	1.31E-04	0.0052	
H	**1.00**	0.0254	1.31E-04	0.0052	
I	**1.00**	0.0254	1.31E-04	0.0052	
J	**1.00**	0.0254	1.31E-04	0.0052	
K	**1.00**	0.0254	1.31E-04	0.0052	
L	**1.25**	0.0318	1.64E-04	0.0052	Elutriation Point
U	**4.0**	0.1016	**4.59E-04**	0.0001	Underflow Zone
Calc. Depth	16.75				
Act. Depth	**16.75**				

Feed Size and Distribution Input (user input in bold font):

Feed Size Distribution										
Screen Size (mesh)	Passing Size (mm)	Retained Size (mm)	Mean Size (mm)	Feed Mass (g)	Feed Mass (%)	Comp. 1 Assay (%)	Comp. 2 Assay (%)	Comp. 1 Mass (%)	Comp. 2 Mass (%)	Mixed Feed Density
Plus 18	***	1.180	1.180	**5.00**	11.11	**50.00**	50.00	5.56	5.56	3.02
18 x 20	1.180	0.850	1.001	**5.00**	11.11	**50.00**	50.00	5.56	5.56	3.02
20 x 30	0.850	0.600	0.714	**5.00**	11.11	**50.00**	50.00	5.56	5.56	3.02
30 x 40	0.600	0.425	0.505	**5.00**	11.11	**50.00**	50.00	5.56	5.56	3.02
40 x 50	0.425	0.300	0.357	**5.00**	11.11	**50.00**	50.00	5.56	5.56	3.02
50 x 70	0.300	0.212	0.252	**5.00**	11.11	**50.00**	50.00	5.56	5.56	3.02
70 x 100	0.212	0.150	0.178	**5.00**	11.11	**50.00**	50.00	5.56	5.56	3.02
100 x 150	0.150	0.106	0.126	**5.00**	11.11	**50.00**	50.00	5.56	5.56	3.02
Minus 150	0.106	***	0.106	**5.00**	11.11	**50.00**	50.00	5.56	5.56	3.02
Overall				45.00				50.00	50.00	

Screen Size (mesh)	Feed Rate kg/s	Comp 1 Rate kg/s	Comp 2 Rate kg/s	Feed Conc. kg/m^3	Comp 1 Conc. kg/m^3	Comp 2 Conc. kg/m^3	Feed Conc. m^3/m^3	Comp 1 Conc. m^3/m^3	Comp 2 Conc. m^3/m^3
Plus 18	0.004	0.002	0.002	83.45	41.72	41.72	0.0277	0.0157	0.0119
18 x 20	0.004	0.002	0.002	83.45	41.72	41.72	0.0277	0.0157	0.0119
20 x 30	0.004	0.002	0.002	83.45	41.72	41.72	0.0277	0.0157	0.0119
30 x 40	0.004	0.002	0.002	83.45	41.72	41.72	0.0277	0.0157	0.0119
40 x 50	0.004	0.002	0.002	83.45	41.72	41.72	0.0277	0.0157	0.0119
50 x 70	0.004	0.002	0.002	83.45	41.72	41.72	0.0277	0.0157	0.0119
70 x 100	0.004	0.002	0.002	83.45	41.72	41.72	0.0277	0.0157	0.0119
100 x 150	0.004	0.002	0.002	83.45	41.72	41.72	0.0277	0.0157	0.0119
Minus 150	0.004	0.002	0.002	83.45	41.72	41.72	0.0277	0.0157	0.0119
Overall	0.035	0.017	0.017	751.01	375.51	375.51	0.2490	0.1417	0.1073
									0.2490

Output Partition Data:

Component No. 1 Partitioning						
Mean Size (μm)	Feed Rate (kg/min)	O/F Rate (kg/min)	U/F Rate (kg/min)	O/F PF (%)	U/F PF (%)	Balance Error (%)
1.180	0.12	0.00	0.12	0.03	99.97	0.00
1.001	0.12	0.00	0.12	0.07	99.93	0.00
0.714	0.12	0.00	0.12	0.49	99.51	0.00
0.505	0.12	0.00	0.11	3.57	96.43	0.00
0.357	0.12	0.02	0.09	19.78	80.22	0.00
0.252	0.12	0.07	0.05	58.27	41.73	0.00
0.178	0.12	0.11	0.01	91.26	8.74	0.00
0.126	0.12	0.12	0.00	99.53	0.47	0.00
0.106	0.12	0.12	0.00	99.93	0.07	0.00
				0.000E+00	0.081920	0.00

Component No. 2 Partitioning						
Mean Size (μm)	Feed Rate (kg/min)	O/F Rate (kg/min)	U/F Rate (kg/min)	O/F PF (%)	U/F PF (%)	Balance Error (%)
1.180	0.12	0.00	0.12	0.01	99.99	0.00
1.001	0.12	0.00	0.12	0.01	99.99	0.00
0.714	0.12	0.00	0.12	0.10	99.90	0.00
0.505	0.12	0.00	0.12	0.78	99.22	0.00
0.357	0.12	0.01	0.11	5.95	94.05	0.00
0.252	0.12	0.04	0.08	30.14	69.86	0.00
0.178	0.12	0.08	0.03	72.30	27.70	0.00
0.126	0.12	0.11	0.00	96.28	3.72	0.00
0.106	0.12	0.12	0.00	99.23	0.77	0.00
						0.00

Output Partition Curves:

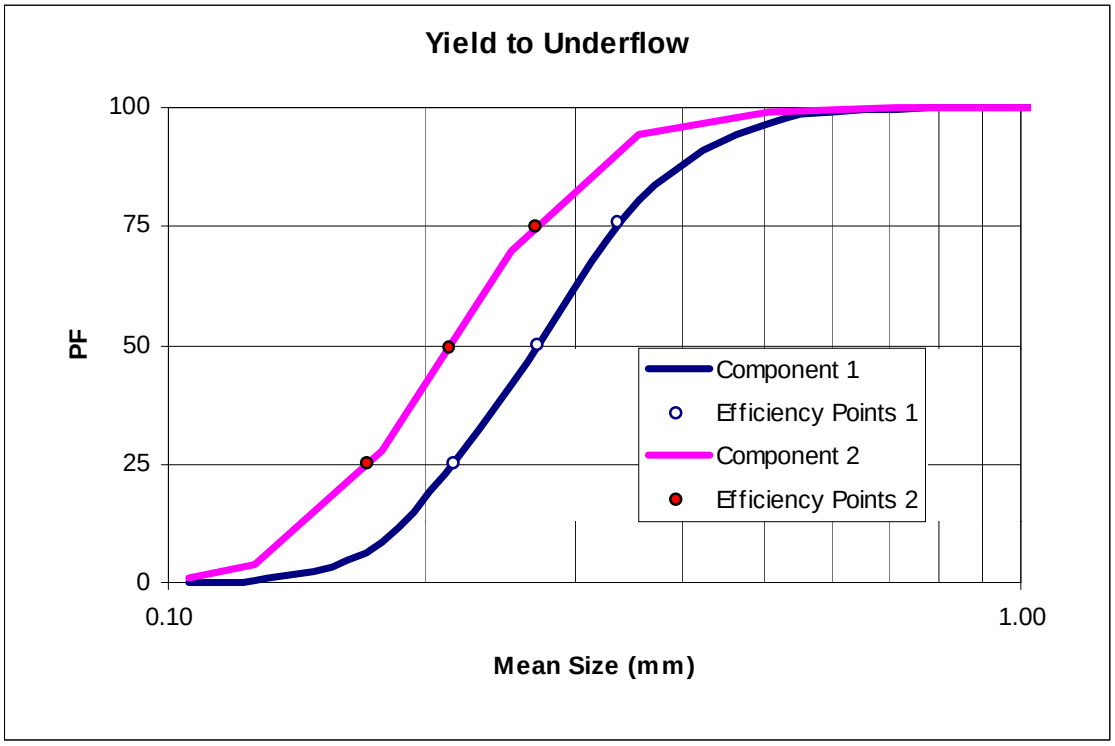

Output Separation Efficiency Data:

Comp. 1 Check		
Feed kg/min	O/F kg/min	U/F kg/min
1.0500	0.4351	0.6149
100.00%	41.44%	58.56%

Comp. 1 Sizing Efficiency		
PF	(mm)	Ep
25.00	0.216	0.060
50.00	0.273	Imp.
75.50	0.337	0.220

Comp. 2 Check		
Feed kg/min	O/F kg/min	U/F kg/min
1.0500	0.3556	0.6944
100.00%	33.87%	66.13%

Comp. 2 Sizing Efficiency		
PF	(mm)	Ep
25.00	0.171	0.050
50.00	0.214	I
75.00	0.270	0.230

Output Volumetric Concentration Data:

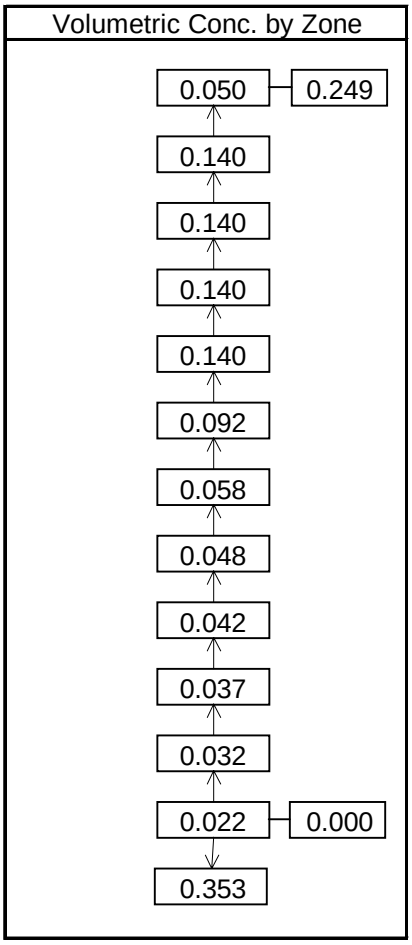

Output Product Recovery and Particle Size Distribution Data:

Combined Products									
	Feed Rate			Underflow Rate			Overflow Rate		
Mean Size	Combined	Comp. 1	Comp. 2	Combined	Comp. 1	Comp. 2	Combined	Comp. 1	Comp. 2
(µm)	kg/min	kg/min	kg/min	kg/min	kg/min	kg/min	kg/min	kg/min	kg/min
1.180	0.23	0.12	0.12	0.23	0.12	0.12	0.00	0.00	0.00
1.001	0.23	0.12	0.12	0.23	0.12	0.12	0.00	0.00	0.00
0.714	0.23	0.12	0.12	0.23	0.12	0.12	0.00	0.00	0.00
0.505	0.23	0.12	0.12	0.23	0.11	0.12	0.01	0.00	0.00
0.357	0.23	0.12	0.12	0.20	0.09	0.11	0.03	0.02	0.01
0.252	0.23	0.12	0.12	0.13	0.05	0.08	0.10	0.07	0.04
0.178	0.23	0.12	0.12	0.04	0.01	0.03	0.19	0.11	0.08
0.126	0.23	0.12	0.12	0.00	0.00	0.00	0.23	0.12	0.11
0.106	0.23	0.12	0.12	0.00	0.00	0.00	0.23	0.12	0.12
Totals	2.10	1.05	1.05	1.31	0.61	0.69	0.79	0.44	0.36

	Feed Assay		Underflow Assay		Overflow Assay		Underflow	Overflow
Mean Size	Comp. 1	Comp. 2	Comp. 1	Comp. 2	Comp. 1	Comp. 2	PSD	PSD
(µm)	%	%	%	%	%	%	%	%
1.180	50.0	50.0	50.0	50.0	83.7	16.3	17.82	0.01
1.001	50.0	50.0	50.0	50.0	83.7	16.3	17.81	0.01
0.714	50.0	50.0	49.9	50.1	83.5	16.5	17.77	0.09
0.505	50.0	50.0	49.3	50.7	82.0	18.0	17.43	0.64
0.357	50.0	50.0	46.0	54.0	76.9	23.1	15.53	3.80
0.252	50.0	50.0	37.4	62.6	65.9	34.1	9.94	13.05
0.178	50.0	50.0	24.0	76.0	55.8	44.2	3.25	24.13
0.126	50.0	50.0	11.2	88.8	50.8	49.2	0.37	28.89
0.106	50.0	50.0	8.4	91.6	50.2	49.8	0.08	29.39
Totals	50.0	50.0	47.0	53.0	55.0	45.0	***	***

Combined Product Recoveries							
Mean Size	Total Mass Recovery			Comp 1 Recovery		Comp 2 Recovery	
	Feed	U/F	O/F	U/F	O/F	U/F	O/F
(µm)	%	%	%	%	%	%	%
1.180	100	100.0	0.0	100.0	0.0	100.0	0.0
1.001	100	100.0	0.0	99.9	0.1	100.0	0.0
0.714	100	99.7	0.3	99.5	0.5	99.9	0.1
0.505	100	97.8	2.2	96.4	3.6	99.2	0.8
0.357	100	87.1	12.9	80.2	19.8	94.0	6.0
0.252	100	55.8	44.2	41.7	58.3	69.9	30.1
0.178	100	18.2	81.8	8.7	91.3	27.7	72.3
0.126	100	2.1	97.9	0.5	99.5	3.7	96.3
0.106	100	0.4	99.6	0.1	99.9	0.8	99.2
Totals	100.0	62.3	37.7	58.6	41.4	66.1	33.9

VITA

Jaisen Nathaniel Kohmuench, son of William C. and Carolyn A. Kohmuench was born in Teaneck, NJ, on the 23rd day of May, 1973. He graduated from Hunterdon Central Regional High School in the spring of 1991. The following fall, he was granted admission to Virginia Polytechnic Institute and State University (Virginia Tech), where he went on to gain a Bachelor of Science degree in Mining and Minerals Engineering. During his time as an undergraduate, he was highly involved in the Burkhart Mining Society, the student chapter of the Society for Mining, Metallurgy and Exploration (SME). It was during the '94-'95 school year that he served as the vice president of this organization. He also successfully passed the EIT exam.

After graduating in the spring of 1995, he remained at Virginia Tech to pursue a Master of Science degree in Mining and Minerals Engineering with an emphasis in minerals processing. He completed his degree in the fall semester of 1997 and immediately enrolled in the Ph.D. program. He is currently a student member of SME. As a doctoral candidate, he conducted several presentations at professional meetings in addition to authoring (or co-authoring) over 11 works, including two full peer-reviewed journal publications. While a student, he earned the Graduate Student of the Year Award for both the 1996 and 1999 school years.

Upon completion of his doctoral dissertation, he and his wife, Kathryn, will relocate to Erie, Pennsylvania. Here, having already accepted a position, Jaisen will begin his professional career as a process engineer for Eriez Magnetics.

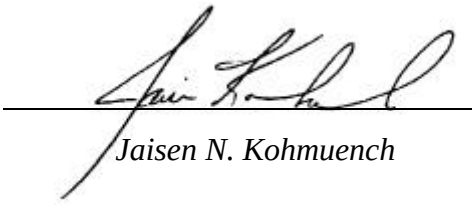

Jaisen N. Kohmuench